AN INVESTIGATION ON ELECTROCHEMICAL PERFORMANCE OF SUPERCAPACITORS ASSEMBLED WITH VERTICALLY ALIGNED&ENTANGLED CARBON NANOTUBE AND CONDUCTIVE POLYMER

by
DİLEK ÇAKIROĞLU

Submitted to the Graduate School of Engineering and Natural Sciences
in partial fulfillment of
the requirements for the degree of
Doctor of Philosophy

Sabancı University
March 2016

AN INVESTIGATION ON ELECTROCHEMICAL PERFORMANCE OF SUPERCAPACITORS ASSEMBLED WITH VERTICALLY ALIGNED&ENTANGLED CARBON NANOTUBE AND CONDUCTIVE POLYMER

APPROVED BY:

Asst. Prof. Fevzi Çakmak Cebeci
(Thesis Supervisor)

Assoc. Prof. Selmiye Alkan Gürsel

Assoc. Prof. Kürşat Şendur

Assoc. Prof. Murat Ateş

Assoc. Prof. Musa Mutlu Can

DATE OF APPROVAL: 14.03.2016

ABSTRACT

AN INVESTIGATION ON ELECTROCHEMICAL PERFORMANCE OF SUPERCAPACITORS ASSEMBLED WITH VERTICALLY ALIGNED&ENTANGLED CARBON NANOTUBE AND CONDUCTIVE POLYMER

Dilek Çakıroğlu

Material Science and Engineering, PhD Thesis, 2016

Thesis Supervisor: Asst. Prof.. Fevzi C. Cebeci

Keywords: Supercapacitor, vertically aligned carbon nanotube, entangled carbon nanotube, conducting polymer, electrochemical characterization, morphological characterization

Supercapacitors or electrochemical double layer capacitors are one of the most important research topics in the energy storage field because they fill the gap between batteries and commercial electrostatic capacitors. Long cycle life, high specific power density and short charge/discharge time offer advantages to supercapacitors over batteries; however, specific energy density of batteries is clearly higher than that of supercapacitors.

After introduction of multi-walled carbon nanotubes (MWCNT) to the scientific community by S. Iijima, carbon nanotubes (CNT) became a very popular electrode active material in supercapacitor applications because of its well-defined porosity, high surface area, chemical stability, and more importantly its high conductivity that might lead high power density. These characteristics are essential for high charge storage which is called double-layer capacitance. Two forms of CNT, which vertically aligned carbon nanotubes (VA-CNT) and the other one is entangled carbon nanotubes (EN-CNT) can be used as an electrode material in supercapacitors.

Implementing CNT with a conducting polymer which will give additional charge storage, called pseudo-capacitance, into a supercapacitor electrode structure ensures to achieve enhanced capacitive behavior. The reason of this is that supercapacitor will store the charge physically in the double-layer and also chemically in the polymer in this way. Among all conducting polymers, polyaniline (PANi) has been studied extensively due to its high conductivity, high theoretical capacitance, good faradic redox reversibility, and high stability in air and solutions.

In the present work, VA-CNT were synthesized by thermal chemical vapor deposition (CVD) on the silicon wafer chips. Free standing EN-CNT film without any binder was prepared from VA-CNT. Hybrid supercapacitor electrodes were fabricated via electrochemical and chemical methods. Electrochemical performances of the supercapacitor cells were evaluated by cyclic voltammetry, electrochemical impedance spectroscopy and galvanostatic charge/discharge tests.

ÖZET

KARBON NANOTÜP VE İLETKEN POLİMER İLE HAZIRLANAN

SÜPERKAPASİTÖRLERİN ELEKTROKİMYASAL PERFORMANSININ

İNCELENMESİ

Dilek Çakıroğlu

Malzeme Bilimi ve Mühendisliği, Doktora tezi, 2016

Tez Danışmanı: Yrd. Doç. Fevzi C. Cebeci

Anahtar Kelimeler: Süperkapasitörler, dikey yönelimli karbon nanotüp, çapraşık karbon nanotüp, iletken polimer, elektrokimyasal karakterizasyon

Süperkapasitörler, bir diğer adıyla elektrokimyasal çift tabakalı kapasitörler, enerji depolama konusunda ki en önemli araştırma konularından biridir çünkü piller ve elektrostatik kapasitörlerin arasındaki boşluğu doldurmaktadır. Uzun kullanım süresi, yüksek spesifik güç yoğunluğu ve kısa sarj/deşarj süresi, süperkapasitörleri pillere kıyasla daha avantajlı hale getirmektedir ancak pillerin spesifik enerji yoğunluğu, kapasitörlere kıyasla çok daha yüksektir.

S. Lijima'nın çok duvarlı karbon nanotüpleri (MWCNT) bulmasından sonra, CNT süperkapasitörlerde elektroaktif madde olarak kullanılmaya başlanmıştır çünkü iyi tanımlanmış porlu yapısı, yüksek yüzey alanı, kimyasal stabilitesi, ve en önemlisi yüksek iletkenliği sahiptir. Bu özellikler, yük depoloma işlemi için çok gerekli olmakla birlikte çift katmanlı kapasitans olarak adlandırılmaktadır. Dikey yönelimli CNT (VA-CNT) ve dolanık CNT (EN-CNT), karbon nanotüpün iki farklı formu olarak elektrode aktif malzemesi olarak kullanılmıştır.

İletken polimerin CNT yapısına dahil edilmesi ile yük depolama mekanizmasina pseudokapasitans olarak adlandırılan yeni bir özellik katılabilmektedir. Bu şekilde yeni bir malzemenin yanısıra daha iyi kapasitesye sahip bir yapı elde edilecektir. Çift katmanlı yük depolama işleminde yükler fiziksel olarak elektrostatik bir şekilde depolanırken, iletken polimer ve CNT ile elde edilen melez yapılarda yük depolama işlemi elektron alışverişinden dolayı kimyasal bir olaydır. Tüm iletken polimerler içinde polianilin (PANi), çok fazla araştırılmıştır çünkü iyi bir iletkenliğe, yüksek bir teorik kapasitansa, ve havada ve çözelti içinde yüksek bir stabiliteye sahiptir.

Bu tez konusunda, VA-CNT kimyasal depolama (CVD) yöntemi ile silikon yonga tabakası üzerinde sentezlenmiştir. EN-CNT elektrodlar ise herhangi bir dolgu yada birleştirici malzeme kullanılmadan direk olarak VA-CNT'den elde edilmiştir. Melez yapılı elektrodlar, elektrokimyasal ve kimyasal yötemler ile hazırlanmıştır. Elde edilen elektrodların ve süperkapasitör hücrelerın elektrokimyasal performansları, dönüşümlü voltametri, elektrokimyasal empedans spektroskopi ve galvanostatik şarj/deşarj yötemleri ile test edilmiştir.

“You are the average of five people you spent the most time with”-Jim Rohn

I present my sincere thanks and gratitude to those honest, hardworking and ethical souls who helped me to accomplish this study...

TABLE OF CONTENTS

LIST OF FIGURES

LIST OF TABLES

LIST OF ABBREVIATIONS

SCs	Supercapacitor
AC	Activated Carbon
CNT	Carbon Nanotube
MWCNT	Multiwall Carbon Nanotube
SWCNT	Singlewall Carbon Nanotube
VA-CNT	Vertically Aligned Carbon Nanotube
EN-CNT	Entangled Carbon Nanotube
ESR	Equivalent Series Resistance
H_2SO_4	Sulfuric Acid
NA_2SO_4	Sodium Sulfate
KOH	Potassium Hydroxide
PANi	Polyaniline
PPy	Polypyrole
$LiPF_6$	Lithium hexafluorophosphate
TEABF4	Tetraethylammonium tetrafluoroborate
TBABF4	Tetrabutylammonium tetrafluoroborate
PC	Propylene Carbonate
AN	Acetonitrile
EMIT-BF4	1-ethyl-3-methyl imidazolium tetrafluoroborate
EMIT-FSI	1-ethyl-3-methyllimidazoliumbis (trifluoromethylsulfonyl) imide
PP	Polypropylene
PE	Polyethylene
EDLCs	Electrochemical Double Layer Capacitors
PCs	Pseudocapacitors

HCs	Hybrid Capacitors
RuO_2	Ruthenium Oxide
MnO_2	Manganese Dioxide
CV	Cyclic Voltammetry
EIS	Electrochemical Impedans Spectroscopy
GCD	Galvanostatic Charge/Discharge
C_{sp}	Specific Capacitance
E_{sp}	Specific Energy Density
P_{sp}	Specific Power Density
SEM	Scanning Electron Microscopy
TEM	Tranmission Electron Microscopy
TGA	Thermogravimetric Analysis
CVD	Chemical Vapor Deposition
SiO_2	Silicone Oxide

1. Introduction

Supercapacitors (SC) or electrochemical capacitors (EC) are one of the most conspicuous research topics in the energy storage field for their fast response time and exceptional cycle life. In spite of all recent extensive studies in the area and especially electrode materials [1-6], supercapacitors still require exhaustive research and through understanding of electrode materials and fundamentals of electrode charge storage mechanism to close the gap between capacitors and batteries. To attain those features, cell assemblies should demonstrate high energy density and high power density without sacrificing the response time and cycle life.

On the other hand nanostructured carbon-based materials, as the primary materials for supercapacitor electrodes, such as activated carbon, porous carbon, carbon nanotubes, graphene have been extensively studied and reported in the literature [7-9]. Carbon based materials exhibit most of the essential properties required by high performance supercapacitor electrodes such as high surface area, conductivity, and stability. Especially, carbon nanotubes (CNT) emerged as an electrode active material in supercapacitor applications along with the most commonly used activated carbon (AC) and become exceptionally popular because of its well-defined porosity, chemical stability, and more importantly its high conductivity that might lead to high power density [10-13].

After the introduction of multi-walled carbon nanotubes (MWCNTs) to the scientific community by S. Iijima [14], synthesis, property and application perspectives of carbon nanotubes have been researched. Terrones and coworkers have reported a controlled production and alignment of the CNT [15] and synthesis of vertical alignment of carbon nanotubes has been followed [16]. Electrochemical performance of the SC cell alters depending on the alignment of the CNT and the type of electrolytes being employed. Vertically aligned carbon nanotubes (VA-CNT) and entangled carbon nanotubes (EN-CNT) have been used as electrode materials in the different form of CNT [17-21]. The main difference between VA-CNT and EN-CNT is the ion pathway, which affects the electric resistance and the ion transport [13, 22, 23]. EN-CNT has tortuous ion pathways similar to that in activated carbon and requires binder to prepare electrode material,

however preparation of VA-CNT electrode does not need binder [23-25]. The electrochemical properties of VA-CNT and EN-CNT were compared and pointed out VA-CNT is a viable choice as a electrode material for supercapacitor applications [17, 24]. The investigation of supercapacitor performance between VA-CNT and EN-CNT differs completely when the growth procedures are not the same, besides the filler and binder presence results in various differences. Furthermore, the same SC device shows different electrochemical behaviour in acidic aqueous electrolyte and organic electrolyte due to the differences of both electrolytes such as the type of ions which are more reactive to the catalyst particle in CNT electrodes, ion radii, voltage window and ionic conductivity [26].

Recently, hybrid nanostructured electrodes gained more importance. Binary and ternary hybrid structures are a good option to enhance the specific energy and power densities, as well as capacitance, of supercapacitors because it possesses both battery and capacitor properties [27] One could fabricate a hybrid electrode structure by the assembly of materials that undergo Faradic redox behavior with capacitive/conductive materials. Faradic materials are divided into two categories; the first is conducting polymers such as polyaniline (PANi), polypyrrole (Ppy), and polythiophene (Pth); the second is inorganic electroactive species such as RuO_2 and MnO_2. Among all conducting polymers, polyaniline is one of the most promising materials due to its high conductivity, high theoretical specific capacitance, good faradic reversibility, and low cost [28]. Besides, as a transition metal oxide, MnO_2 recently has received greater attention from researchers due to its high energy density, low cost, natural abundance, environmental friendliness, and high theoretical specific capacitance [29].

In this work, I present a study on the electrochemical properties of symmetric supercapacitor (SC) cells fabricated by VA-CNT electrodes and EN-CNT electrodes. The effects of alignment and entanglement of CNT and the procedure of electrode preparation on the electrochemical performance were investigated in detail. In order to limit the set of the parameters affecting the electrochemical test results, EN-CNT used in this work was directly obtained from VA-CNT as binder and filler free. I also show the effect of electrolytes on the electrode structure using acidic aqueous electrolyte and organic electrolyte for long term usage. Addition to this, I focus on the preparation of a hybrid electrode structure using polyaniline and EN-CNT via electrochemical and chemical methods. Morphological characterizations of the prepared electrode samples were conducted by scanningin electron microscopy (SEM) and tranmission electron microscopy (TEM) and Raman spectroscopy. Electrochemical properties of the electrodes and SC cells

were investigated using cyclic voltammetry (CV), electrochemical impedance spectroscopy (EIS) and galvanostatic charge/discharge (GCD) tests methods.

2. Energy Storage Technologies

Energy crisis in the world forces researchers to find new energy sources and also efficient energy storage systems. There are many different electrochemical energy storage systems on the market and supercapacitors, named as also ultracapacitors and electrochemical capacitors, are one of those systems in addition to the electrostatic capacitors, batteries and fuel cells. The plot in Figure 2.1 [30] is called as Ragone plot and compares the different energy storage and conversion systems based on their specific power and energy density. Fuel cells are the one which have the highest specific energy density and the electrostatic capacitors are the one which have the highest specific power density. Batteries and SCs have moderate power and energy densities and fill the middle part of the plot.

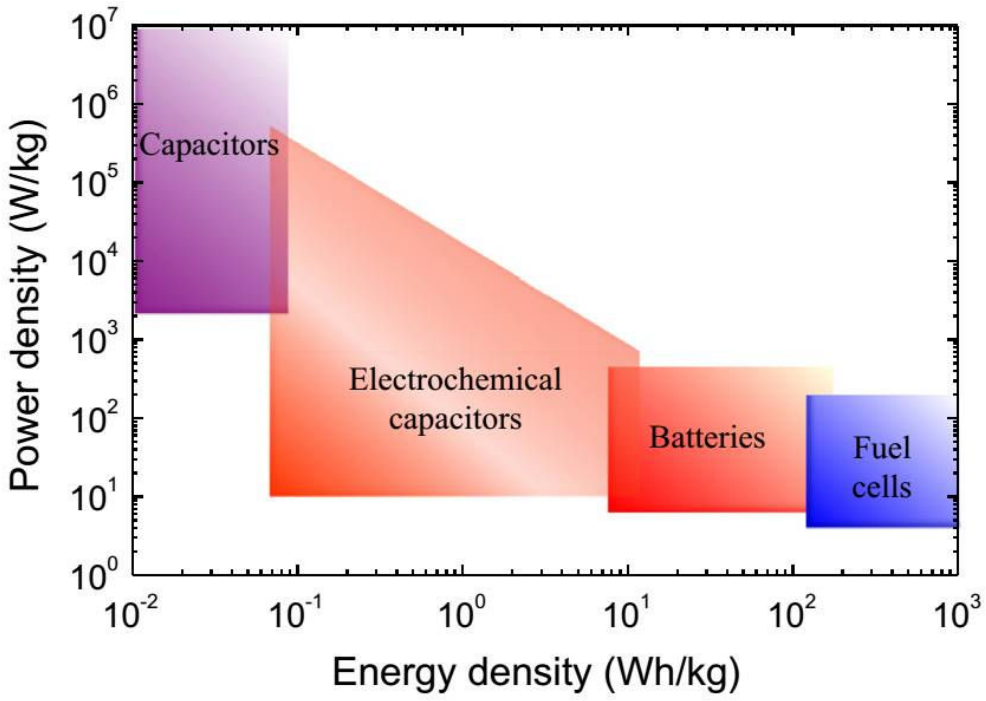

Figure 2.1.Performance comparison of various energy storing devices [30]

Table 2.1 summarizes the main differences between batteries, capacitors and supercapacitors [31]. As seen in table, capacitors have more advantages than supercapacitors except the specific energy density. SCs have higher energy density than

capacitors. Among all these three energy storage technology, batteries have higher energy density. When the battery and SCs are compared SCs have better properties than batteries in some aspects such as shor charge/discharge time, high power density and more cycle life. Cycle efficiency is very high in SCs due to the non-faradic physical reactions in the electrode surface.

Table 2.1. Characteristic of Li-ion battery, supercapacitor and electrostatic capacitor [31]

Characteristic	**Li-ion Battery**	**Supercapacitor**	**Capacitor**
Charge Time	1-5h	sec to min	10^{-6} to 10^{-3}
Discharge Time	0.3-3h	sec to min	10^{-6} to 10^{-3}
Cycle Life (#)	<5000	>500000	Almost infinite
Specific Power (W/kg)	<1000	5000-10000	>10000
Specific Energy (Wh/kg)	10-100	1 to 10	<0.1
Cyclic Efficiency (%)	%70 to %85	%70 to %95	>%95

An important difference between battery and capacitor is that there is an increase at the beginning of charge and a decrease at the beginning of discharge of the capacitor as seen in Figure 2.2 [32]. The sudden drop at the voltage is called as equivalent series resistance (ESR). Battery does not show any increase or decrease during charge and discharge except when it approaches to the 100% charge named as TOC (top of charge) and 100% discharge names as EOD (end of discharge). For this reason, capacitor requires DC-DC converter to provide a constant output voltage.

Table 2.2 compares the battery and SCs in different aspects. Storage mechanism in battery and SCs is totaly different. Batteries use chemical reactions to work during charging and discharging whereas SCs use physical reactions. Power of the systems are limited. In battery, this limitation is due to the reaction kinetics and mass transport. Power limitation of SCs depends on the used electrolyte. Energy is stored in bulk structure of battery electrodes whereas energy storage is limited by the surface area of the electrodes. Because, in SCs charge storage takes place on the surface of the electrode materials. Cycle life is also limited by the side reactions in SCs and by mechanical and chemical stability in batteries. Charge and discharge rate is very high in SCs but batteries have very slow charge/discharge rate due to the kinetical limitations.

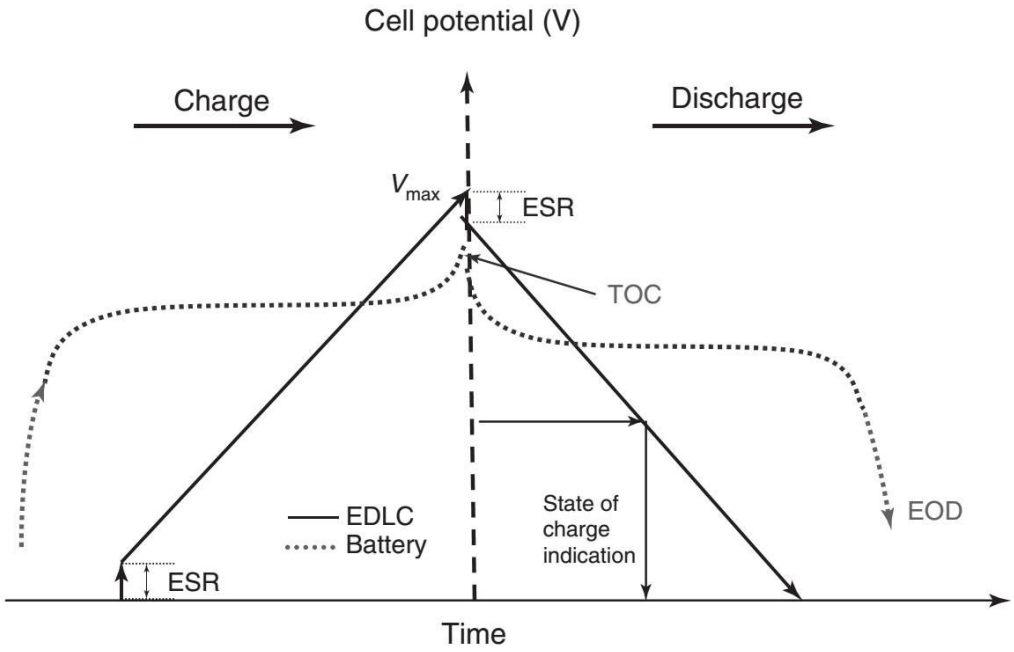

Figure 2.2. Charge-discharge behaviour of capacitor and battery [47]

Table 2.2. Comparison between battery and supercapacitors [31]

Parameters	**Battery**	**Supercapacitor**
Storage mechanism	Chemical	Physical
Power limitation	Reaction kinetics, mass transport	Electrolyte conductivity
Energy storage	High	Limited
Charge rate	Kinetically limited	High
Cycle life limitations	Mechanical stability, chemical reversibility	Side reactions

Due to the improving technologies in SCs, they are used in different applications such as supplementary storage for battery vehicles, Boeing plane emergency doors, light rail systems [33]. However low operating voltage and low energy density are the drawbacks of SCs. To overcome those drawbacks, the components of the SCs system should be investigated more deeply and there are several ongoing researches on this area recently [2, 4, 5, 34].

2.1. Elements of Supercapacitor Cell

SC cells consist of two electrodes (positive and negative), electrolyte, seperator and current collectors. Figure 2.3 illustrates the components of the SC cells [35]. The used electrodes might be the same on the both side or different based on the SC configuration. In the symmetric SC configuration, positive and negative electrodes have the same material structure. In asymmetric SC configuration, positive and negative electrodes have different material structure.

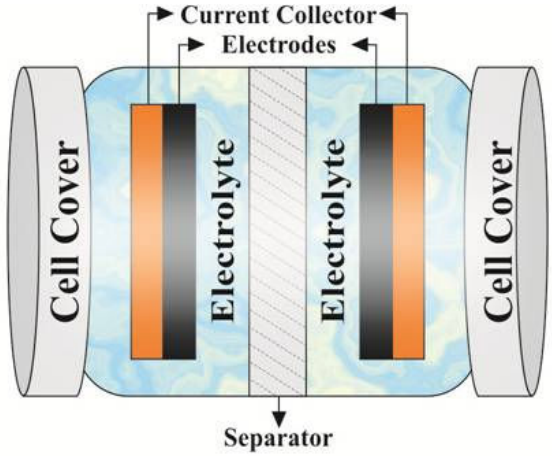

Figure 2.3. The components of the supercapacitor cell [35]

2.2. Electrodes Used in Supercapacitor Cell

Electrodes are the most essential elements of the SC cells. The electrochemical performance of the electrodes are directly related to their specific surface area, pore size distrubition, pore shape and structure, electrical conductivity, and surface functionality [4]. The most important electrode materials such as activated carbon, carbon nanotube and conducting polymers are briefly explained here.

2.2.1. Activated Carbon

Activated carbon (AC) is one of the mostly used as electroactive material for SC electrodes because of its high surface area which is about 800-3000 m^2/g and relativly low cost. It can be synthesized with carbonization of carbon-rich organic precursors under inert atmosphere. These precursors can be obtained from coconut shells wood, coal, and fossil

fuels, also from synthetic materials like polymers [31]. However complex and tortuous microporous structure as well as pore size distribution which is less than 2 nm do not make them ideal for an easy ion transport [12]. For aqueous electrolyts usually 3-5 nm pore size is required [12]. Most of the commercial SC devices are constructred with AC. To prepare electrode materials, AC is usally mixed with carbon black and organic binder. Most of the case, electrode prepared with AC is underused so that full capacitance is never be achieved eventhough it has very high specifif capacitance. Based on the used electrolyte, specific capacitance can reach at 300 Fg^{-1} [31].

2.2.2. **Carbon Nanotube**

CNT became a very popular electrode active materials because of its well defined porosity, chemical and mechanical stability, high surface area (bigger than $1600m^2g^{-1}$ for single wall CNT (SWCNT) and bigger than $430m^2g^{-1}$) and more importantly its high conductivity (~$5000Scm^{-1}$) [7, 8, 11, 12, 34, 36]. However, it has hydrophobic property so its specific capacitance is in the range of $20Fg^{-1}$ to $80Fg^{-1}$ [2, 37]. The specific capacitance can be increased to the high values like 130 Fg^{-1} while creating functional groups with oxidative processes [31].

The electrochemical performance of CNT depends on the some factors such as CNT orientation and dispersion, contact between electrodes and current collectors, and fabrication process which directly affect the conductivity and pore size. Vertically aligned carbon nanotube (VA-CNT) and entangled carbon nanotube (EN-CNT) are two different forms of CNTs and have been used as electrode materials in supercapacitor applications [17-21]. The main difference between VA-CNT and AC or EN-CNT is shown in Figure 2.4 schematically [13]. AC and EN-CNT have tortuous ion pathways and requires binder to prepare electrode material, however preparation of VA-CNT electrode does not need binder and has well ordered ion pathway [23-25]. EN-CNT electrode is prepared from carbon nanotubes but it has randomly oriented CNT different than VA-CNT. EN-CNT has similarity to the AC in terms of tortous ion pathway, meanwile according to recent studies, preparation of EN-CNT electrodes does not require any binder and filler if the CNT disperse and dry well enough [18, 38-40]. Ion pathway signifacantly affects the electric resistance and the ion transport [13, 22, 23]. The problem in binders is that they are insulator which increases the internal resistance and also add impurities which can degrade the performance of the SCs [12]. The dispersion process is also important because it can

decrease the effective surface area because of the formation of entangled and unpercolated CNT [12]. VA-CNT have high number of mesopores (2-5nm) and more accessible surface area [12].

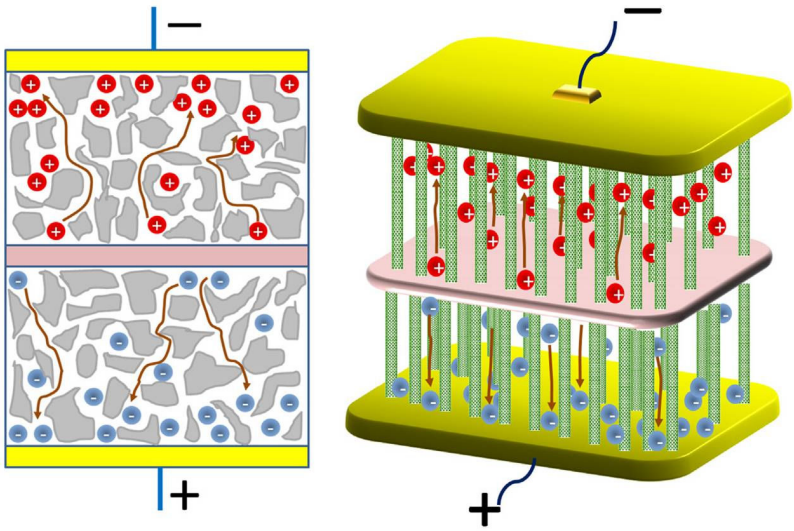

Figure 2.4.Illustration of ion pathways in EN-CNT and VA-CNT electrodes [13]

2.2.3. **Conducting Polymer**

Conducting polymers (CP) are commonly known as “synthetic metals” and composed of pi-conjugation which is alternating single and double bound along the polymer chains [41]. There are three types of CP; electron-conducing polymers, proton conducting polymers and ion-conducting polymers. Each of them has a wide application area from smart windows to energy storage and conversion.

In the case of electron-conducting polymers electrons can move freely along the polymer chain due to the partially filled molecular orbitals [41]. Electronic conductivity of CP could be altered with doping process which is the partially oxidation and reduction of the chain. Chemical and electrochemical methods are used for the doping process. The well known electron-conducting polymers used in SC applications are polypyrrol (PPy), polyaniline (PANi), polythiophene (PTh) and the derivatives of these polymers [4]. CP can be negatively or positively charged based on the doping process. Positively charged polymers such as PANi and PPy are called as p-doped and negatively charged polymers such as PTh are called as n-doped.

In SC applications, PANi is considered to be one of the most promising material due to its high conductivity and high capacity for energy storage because of multiple redox reactions

during charge/discharge process as well as low cost when it is compared with other conducting polymers [42]. It has high theoretical capacity of 500-2200 Fg^{-1} [43]. Beside it is cheap and very stable material. When the PANi is used in SC applications, it requires proton to charge and discharge properly, therefore, a protic solvent, an acidic solution or a protic ionic liquid is used as an electrolyte material [4].

Chemical ctructure of PANi is determined with redox state and doping level and mainly has three distinguishable states. Figure 2.5 shows the general chemical structure of PANi and the repeating units [44]. When the x is 1, PANi will be in the leucoemeraldine state (fully reduced), if it is 0.5, PANi will be in emeraldine state (half oxidized) and if it is 0, it will be in pernigraniline state (fully oxidized).

In the acidic environment, the imine group in oxidized repeating unit is protonated and radical cations are generated. Unprotonated PANi is called as base and protonated one is called as salt. Figure 2.6 shows the base and salt form of three different states of PANi [44]. These states have also different colors and based on the colors one can guess whether PANi is conductive or not. The main source of conduction in PANi is the delocolized positively charged free radicals so to increase the conductivity, radical cations should be maximized in polymer chains [44]. Based on these informations we can say that the only conductive form of PANi is emeraldine state. In addition to this, conductive form of PANi has green color and non-conductive form has blue color. The conductivity of the PANi changes with the pH level of the electrolyte. Figure 2.7 shows that with increasing pH level conductivity decreases [44].

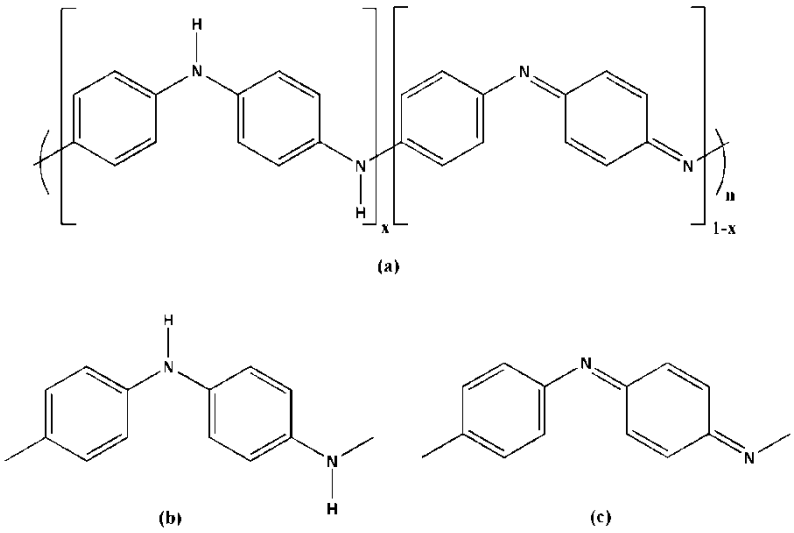

Figure 2.5. a) Chemical structure of PANi with repeating units b) reduced repeating unit c) oxidized repeating unit [43]

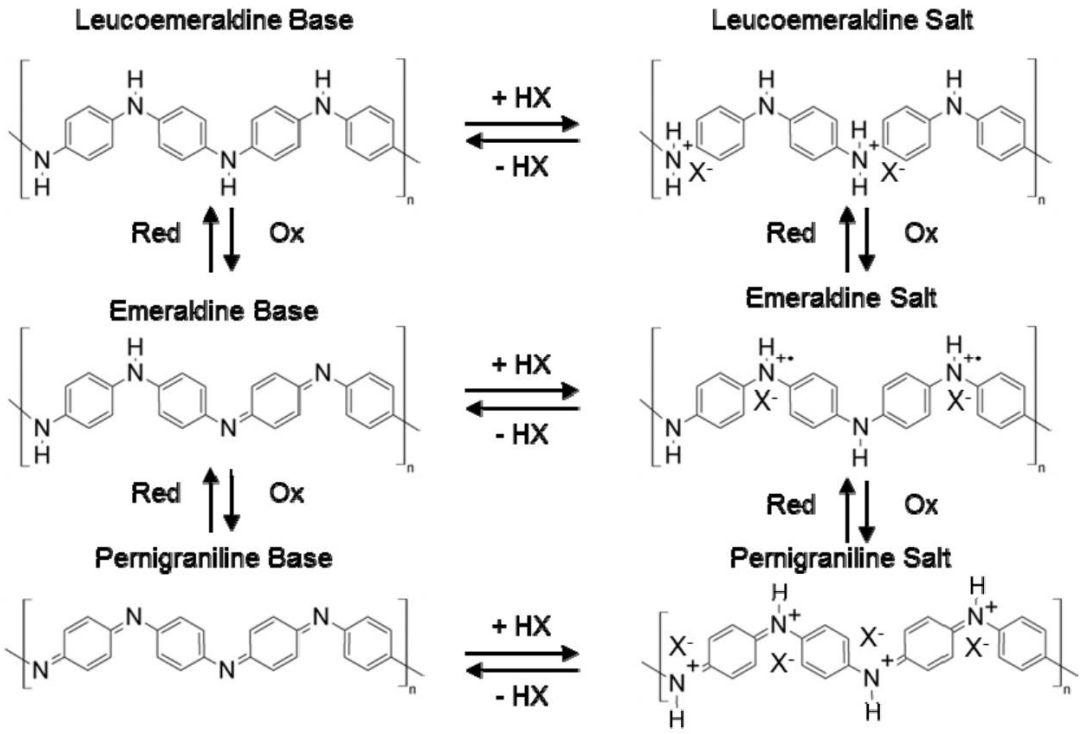

Figure 2.6. Protonated and unprotonated form of PANi with acid [43]

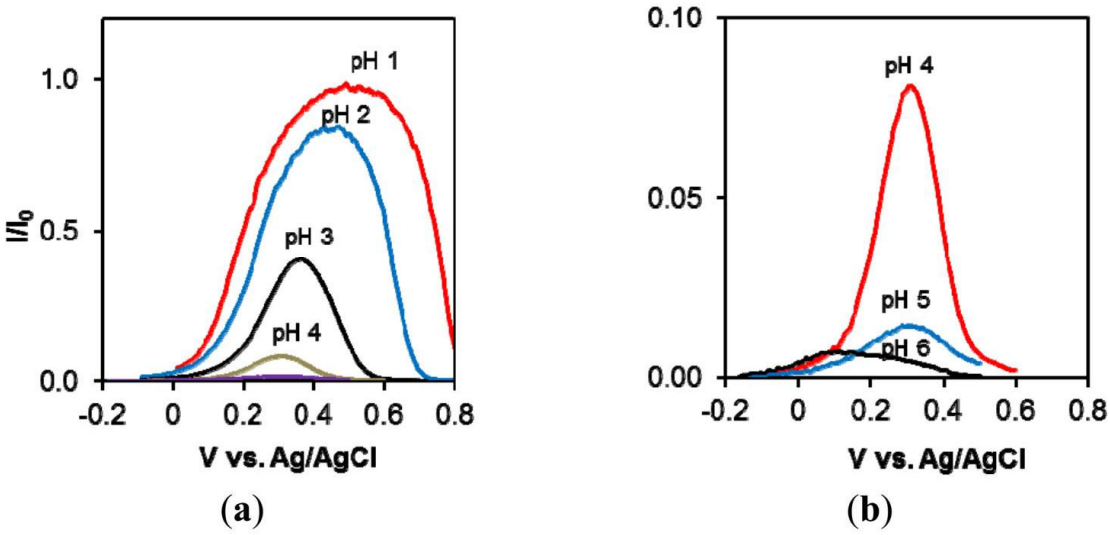

Figure 2.7. Conductance current vs potential of PANi in various pH solutions [43]

Generally conducting polymers have low cyclic stability when they are used as electrode materials in SC applications. These problems are due to the large volume of swelling and shrinking during charge and discharge and also the charge trapping in the bulk PANi chains [4, 45]. This degradation can lead to lower specific capacitance. To overcome this problem, instead of using only PANi, hybrid structure is created with carbon based

material such as CNT [4]. Here, CNT behaves like a mechanically strong substrate for PANi.

2.3. Electrolytes used in Supercapacitor Cell

The electrolyte is also another important parameter in supercapacitor cell performance because cell voltage is directly related to the electrolyte stability. The electrolyte concentration should be more than 0.2 molar to avoid the depletion problems during charging and discharging [31]. High conductivity, wide voltage window, high electrochemical stability, high ionic concentration, low solvated ionic radius, low viscosity, low volatility, low toxicity, low cost and high purity are the requirements for the electrolytes [4]. Equivalent series resistance (ESR) of the SC cell is determined with mainly conductivity of the electrolyte. There are mainly three types of electrolytes; aqueous based, organic solvent based and ionic liquids (IL).

2.3.1. **Aqueous Electrolytes**

Aqueous electrolytes limit the cell voltage up to 1.23V, which is the dissociation voltage for water and they have higher ionic conductivity, around 1 S cm^{-1} [46]. H_2SO_4, KOH and Na_2SO_4 are commonly used aqueous electrolytes. The requirement of pore size is lower for aqueous electrolytes compared to organic electrolyte due to the smaller ion size [31]. For example, HSO^-_4 has an ion size of 0.37 nm and K^+ has 0.26 nm ion size [47]. Low voltage window of aqueous electrolyte limit the energy of the SC cell however they can provide high power with low cost. The high ionic conductivity reduces the internal resistance of the cell and increases the power [47]. Also, SC cell with aqueous electrolyte can be fabricated in air atmosphere.

2.3.2. **Organic Electrolytes**

Organic electrolytes such as polypropylene (PC) and acetonitrile (ACN) limit the cell voltage upto 2.7V or higher [32]. These electrolytes are used with alkyl ammonium salts such as lithium hexafluorophosphate in polypropylene carbonate ($LiPF_6$) and tetraethylammonium tetrafluoroborate ($TEABF_4$). SC cell can have higher energy when it

is assembled with organic electrolyte because of the high voltage window. However organic electrolyte has higher resistivity than aqueous one, therefore SC has higher ESR value. This high ESR value limits the maximum power of the SC cell. For example, 1M $TEABF_4$ has an ionic conductivity of 60 $mScm^{-1}$ in ACN, whereas aorund 11 $mScm^{-1}$ in PC [47]. One of the drawbacks of the organic electrolytes is their toxiticy and intolarence to the humudity so that they require inert atmosphere.

If all parameters are taken into account, aqueous based electrolytes have more advantages than organic based electrolytes because they have high conductivity, low cost, easy handling and low resistance when compared to organic one [4, 32, 36, 46, 48-50].

2.3.3. **Ionic Liquids**

Ionic liquids (IL) are a class of organic salts and they are in liquid form at temperatures below 100^{o}C. 1-ethyl-3-methyl imidazolium tetrafluoroborate (EMI-BF_4), 1-ethyl-3-methyllimidazoliumbis (trifluoromethylsulfonyl) imide (EMIT-FSI) are well known ionic liquids. They also provide wide potential window along with non-flammability, high thermal and chemical stabilities which make them more safe than organic solvent based electrolytes [51]. IL is very resistant to the oxidation and reduction so that they can be used in very high potential range upto 4.5V, some of them can reach 6V [31].

When the ionic liquids are used with organic electrolytes such as PC and ACN, they will have a higher conductivity than pure ionic liquid [13]. The conductivity of the ionic liquids are in the range of between 0.1 and 15 $mScm^{-1}$ [47]. The cost of the IL and inert atmosphere limit the their usage in SC applications. Also their compatibility with microporous carbon is very poor.

2.4. Separator used in Supercapacitor Cell

A porous separator is used to prevent electric short cut between two electrodes. Separator should be chemically and mechanically stable and must be thin enough not to increase internal resistance of the cell [52]. Polypropylene (PP) and polyethylene (PE) seperator are mostly used in organic based electrolytes and cellulose based seperators are preferred for aqueous based electrolytes due to the easy wetting [52]. Current collectors should also be

chemically stable and its contribution to the internal resistance should not be disregarded [48, 52].

2.5. Classifications of Supercapacitor Cells

SCs can be classified into three different types depending on the charge storage mechanism as well as the active materials [35];

1. Electrochemical double-layer capacitors (EDLCs)
2. Pseudo capacitors (PCs)
3. Hybrid capacitors (HCs)

2.5.1. Electrochemical Double Layer Capacitors

EDLCs store the charge electrostatically using reversible adsorption of ions of the electrolyte on the electrode/electrolyte interface [11, 34, 53, 54]. Helmholtz described this charge separation as a double layer capacitance and the thickness of this layer is between 2^{o}A-10^{o}A. Figure 2.8 illustrates the potential drop at the electrode/electrolyte interface [48]. When the potential difference is created between electrodes, one side becomes positively charged which has a higher potential than the other side and the other side becomes negatively charged which has a lower potential than the other side. Figure 2.9 depicts the charge and discharge mechanism in EDLCs [35]. During charging of the EDLCs, positively charged electrode will attract negative ions in the electrolyte and negatively charged electrode will attract positive ions. Besides, electron will travel from negative side to the positive side. During charging/discharging, electrode surface is always electrochemically stable so that EDLCs have very high cycle life.

The equivalent circuit of EDLC is modeled with RC circuit as seen in Figure 2.10 [47]. Where, C_{-} and C_{+} are the capacitance of negative and positive electrodes and R_{f-} and R_{f+} are the faradic resistance of negative and positive electrodes. R_s is the ESR of the cell. Two main factors determine the performance of the EDLC cell, one is the active electrode material and the other one is electrolyte [47]. While active material directly defines the capacitance, electrolytes define the operational voltage.

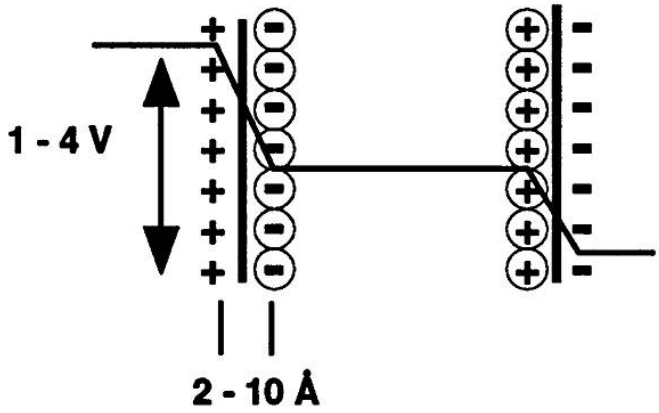

Figure 2.8. Illustration of the potential drop at the electrode/electrolyte interface [48]

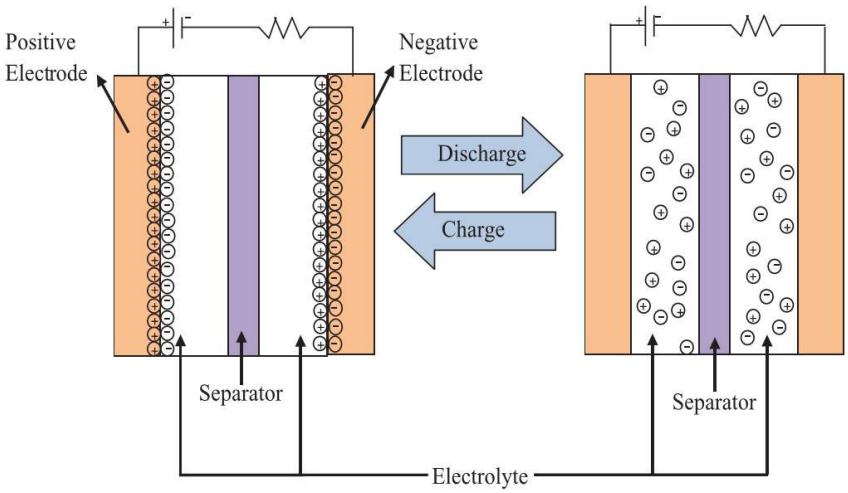

Figure 2.9. Illustration of the charging and discharging mechanism in electrochemical double layer capacitor [35]

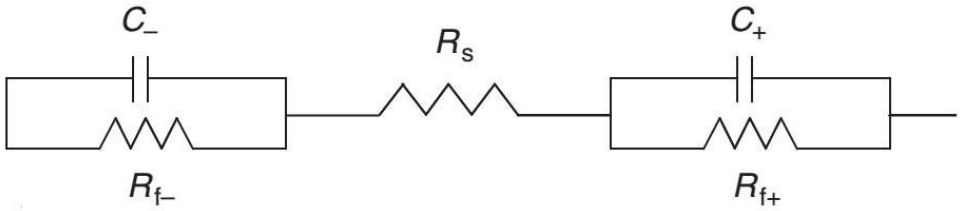

Figure 2.10. Equivalent circuit model of electrochemical double layer capacitor [47]

These factors and some additional factors influence the internal resistance (ESR) of the device and here are the summary of these factors [47]:

1. Intrinsic electronic resistance of the electrode material
2. The interfacial resistance between electrode material and current collector

3. The ionic resistance of the ions in porous structure
4. The ionic resistance of the ions passing through the seperator
5. Ionic resistance of electrolyte

The power capability of the capacitor is limited by the internal resistance of the device.

2.5.2. **Pseudo Capacitors**

Different than the EDLCs, PCs store the charge with reversible redox reactions at the electrode surface [5, 13, 34, 54]. Figure 2.11 depicts the charge and discharge mechanism in PCs [35]. Due to the these Faradic reactions, PCs generally suffer shorter cycle life than EDLCs [4]. Metal oxides such as RuO_2 and MnO_2 and conducting polymers such as polyaniline (PANi) and polypyrrole (PPy) are commonly used electrode active materials in PCs system [55-61]. Faradic reactions taking place in PCs involve electrosorption, oxidation and reductions, and also intercalaction processes [35]. SCs have high specific capacitance and specific energy density in addition to the lower specific power density than EDLCs because electrochemical proceses take place on the electrode surface and also in the bulk structure, besides faradic process is slower than non-faradic one [4]. Generally, specific capacitance of the SCs has 10-100 times more than EDLCs [62]. The main difference between EDLCs and PCs are the faradic reactions on the electrode surface. EDLCs generally show good cycling stability but low specific capacitance, whereas PCs suffer from lack of stability during cycling due to the faradic reactions but have high specific capacitance [63]. To get rid of this problem, researchers recently focus on the hybrid system of EDLCs and PCs and it is called as HCs.

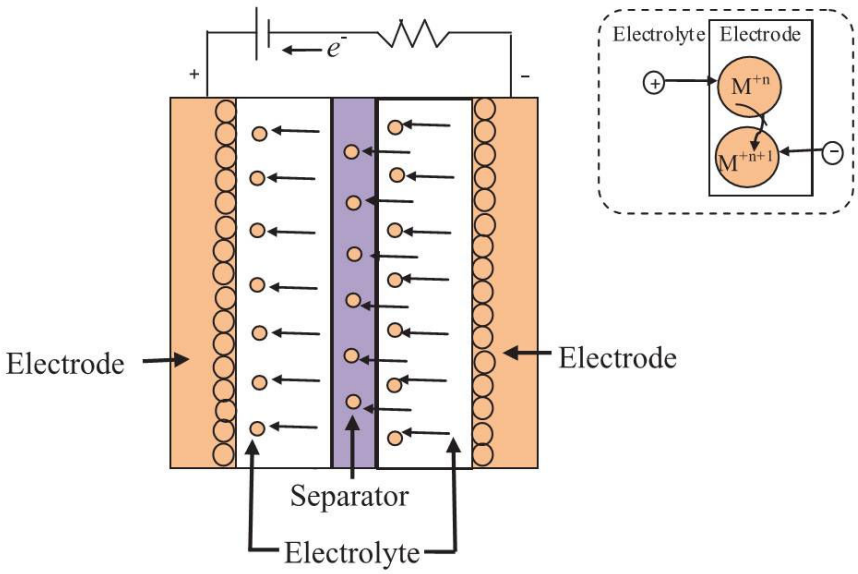

Figure 2.11. Illustration of charging and discharging mechanism in pseudocapacitor [35]

2.5.3. **Hybrid Capacitors**

In HCs system, metal-oxide or a battery like electrode (eg. conducting polymer as a energy source) and capacitor like electrode (eg. carbon nanotube as a power source) are combined together [13, 27, 64, 65]. HCs have the asymetric electrode configuration different than the EDLCs and PCs which they have the same active material as positive and negative electrodes. Generally, non-faradic active materials are used as negative electrode and faradic active materials are used as positive electrodes. During the charging process of HCs, when the voltage applied to the electrodes, negative ions will be attracted by positive electrode and oxidation will take place there. The released electrons will travel from positive electrode to the negative one and negative electrode will attract positive ions. During discharging, process will be reversed. Figure 2.12 shows the schematic of HCs [47]. To design HCs, electrode material should be choosen very carefully and some of the requirements are as follows [47]:

1. The charge/discharge rate capability of the faradic and non-faradic electrodes should be high
2. Faradic electrodes exhibit higher capacitance value than non-faradic electrodes, therefore to balance the capacitance value of the both sides thicker non-faradic electrode should be used.
3. Non-faradic electrodes should have the highest possible electronic conductivity, porosity and surface area.

Figure 2.13 compares the specific capacitance of electrode materials used in EDLCs, PCs and HCs [66]. HCs have higher specific capacitance than PCs and EDLCs so that it provides higher specific energy density than the others.

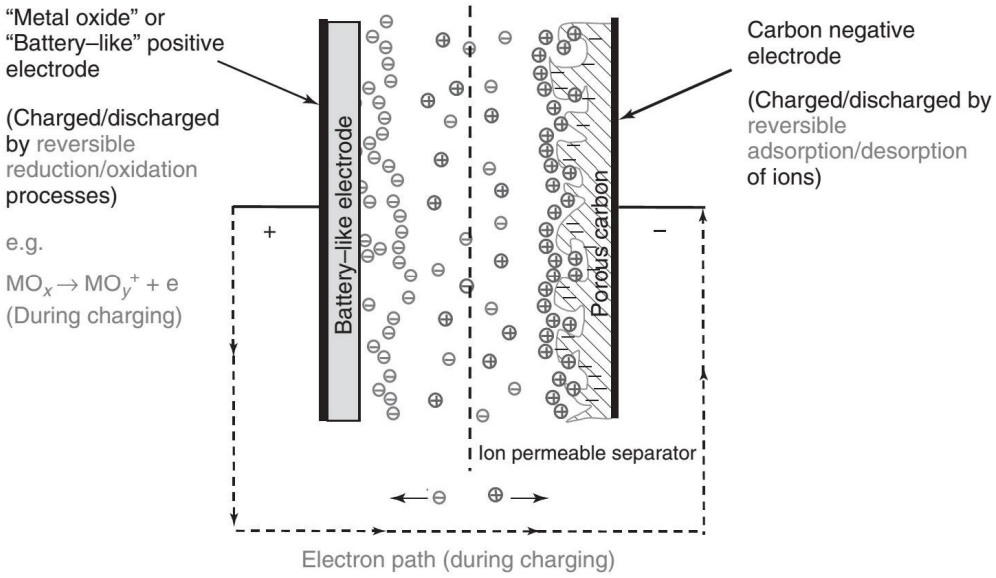

Figure 2.12. Illustration of charging and discharging mechanism in hybrid capacitor[47]

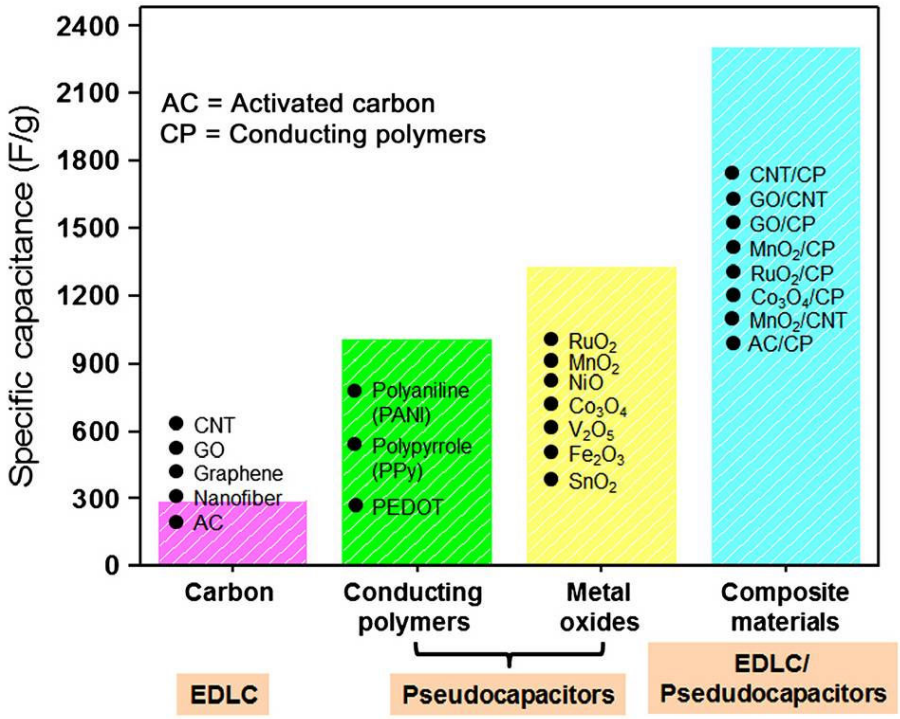

Figure 2.13. Specific capacitance values of EDLC, PC and HC [66]

2.6. Electrochemical Performance Evaluation Techniques

The electrochemical performances of the SCs are evaluated by mainly three different test methods; cyclic voltammetry (CV), electrochemical impedance spectroscopy (EIS) and galvanostatic charge/discharge (GCD) [4, 67]. Based on the experimental results from the test, the parameters such as equivalent series resistance (EIS), voltage (IR) drop, capacitance, energy and power densities, cyclic stability and time constant are evaluated [54, 68]. Cell configuration directly effects the calculated capacitance value of a supercapacitor and it is always higher when the three-electrode system is used [69]. Two electrode cell configuration provides more accurate measurement of the material performance [70].

2.6.1. Cyclic Voltammetry

CV test works based on the scanning the electrodes between two voltage limit and recording the current instantaneously [4, 67]. CV data is plotted as current vs applied potential and CV curve for an ideal EDLC is a rectangular shape [10, 17, 35, 71, 72]. This technique is very helpful to obtain fast information about electrode materials and to decide about which operating voltage should be used for the device [4]. The specific capacitances of the electrode (C_p) can be calculated by integrating area under the CV curves using the following equation [12]:

$$C_{sp}(F/g) = \frac{\int_{Vi}^{Vf} i(V)dV}{\Delta V \nu m} \qquad \text{(Eqn. 2.1)}$$

where, ϑ (V/s) is the scan rate, m(g) is the mass of a single electrode, ΔV is the voltage range and i(V) is the current response of the applied voltage. To obtain a reliable specific capacitance value from CV test, slow scan rates should be used.

2.6.2. Galvanostatic Charge Discharge

GCD test characterizes the SCs under a constant current charging/disharging up to the desired voltage limit. The test results give access to the paramaters such as capacitance, resistance and cyclability [73]. Based on the applied current, SCs will provide different

specific capacitance. Equation 2.2 is used to calculate C_{sp} from GCD test discharge curve [74].

$$C_{sp} = \frac{2I\Delta t}{\Delta V m} \qquad \text{(Eqn. 2.2)}$$

Where, I is the discharge current (A), Δt is discharge time and ΔV is potential window after the IR drop which is attributed to the internal resistance of the cell, and m is the total weight of both electrodes. The specific energy density, E_{sp}, and specific power density, P_{sp}, of the supercapacitor cell are deduced from the equations 2.3 and 2.4 [75].

$$E_{sp} = \frac{C_{sp}\Delta V^2}{7.2} \qquad \text{(Eqn.2.3)}$$

$$P_{sp} = \frac{E_{sp}}{\Delta t} \qquad \text{(Eqn. 2.4)}$$

2.6.3. **Electrochemical Impedance Spectroscopy**

Electrohemical impedance spectroscopy (EIS) is also very helpful technique to obtain information about mass transport and diffusion as well as capacitance and resistance in the electrode system. Measurements are made at the open circuit potential perturbating the system with a small AC voltage like 5 or 10 mV over a frequency regime which is usually from 1mHz to 1MHz [4, 73]. SCs behave like resistance at high frequencies and capacitive at low frequencies. In the middle freqeuncies they behave like a RC circuit [37]. Equivalent RC circuit is modeled using EIS data.

EIS data is expressed as a Nyquist plot which plots the real part of the impedance data versus imaginary part of it, also as a Bode phase plot where the frequency is ploted against the phase difference [4]. The impedance in Nyquist plot at frequencies up to 10^4 implies the conductivity of both electrode material and electrolyte, it shows charge transfer resistance which is attributed to the mass transfer of electrolyte to the porous electrodes at frequencies between 10^4Hz and 1Hz, and pure capacitive behavior shows up at frequencies less than 1Hz [4]. Electrochemical systems are more complex systems and usually resistance (R) and capacitance (C) are used for circuit components. R is identified with electrochemical processes and kinetics and C is identified with charge accumulation at the interfaces [47]. Figure 2.14 shows the Nyquist plot of an ideal EDLCs and an ideal PCs,

also equivalent circuit model of ideal EDLCs and an ideal PCs is seen in Figure 2.15 [47]. In the figures, R_s is the series resistance which is related to the electrolyte resistance, R_{ct} is the charge transfer resistance, C_{dl} is double layer capacitance and C_p is pseudocapacitance.

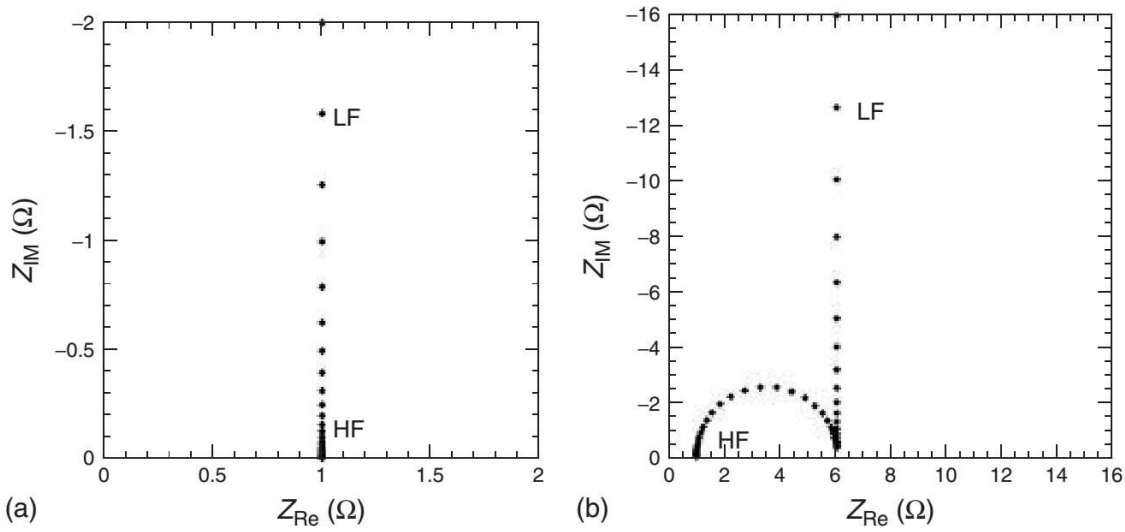

Figure 2.14. Nyquist plot of a) an ideal EDLCs b) an ideal PCs [47]

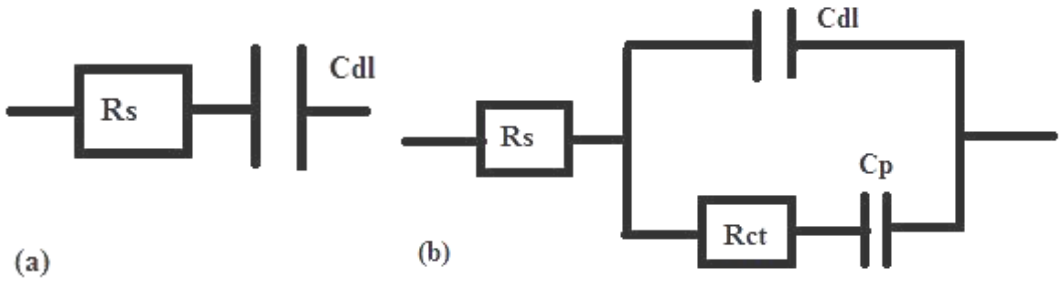

Figure 2.15. Equivalent circuit model of a) an ideal EDLCs b) an ideal PCs [47]

The transition region from the high frequency to low frequency is called Warburg region, which is observed as the result of ion penetration resistance in the electrode/electrolyte interface and the inside of porous electrode [76]. The frequency at this transition point is known as knee frequency and the value of knee frequency is the indication of how fast the system responds to the applied AC voltage [77]. In an ideal capacitor, the line in the low frequency region makes 90 degree with x-axis and this is the result of capacitive behavior of the electrode [71]. Figure 2.16 shows Nyquist plot under the restricted diffusion limitation. The Warburg region is clearly seen in Figure 2.16. Figure 2.17 represents the equivalent circuit model of diffusion limited system [47]. Capacitors do not behave ideally, therefore If one want to generalize the electrical dispersions which occurs in real electrode material, constant phase element (CPE) is used as a mathematical tool [47].

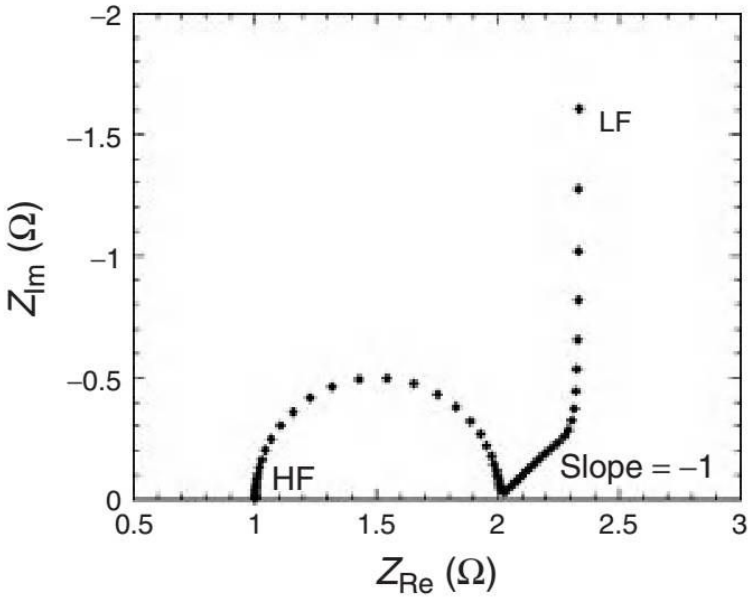

Figure 2.16. Nyquist plot under the restricted diffusion limitation [47]

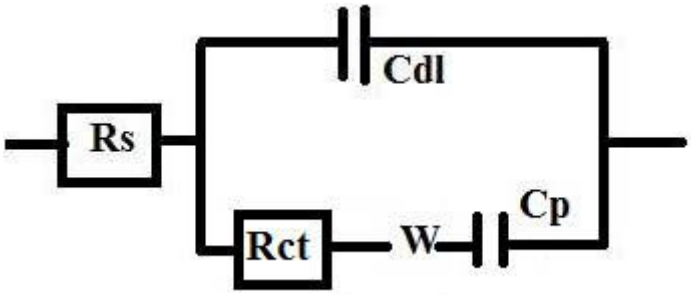

Figure 2.17. Equivalent circuit for diffuison limited systems [47]

It is expressed as,

$$Z_{CPE} = \frac{|Z|}{(jw)^{\alpha}} \qquad \text{(Eqn.2.5)}$$

where, Z_{CPE} is the equivalent impedance, w is the frequency, |Z| is the magnitude of the impedance and α is the dispersion exponent. Depending of the α value, three possible situations are given in Table 2.3. Figure 2.18 shows the Nyquist plot of CPE depending on the α value.

Table 2.3. Possible situations for impedance depending on the dispersion exponent

	α=0	**α=0.5**	**α=1**
Impedance	Resistor	Warburg	Capacitor
	$R = \|Z\|$	$W = \frac{\|Z\|}{(jw)^{0.5}}$	$C = \frac{\|Z\|}{jw}$

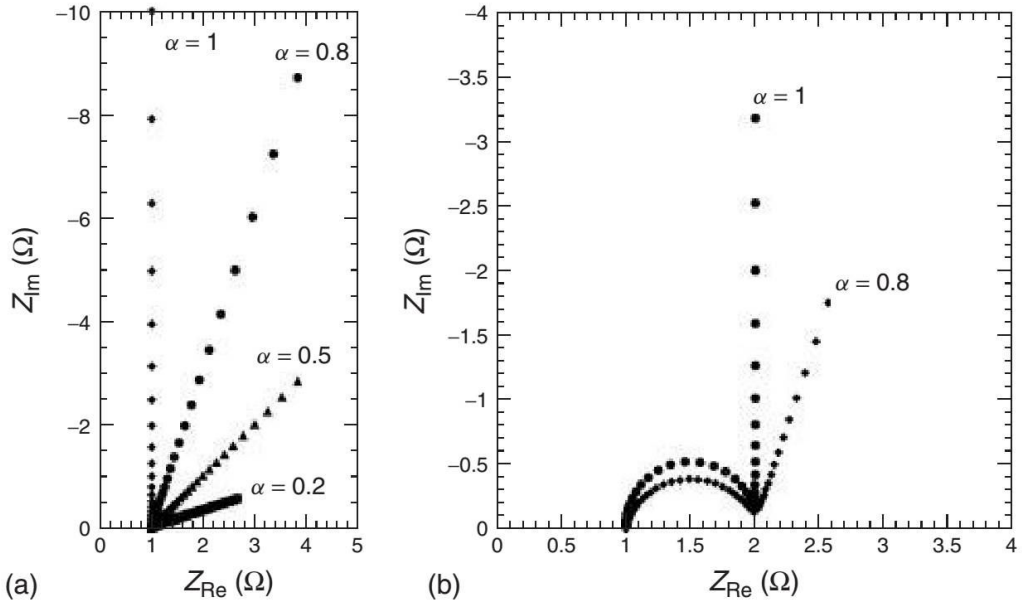

Figure 2.18. Nyquist plot of (a) a CPE for different values of α (b) pseudocapacitor including CPE [47]

A real electrode is modeled using the combination of several CPE elements seen in equation 2.6 [47],

$$Z = \frac{|Z|}{(jw)^{a_0}} + \frac{|Z|}{(jw)^{a_1}} + \frac{|Z|}{(jw)^{a_2}} \qquad \text{(Eqn. 2.6)}$$

Frequency behavior of the SC cell is also analyzed using the impedance data. Complex capacitance of the SC cell, C(f), is defined using equation 2.7 [78];

$$C(f) = C'(f) - jC''(f) \qquad \text{(Eqn. 2.7)}$$

The imaginary and real part of the complex capacitance is calculated using equation 2.8 and 2.9,

$$C'' = -\frac{Z'(f)}{2\pi f\,|Z(f)|^2} \qquad \text{(Eqn. 2.8)}$$

$$C' = \frac{Z''(f)}{2\pi f\,|Z(f)|^2} \qquad \text{(Eqn. 2.9)}$$

where, C'' is the imaginary part of the complex capacitance and C' is the real part of the complex capacitance. *Z''(f)* is imaginary part of the complex impedance and *Z'(f)* is the real part of the complex impedance. *Z(f)* is the complex impedance at frequency *f*. The value of C' at low frequency corresponds to the cell capacitance which is measured in GCD test. C'' corresponds to the energy loss in the system.

Rate capability of the SC cells can be determined from maximum point of the C'' versus frequency plot [79]. This characteristic frequency, f_o, of the cell which is also obtained at the 45 degree phase angle of the impedance [79, 80]. Time constant, τ_o, in equation 2.10 shows how fast the capacitor discharges to the half of the capacitance [81].

$$\tau_0 = \frac{1}{f_0} \qquad \text{(Eqn. 2.10)}$$

3. Experimental Procedure

3.1. Comprasion of Carbon Nanotube Growth Methods

There are several methods to sythesis CNT and arc discharge, laser ablation and chemical vapor deposition (CVD) are mainly used methods. Each of them has pros and cons. Arc discharge method is the first method used for CNT synthesis. The end product generally includes different form of carbon as well as CNT and needs purification step. Yield for this method is 30% [82]. Laser ablation gives high quality CNT and yield is 70%. Again purification step is required [82]. Both methods consume too much energy and time and also it is not easy to control the quality of end product using these two methods. CVD is one of the commonly used methods to synthesize CNT [7]. Compared with other techniques it is easy and gives user the chance to control the dimension and direction of the growth as well as obtaning high purity product [83].

3.1.1. VA-CNT Growth with Chemical Vapor Deposition

CVD is very effective technique for VA-CNT growth and requires different catalst particles (cobalt, molibdenium, iron etc), and carbon contaning gases (methane, acetilen, ethylen etc.). Process parameters such as growth temprature, used gases, and humidity directly affect the quality and morphology of the end product [83]. The growth process with CVD method involves decomposition of the carbon sources on the catalist surface at high temprature. This catalist particles act as the nucleation site for the CNT and as long as the system is feeded with carbon source, growth continues. Depends on the particle size and the growth temperature, either SWCNT or MWCNT are obtained. Low temperature which is between 600-900 ^{o}C favors MWCNT growth and high temperature which is between 900-1200 ^{o}C favors SWCNT growth, also yield is 20-100% [82].

Figure 3.1 illustrates the growth steps [84]. First step is subtrate preparation, second one is nucleation and third one is growth. In the following sections, each steps are explained in detail.

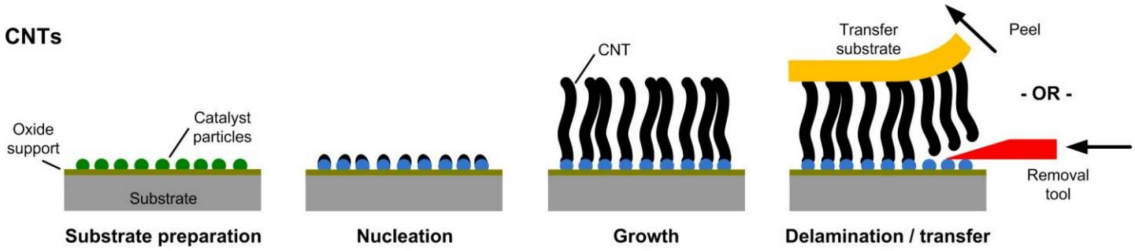

Figure 3.1. Illustration of CNT growth with chemical vapor deposition method [84]

3.1.1.1. Substrate Preparation

VA-CNT growth requires a solid substrate which is durable to the high temperature. In this study, the growth of VA-CNT was made on silicon substrate. Before the growth, silicon substrate firstly was coated with 300 nm thick silicon dioxide (SiO_2) layers via plasma enhanced chemical vapor deposition method (PECVD), which is an Oxford Instrument. SiO_2 layer prevents the silicide formation between catalyst particles and silicon wafer at elevated temperature [85]. Table 3.1 shows parameters used in fomation of SiO_2 layer:

Table 3.1. Parameters used in formation of silicon oxide layer

Parameters	Values
SiH_4	170 sccm
N_2O	710 sccm
Pressure	1000 mTorr
RF	20 W
Temperature	300^oC
Time	255 s

Secondly, 5 nm thick Alumina (Al_2O_3) and 1-3 nm iron (Fe) was coated via e-beam thermal evaporation method (TORR International, Inc) on 300 nm SiO_2 layer. Tickness of both alumina and iron are very important parameters. To ensure about the tickness of those layers, equipments should be used at low vacuum values such as 10^{-5} Torr because at high vacuum atoms ejected from iron or alumina can not trace a straight line to reach the

substrate so that the desired thickness can not be obtained [85]. In this research, evaporator chamber was left almost 3.5 hours to come down 10^{-6} Torr vacuum level. Table 3.2 presents the parameters used in e-beam evaporator:

Table 3.2. Parameters used in alumina and iron coating

Parameters	**Al_20_3**	**Fe**
Density (cm^3)	3.97	7.86
Z-ratio	0.336	0.349
Tooling factor	156	113
Rate (A^o/s)	0.2	0.1

Alumina creates a barrier layer between Fe and SiO_2 [86] and in additon to this it affects the CNT morphology, growth rate and direction [87, 88]. The thickness of Fe layer is one of the important parameters because it determines the wall number of VA-CNT [89] and inter-tube spacing between tubes so that the thickness should not be more than 5 nm [86].

3.1.1.2. Nucleation and Growth

There are many parameters which affect the CNT growth such as the amount of gases, expecially H_2 and C_2H_4, growth time and temperature, even the place of the silicon substrated in the tube [84, 90]. VA-CNT growth was carried out in a quartz tube while feeding the system with helium (He), hydrogen (H_2) and ethylen (C_2H_4) gases at 750^{o}C in furnace. Figure 3.2 presents the steps used in CNT growth.

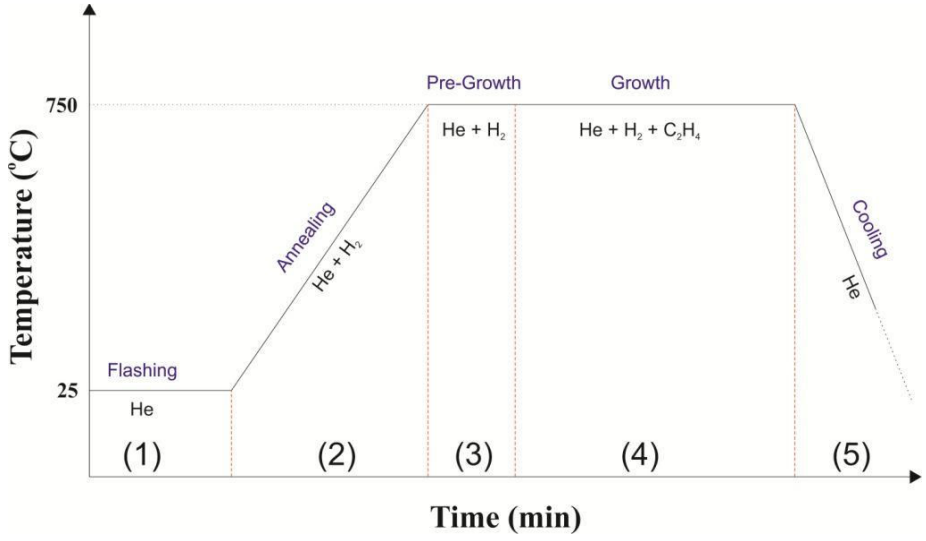

Figure 3.2. Time vs temperature steps used in CNT growth

Prior to the growth, first step is flashing the system with He gas for 5 minutes in room temprature to clean the tube and also to ensure about absence of oxygen. After that,

furnace is heated to the 750 degree in 13 minutes under He and H_2 atmosphere, which is the annealing step. Hydrogen reduce iron film to iron particle as seen SEM image in Figure 3.3. The radius of iron is directly effected by the amount of hydrogen used in annealing process [89]. System is leaved at 750 degrees for 5 minutes to stabilize the temperature of the quartz tube in pre-growth step. Growh is started feeding the system with C_2H_4, He and H_2 gases for several minutes. Last step is the cooling part. System was first cooled down 600 degrees under He atmosphere and then the lif of the furnace was opened. Then system was left to cool down to 300 degrees under He atmosphere.

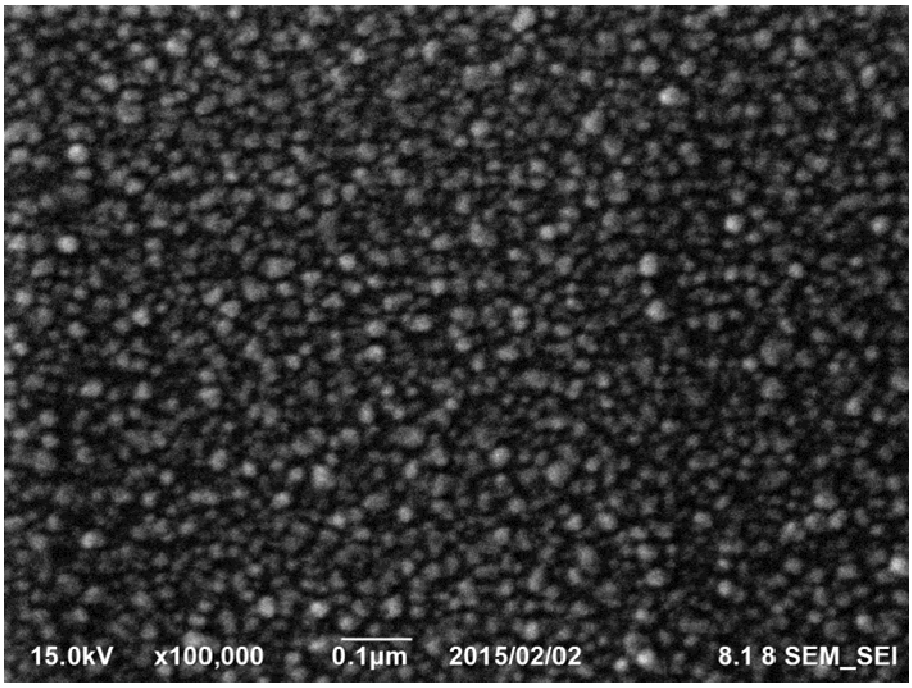

Figure 3.3. Iron nanoparticles on the silicon substrate before the growth take places

Table 3.3. Some of the paramaters used in growth of vertically aligned CNT

Growth #	**Annealing**		**Growth**		
	He	H_2	H_2	C_2H_4	He
1	350	200	150	200	250
2	350	250	150	200	250
3	350	300	150	200	250
4	350	250	200	200	250
5	300	350	250	200	200
6	300	350	275	200	150
7	300	350	300	200	0
8	300	350	350	200	0

3.2. Preparation of EN-CNT electrodes

EN-CNT is the entangled form of CNT and used as electrode material in SC. EN-CNT electrodes were prepared by releasing the VA-CNT from the substrate with a razor blade and dispersing it in ethanol using probe sonicator for 10 minutes under 10% amplitude (Q700 Sonicator). The slurry was dried on silicon wafer in a conventional oven at 80˚C for 4 hours and then removed from the surface using DI water to obtain freestanding film. Prepared EN-CNT electrodes does not consist of any binder such as PVDF or PTFE, which are insulator and increase the ESR in the electrode. EN-CNT electrode did not need binder because the length of the used VA-CNT was enough to facilitate the fabrication of flexible electrode. Figure 3.4 presents the digital image of EN-CNTs electrode.

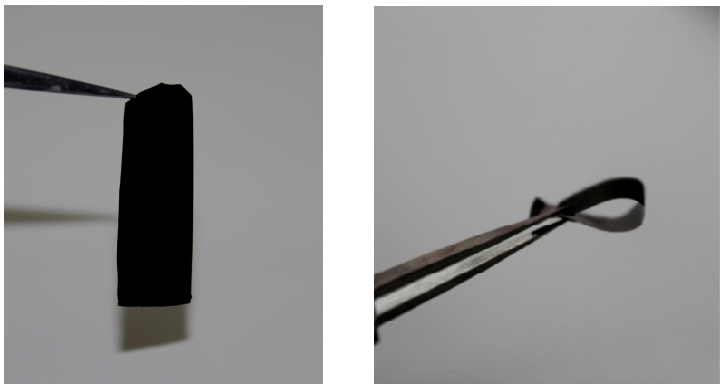

Figure 3.4. Digital image of entangled CNT electrodes

3.3. Preparation of Hybrid Electrodes

Recent studies focus on the binary and ternary hybrid electrode structures because it offers improved properties. In this study, hybrid electrodes were prepared from CNT and PANi using two types of methods; electrochemical method and chemical method.

3.3.1. Hybrid Electrode Preparation with Electrochemical Method

Electrochemical deposition was made using three terminal electrochemical cell which includes working electrode, counter electrode and reference electrode. In this system, CNT film was used as working electrode, Pt wire was used as ocunter electrode and Ag/AgCI

was used as reference electrode (Figure 3.5). Solution was prepared solving 0.1 M aniline in 1M H_2SO_4. Nickel foil with 0.5cmx0.5cm dimensions was used to ensure about the contact between CNT film and the terminal of the cell.

Figure 3.5. Digital image of three terminal electrochemical cell

Aniline monomer was polymerized on the CNT film using galvanostatic pulse deposition (RGP) method. In this method, 1 mA current was applied for 5 sn for polymerization step and then system left on the open circuit potential for 60 s (seen in Figure 3.6). These 2 steps repated 18 times so total polymerization time was 1.5 minutes. The advantage of this method is that monomer finds enough time to reach to the deeper region of the electrode materials [91].

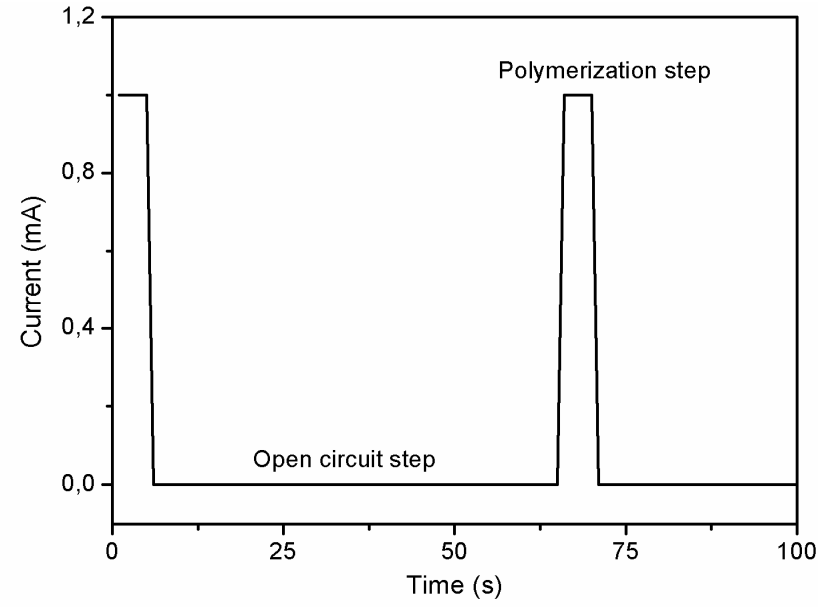

Figure 3.6. Galvonastatic pulse deposition steps

3.3.2. **Hybrid Electrode Preparation with Chemical Method**

There are two type of synthesis methods to obtaine PANi nanowires which are interfacial polymerization and rapid mixing polymerization [92]. In this study, rapid mixing polymerization method was used to prepare hybrid electrodes. Polymerization of aniline took place on the CNT film. Here are the steps; Firstly, 0.004 mol aniline was dissolved in 50 ml of 1M H_2SO_4. Secondly, 0.001 mol ammonium peroxydisulfate (APS), which is oxidant, was dissolved in another 50 ml of 1M H_2SO_4. Thirdly, CNT film was waited in the first solution for few minutes to ensure about aniline monomer was absorbed by CNT film. Finally, APS was put into the aniline and cnt film mixture and shaked very well. All mixture was put into the refrigerator for 24h. After one day polymerization, CNT film was washed and dried in 60 degree furnace.

3.4. Characterization Process of the Prepared Electrodes

Morphological characterizations of the electrodes used in SCs are usually performed with scanning electron microscopy (SEM) and transmission electron microscopy (TEM) and Raman spectroscopy is used for spectral characterization. SEM imaging provides opportunity to measure the length of the sample, to see the direction of the growth etc. TEM is very useful tool to determine the wall number of the grown CNT, radius of the tube etc. Raman spectroscopy yield information about the the quality, purity and defects in addition to the distinction between MWCNT and the other forms of CNT [93]. Thermal stability, composition of the sample and also the purity of the samples are investigated with thermal gravimetric analysis (TGA).

3.4.1. **Morphological Characterization**

Morphological characterizations of prepared electrodes were performed by SEM (FEG-SEM Leo Supra 35, Oberkochen, Germany) and TEM (JEOL JEM-ARM 200FEG UHR). SEM does not require any special specimen preparation so prepared electrodes were used directly. Secondry electron detector and in-lens detector are very common in SEM imaging. Based on the sample, any of them can be choosed and in CNT case in-lens detector is more helpful to get imaging. To accelarate the electron beam, usually 3kV was

used and working distance was kept under 6 mm. To measure the height of the synthesized VA-CNT, specimen was tilted and then imaged.

TEM imaging require special specimen preparation because electron transmit through the samples and then data is collected. TEM specimen was prepared after VA-CNT relased from silicon substrate, sonicated in ethanol for 10 minutes and collected the suspension on lacey carbon TEM grid. The problem in taking the TEM image of CNT is that nanotubes come to the top of each other so that sometimes it can not be possible to take a well clear image to obtain the information related to the wall number etc.

3.4.2. **Spectral Characterization**

Raman spectroscopy is a very effective techniques for spectral characterization of the materials. The quality of obtained CNT was analysed with Renishaw inVia Raman spectrometry with a laser with an excitation line at 532 nm, as a spectral range of 100 to 3200 cm^{-1}. The power of the laser used in Raman measurements should be chosen carefully because one can damage the sample and may not be obtain correct data. When the 5% power of the laser was used, a small hole was created in CNT surface so that in all measurements 1% power was used to ensure about not giving any damage to the sample.

3.4.3. **Thermal Characterization**

Thermal characterization was performed via Shimadzu DTG-60H differential thermal gravimetric analyser under different atmosphere. Decomposition of the materials were analyzed between 30^{o}C and 800^{o}C at a heating rate of 10^{o}C/min. Also nitrogene gas was used to create an inert or oxygen free atmosphere. Hybrid CNT/PANi electrodes were analyzed under nitrogen atmosphere between 30^{o}C and 800^{o}C at a heating rate of 10^{o}C/min. This method was used to calculate the amount of conducting polymer in hybrid structure.

3.5. Fabrication of Supercapacitor Cell

There are many test cells in the market such as split cell, swegolak cell. Based on the user wish, any of them can be used in the reseach. In this research, custom made swagelok cell

was used in all electrochemical measurements. Figure 3.7 shows the schematic of custom made swagelok cell. Symmetric and asymmetric SC cells were fabricated from VA-CNT, EN-CNT and hybrid CNT/PANi electrodes. The whole assembly was sandwiched in custom -made swagelok type test cell using platinum (Pt) foil as current collectors, Celgard PP as a separator. 1 M sulfuric acid (H_2SO_4) and 1M tetrabutylammonium tetrafluoroborate ($TBABF_4$) in acetonitrile (AN) were used as electrolytes. Here, 0.05 nm thick platinium foil was used as current collector and 0.25 nm platinium wire was used to get the data from test cell. Parstat MC multichannel potentiostat was used for the electrochemical testing. Figure 3.8 presents the cell used in the entire experiments.

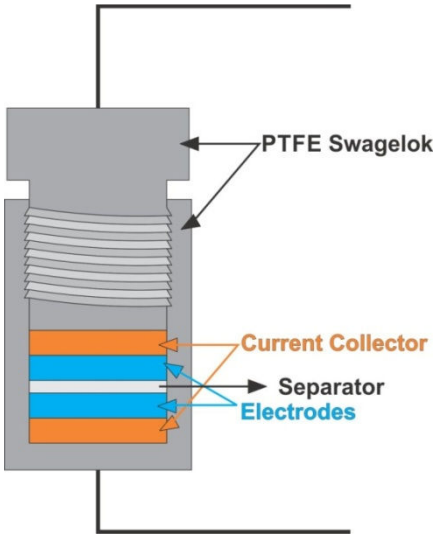

Figure 3.7. Schematic of custom made swagelok cell

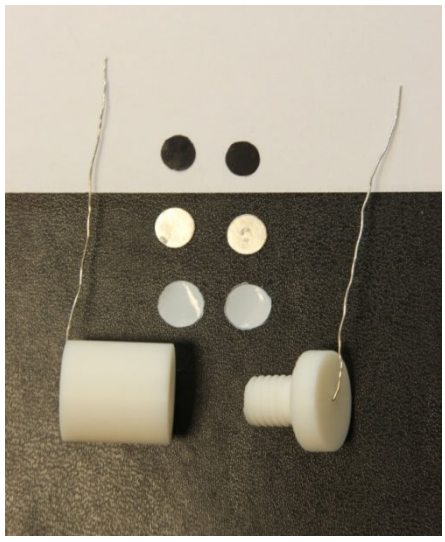

Figure 3.8. Custom made swagelok test cell used in the electrochemical tests

4. Supercapacitor Cell Assembled With VA-CNT electrodes

4.1. Characterization of VA-CNT electrodes

4.1.1. Morphological Characterization of VA-CNT Electrodes

Figure 4.1 and Figure 4.2 show the SEM images of VA-CNTs from different perspective at different magnifications. SEM image in Figure 4.1 shows that VA-CNT has ~0.4 mm length at 13 minutes growth time. Length of the VA-CNT can be changed playing with the growth time and 13 minutes growth time results in approximetly 400 micron length of end product. The image in Figure 4.2 was taken from middle part of the sample after tilted and shows the wavy character of the VA-CNT.

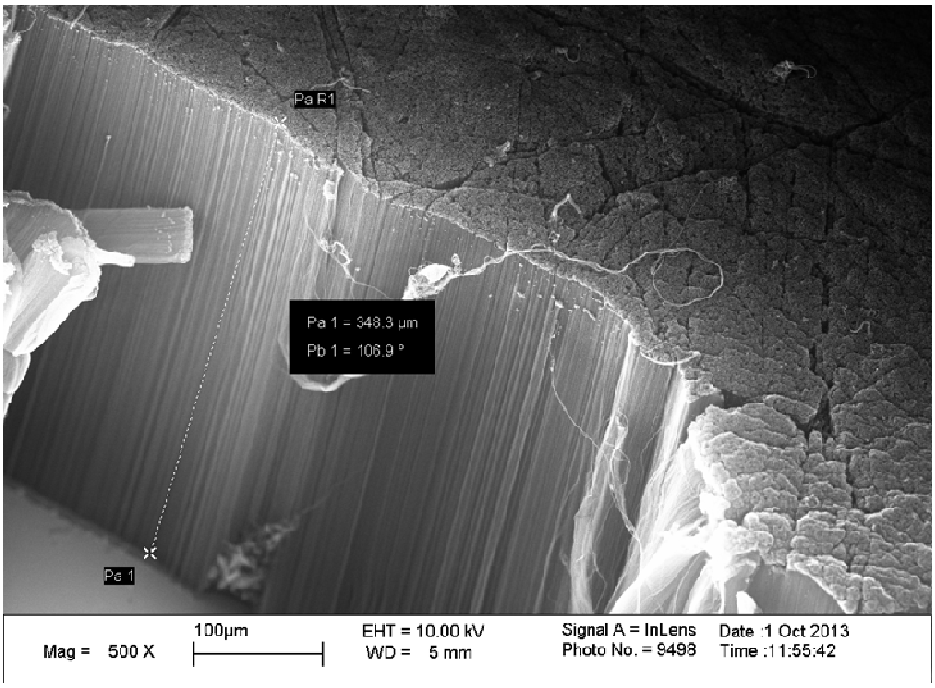

Figure 4.1. Scanning electron microscopy image of VA-CNT in low magnification

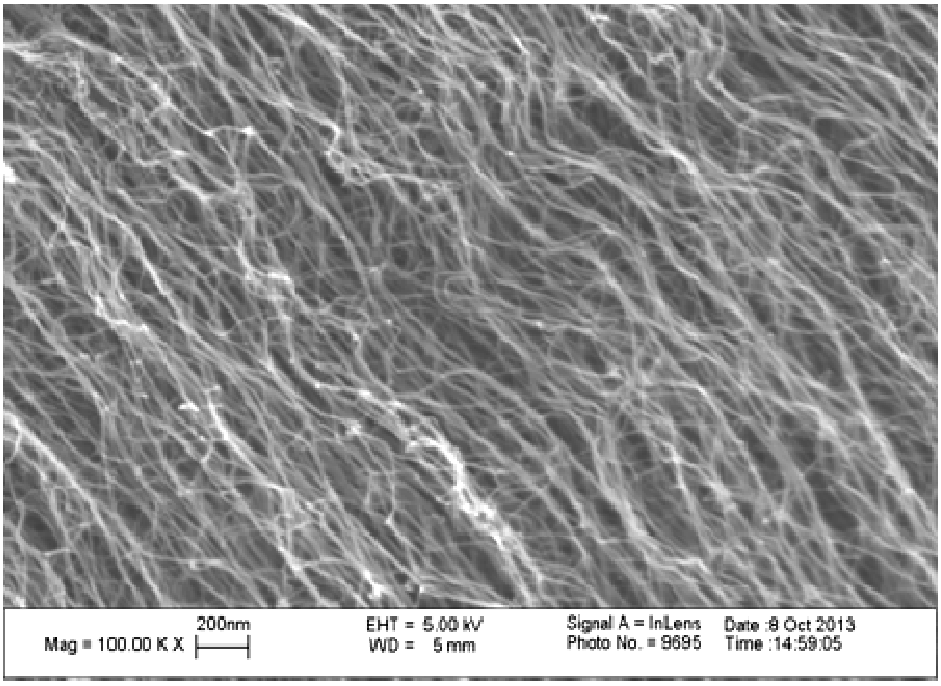

Figure 4.2. Scanning electron microscopy image of VA-CNT at high magnification

Sometimes even the same procedures are followed for the growth, instead of vertically aligned CNT, randomly growth CNT bundles are obtained as seen in Figure 4.3. Researchers in MIT explained that humidity level in quarts tube effect the iron particle size and they used atomic force microscope (AFM) to prove it [90]. According to their findings which is presented in Figure 4.4, If the quartz tube has high level of humidity like 1668 ppm, density of iron particles will not be enough to obtain oriented and densified CNT. However, in the low humidity in quartz tube, well oriented CNT can be obtained. They claim that even the zone of the silicon substrates in quartz tube is important. So substrates were always placed in quartz tube close to the exit of the gas because gases will reach certain temperature when they reach to the substrate surface.

To find out the wall number of CNT, we used TEM. Figure 4.5 shows a clear TEM image of as-grown CNT. As seen in the image, of the as-grown CNT had 2-3 wall numbers with around 8 nm in diameter. More SEM and TEM images can be seen in Appendix A.

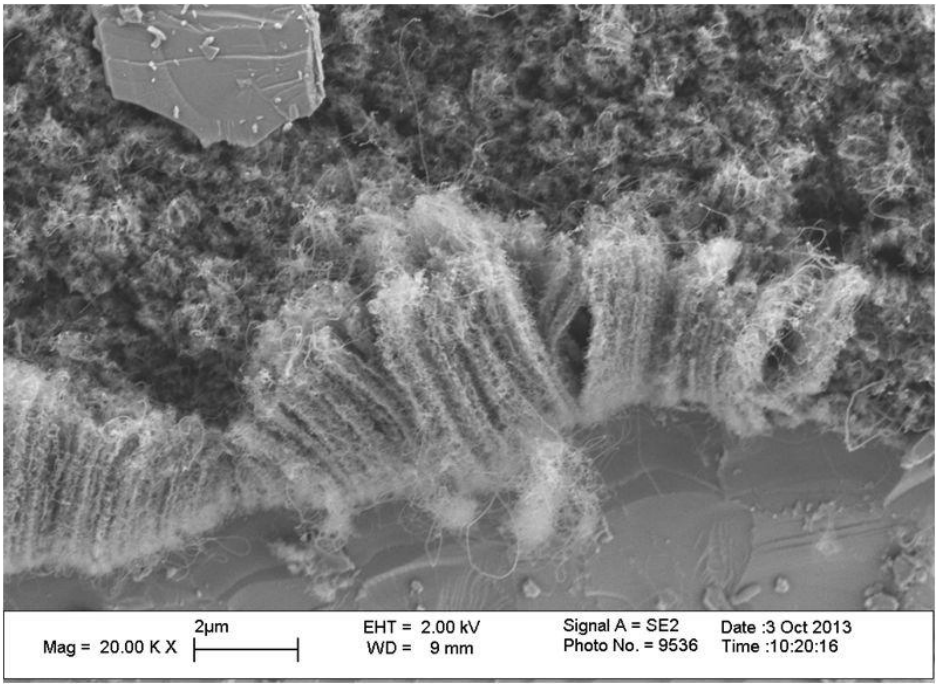

Figure 4.3. Randomly oriented CNT bundles

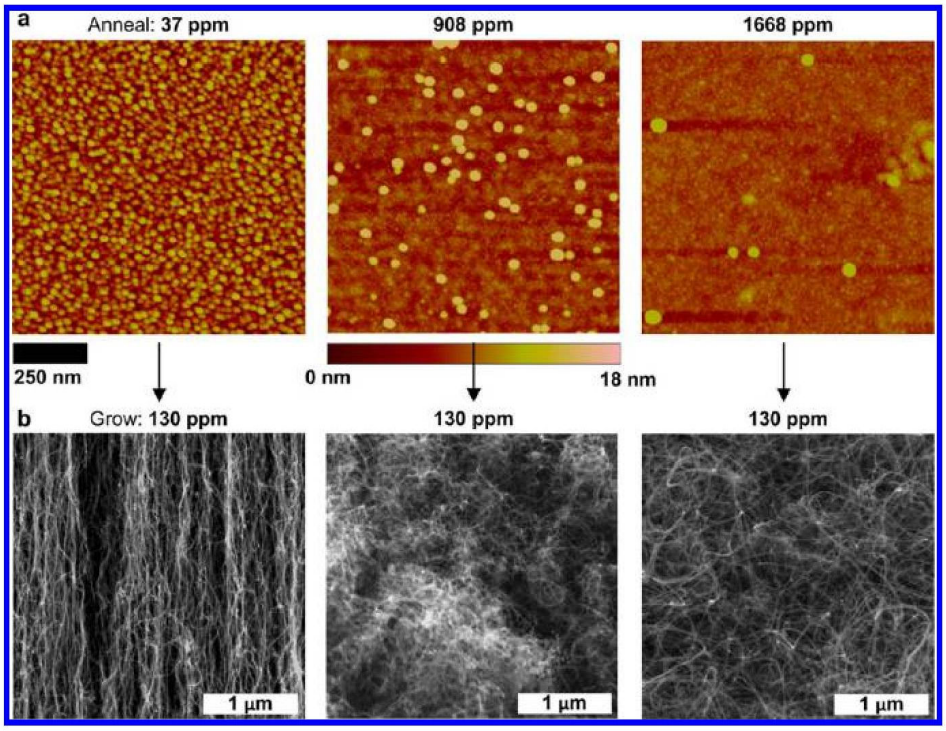

Figure 4.4. The effect of humidity on the CNT growth

.

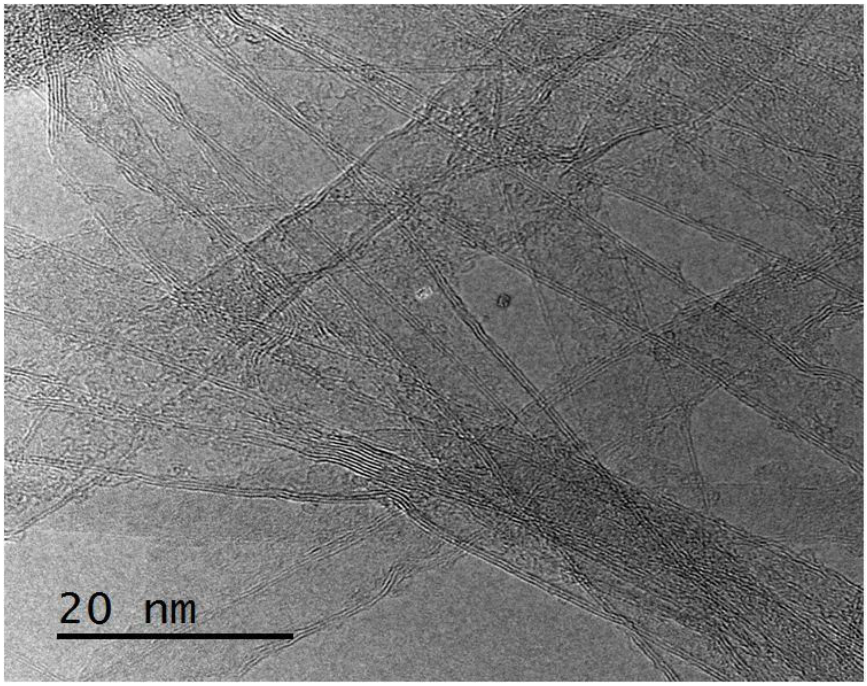

Figure 4.5. Transmission electron microscopy image of synthesized VA-CNT

4.1.2. **Spectral Characterization of VA-CNT Electrodes**

Table 4.1 gives summary of the peaks observed in Raman data of MWCNT [93]. The peak around 1350 cm^{-1} is attributed to the disorded amorph carbon not the defect, and called as D. According to the Lehman et. all paper, in carbon nanotube system defects stems from a) vacancies, b) heptagon-pentagon pairs type transformation, c) doping d) interstitials, edges and add atoms [93]. Figure 4.6 shows the type of defects in CNT system. Density of D peak increases with increasing laser energy so that generally all Raman analysis was conducted at using only 1% of laser energy. The peak around 1580 cm^{-1} corresponds to graphite mode, G, which is related to the sp^2 hybdrized carbon [94].

The peak called as G' or 2D around 2700 cm^{-1} is sensitive to the defect density and when the metallicity of the nanotube increases the intensity of this peak also increases. The last peak called as G+D is defect induced and its intensity also changes with defects. Figure 4.7 shows one of the Raman data of VA-CNT which were synthesed in the laboratory using the growth condition given in Table 3.3. I_G/I_D, which is the ratio of intensities, is generally appeared in articles, and provides information for the graphitic property of the samples. Based on the this ratio, researches decide which growth condition works well.

Table 4.1. Summary of spectral features derived from Raman spectroscopy [91]

Mode	Designation	Description
Sub 500 cm^{-1}		Presence of catalyst
Sub 500 cm^{-1}		Radial breathing modes. Evidance of MWCNTs with high-purity, low-defect material, thin innermost layers
650 cm^{-1}		Appears following intense laser irradiance
1350 cm^{-1}	D	Attributable to the presence of disordered amorphous carbon, double resonance effect in sp^2 carbon [58]. The frequency of the D band peak increase with increasing laser energy. note that this peak results from amorphous carbon, not defects, in the tube walls [59, 60]
1590 cm^{-1}	G	This band corresponds to the tangential vibrations of the grapthitic carbon atoms. In graphite, a single peak is present at 1582 cm^{-1}
1617-1625 cm^{-1}	D'	Associated with interclated graphite compounds (but not graphite), increasing disorder by functionalization and strain in the C-C bond vibrations [56]
2700 cm^{-1}	G'	The G' band is caused by two-phonon scattering around the K point of the Brillouin zone. This mode is known to be senstive to increasing defects density, but not as significantly as the first-order mode. The mode has significant contributions from regions near the K and M points, yielding peaks at approximately 2700 cm^{-1} and approximately 2730 cm^{-1} respectively [56]. The intensity of this peak depends strongly on the metalicity of the nanotube [62]
3240 cm^{-1}	G+D	Second-order mode of D': increases in intensity with increase in defects in a manner similar to the D' peak at 1617 cm^{-1} , it can be seen as part of the density of states. Defect induced [56].

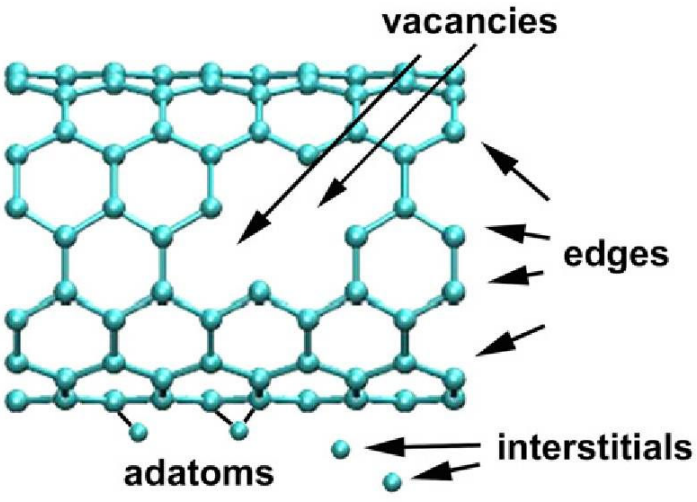

Figure 4.6. Possible defects in carbon nanotube [91]

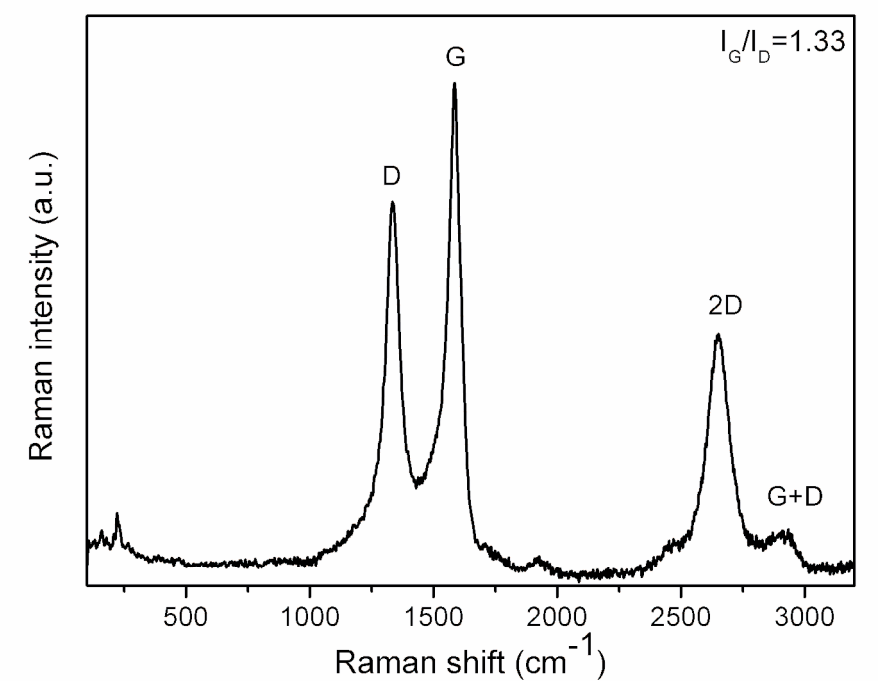

Figure 4.7. Raman spectra of the synthesized VA-CNT

4.1.3. **Thermal Characterizaiton of VA-CNT Electrodes**

TGA experiment was carried out under dry air enviroment to evaluate the thermal stability and characterize the purity of the sample. Impurities would be the other forms of carbon or other structured carbons, metal impurities and other chemical species such as nitrogen [82]. TGA is displayed in the form of the weight-loss vs temperature and one can determine the initiation temperature, oxidation temperature and residiual mass looking at the TGA graph. Inition temperature is where the material starts to decompose, and oxidation temperature is where the maximum weight loss is observed. This temperature is indentified taking the derivative of the weight loss with respect to the temperature. Residiual mass is the mass after heating process and attributed to the metal catalyst. Thermal stability of the sample is indentified with oxidation temperature. According to these informations, Initiation temperature of VA-CNT sample is 600 ^{o}C and oxidation temperature is 700 ^{o}C as seen in Figure 4.8. TGA result confirms the high purity of VA-CNT.

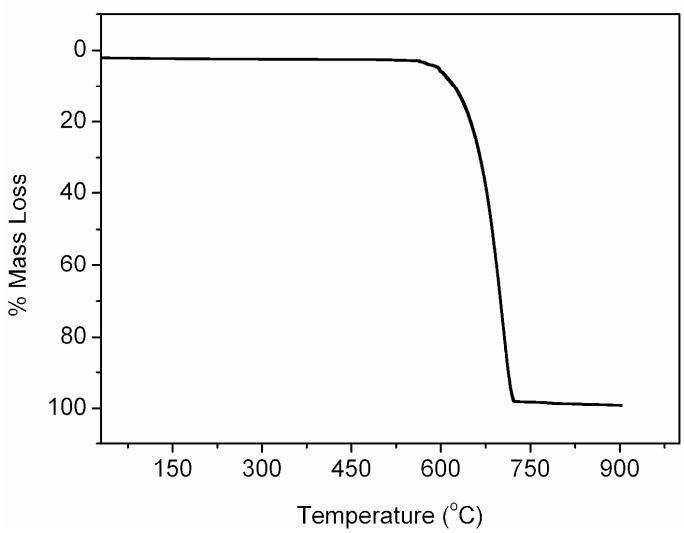

Figure 4.8. Thermogravimetric analysis of the synthesized VA-CNT

4.2. Electrochemical Performance of the Supercapacitor Cell with VA-CNT Electrodes

Figure 4.9 and Figure 4.10 show the CV curves of supercapacitor cells assembled with VA-CNT electrodes, which weight 0.22 mg in total, at different voltage scan rates with a range of 0V-1V in 1M H_2SO_4. All CV curves exhibit rectangular shape and that is very typical to supercapacitor [10, 17, 71, 72]. The curves keep their rectangular shape upto the very high scan rates so it seems that these electrodes show very good performance even at high scan rates.

SC with VA-CNT electrodes is scan rate independent because even at higher scan rates such as 2V/s rectangular shape is conserved. It is suggested that this electrode material is a good candidate for a high scan rate applications.

Galvanostatic charge/discharge (GCD) behaviours of the SC given in Figure 4.11 were tested at current densities from 0.2A/g to 1A/g between 0V and 1V in 1M H_2SO_4. SC cell with VA-CNT electrodes exhibit almost triangular shape of GCD tests without any significant voltage drop (IR drop), which also confirms capacitance of the cell being stable during charge/discharge even at 1A/g current density with 29s discharge time.

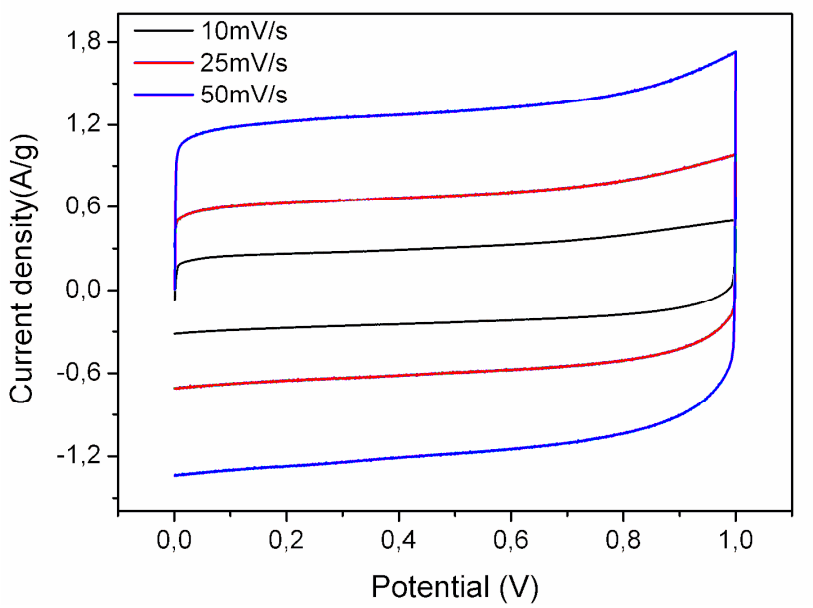

Figure 4.9. Cyclic voltammetry data of supercapacito cell with VA-CNT electrodes at low scan rates

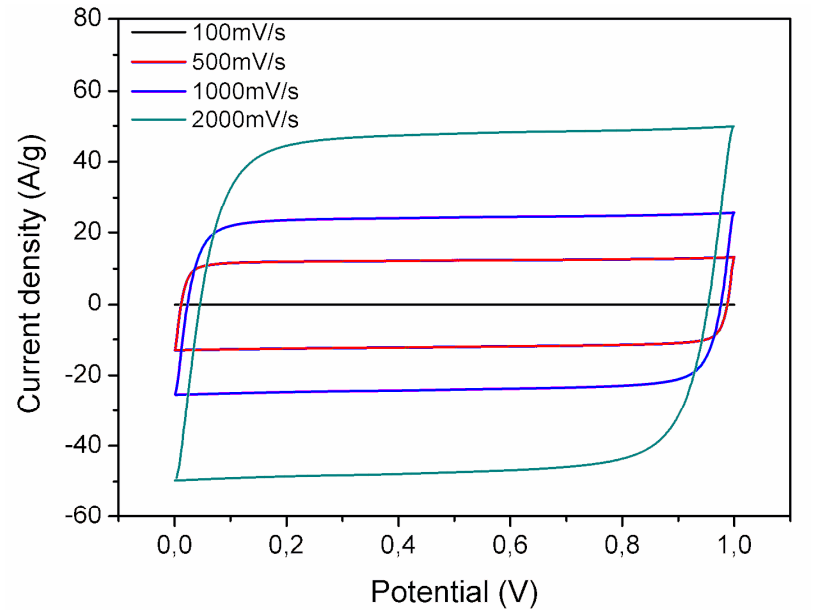

Figure 4.10. Cyclic voltammetry data of supercapacitor cell with VA-CNT electrodes at high scan rates

Stability of the device was tested up to 5000 GCD cycles at 0.3A/g current density and presented in Figure 4.12. Specific capacitance were calculated using Eqn. 2.1. Specific capacitance reaches up to the around 60F/g in the 500 cyles and but then stars to decrease up to 35F/g. Both these specific capacitances are very good values and have good agreement with literature. The increase in the 500 cycles might be explained with the wetting property of the electrode and also as more ions reach deeper surface with time at

VA-CNT electrodes. Upto the 5000 cycles, capacitance retention is 60% and this amount of decrease can be associated with the effect of the electrolyte because in electrolytes there will be insertion and desertion of H^+ and SO_4^- ions to the surface of the electrodes. During this process, H^+ ions might have effected negative electrodes.

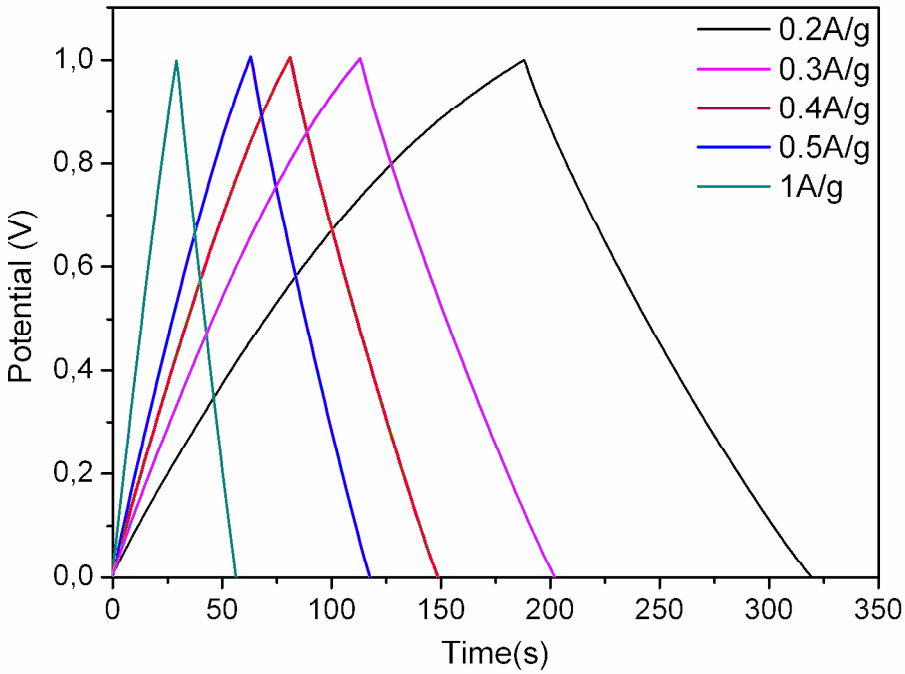

Figure 4.11. Galvanostatic charge/discharge data of supercapacitor cell with VA-CNT electrodes

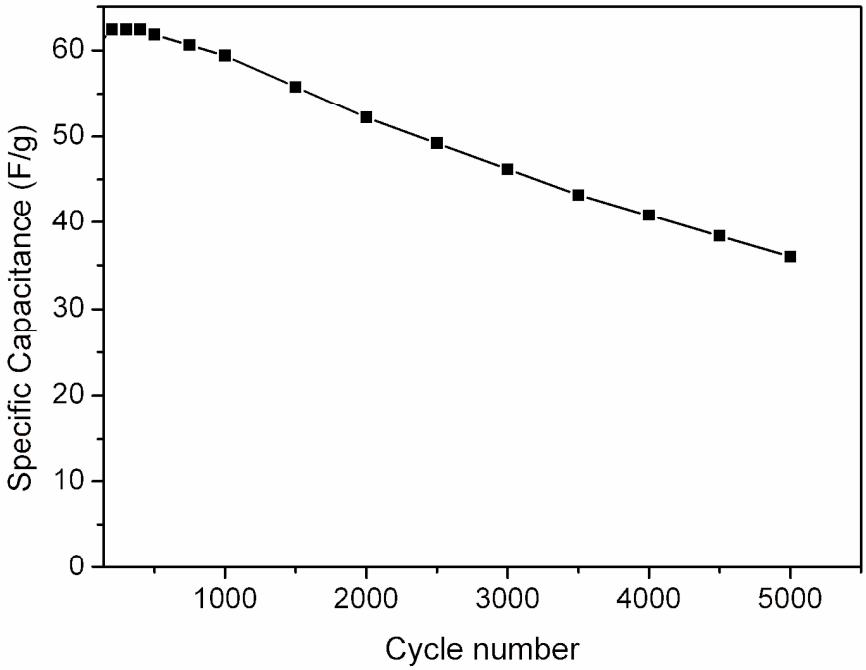

Figure 4.12. Capacitance retention of supercapacitor cell with VA-CNT electrodes

The electrochemical impedance spectroscopy (EIS) analysis was also performed in the frequency range of 100 kHz to 0.01 Hz at 10 mV AC voltage to confirm the capacitive behavior of the VA-CNTs electrodes in 1 M H_2SO_4 and the results are presented in Figure 4.13, Figure 4.14 and Figure 4.15. Figure 4.13 shows Nyquist plot before and after 5000 cycles. As seen in the graph, the radius of semi-circle increased with the repeating charge/discharge process and which can be concluded as the change in the electrode surface. Furthermore, specific capacitance values in Figure 4.15 based on the EIS are matched with the values calculated from GCD data. According to high frequency region of the Bode phase in Figure 4.14, there is a change in electrode materials before and after 5000 cycles however in low frequency region capacitive behaviour is still preserved which means that ion diffusion mechanism changed slightly with cycling process [4].

Rate capability of the SC device is also determined using Eqn. 2.7 from C_{im} data in Figure 4.15. C_{im} values were calculated using Eqn. 2.6 Actually there is not any clear change in the maxiumum point of the C_{im} data before and after 5000 cycles. Both have 0.06 s time constant and those values are very comparable with literature.

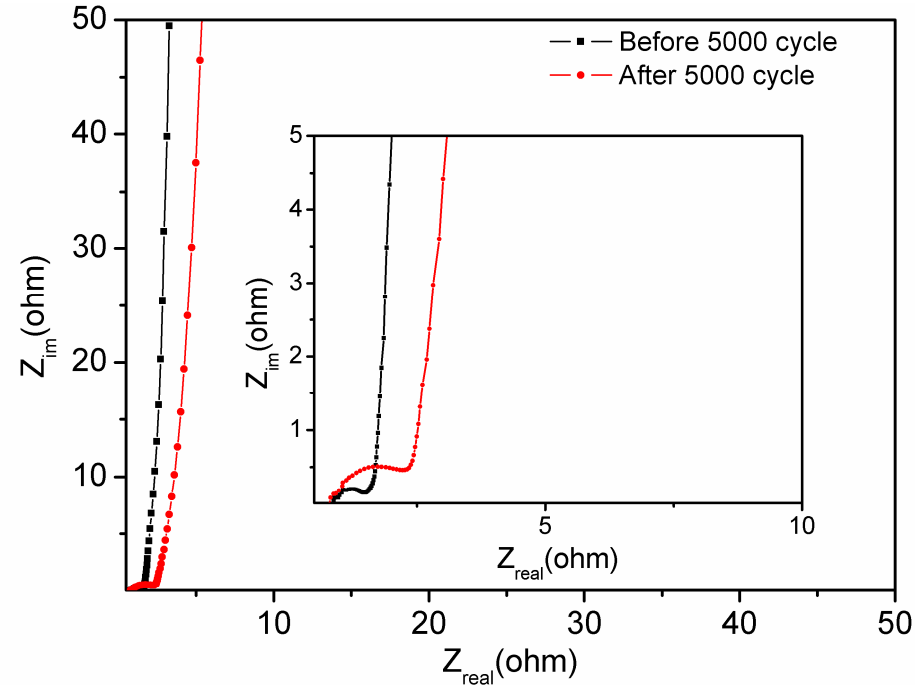

Figure 4.13. Electrochemical impedance spectra of supercapacitor cell with VA-CNT electrodes

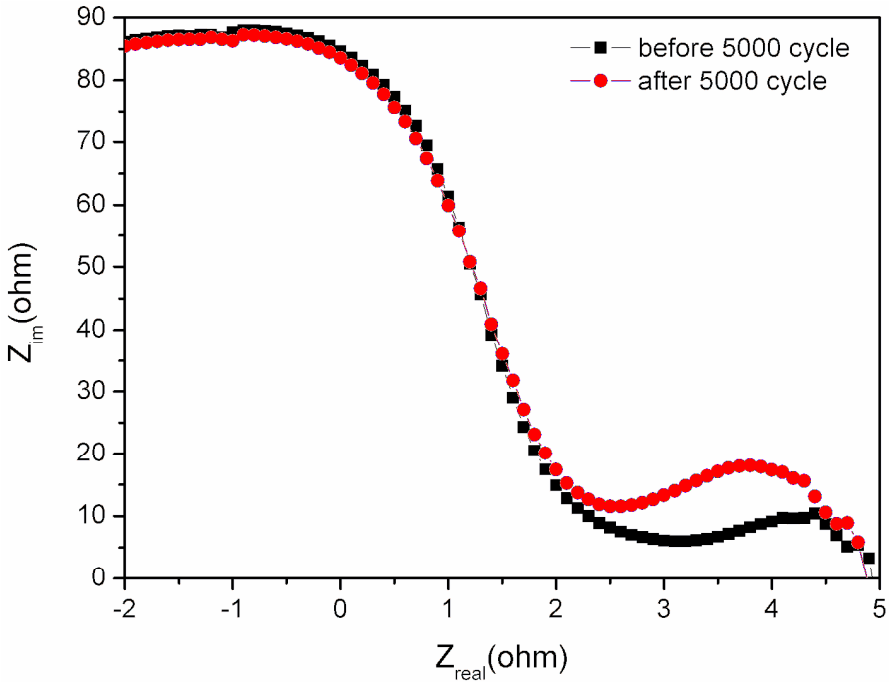

Figure 4.14. Bode phase data of supercapacitor cell with VA-CNT electrodes

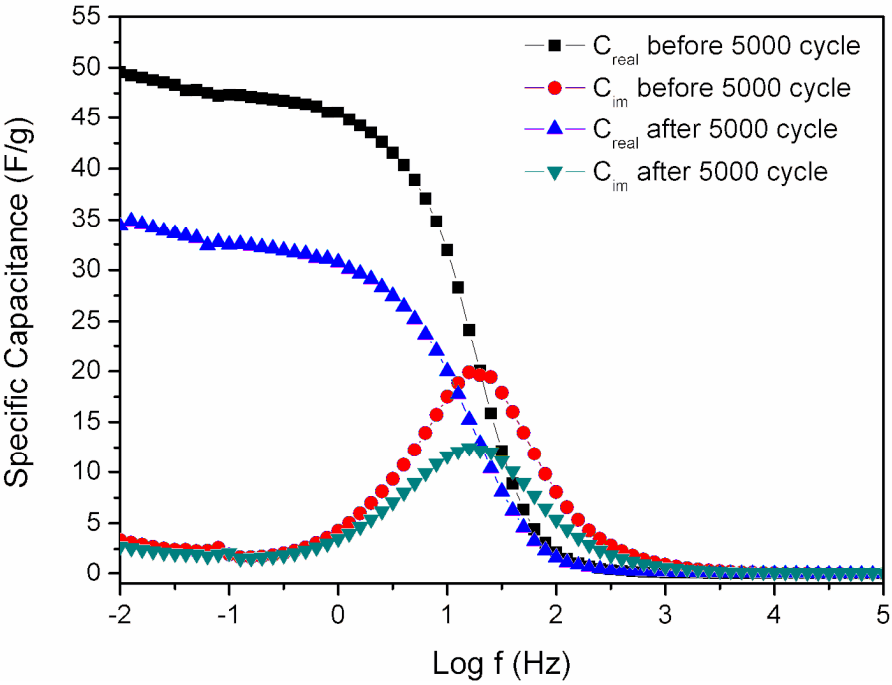

Figure 4.15. Complex capacitance data of supercapacitor cell with VA-CNT electrodes

Specific power and energy densities of SC device before and after 5000 cycles were calculated using Eqn. 2.3. and 2.4 and given in Table 4.2. Specific energy density of the

device after 5000 cycles decreases however specific power density remain stable. Figure 4.16 shows the specific energy and power densities versus cycling number. As seen in the graph, energy density decreases %36 of its begining value at the end of 5000 cycles whereas power density keeps begining value. This result is very desired for the power density required applications.

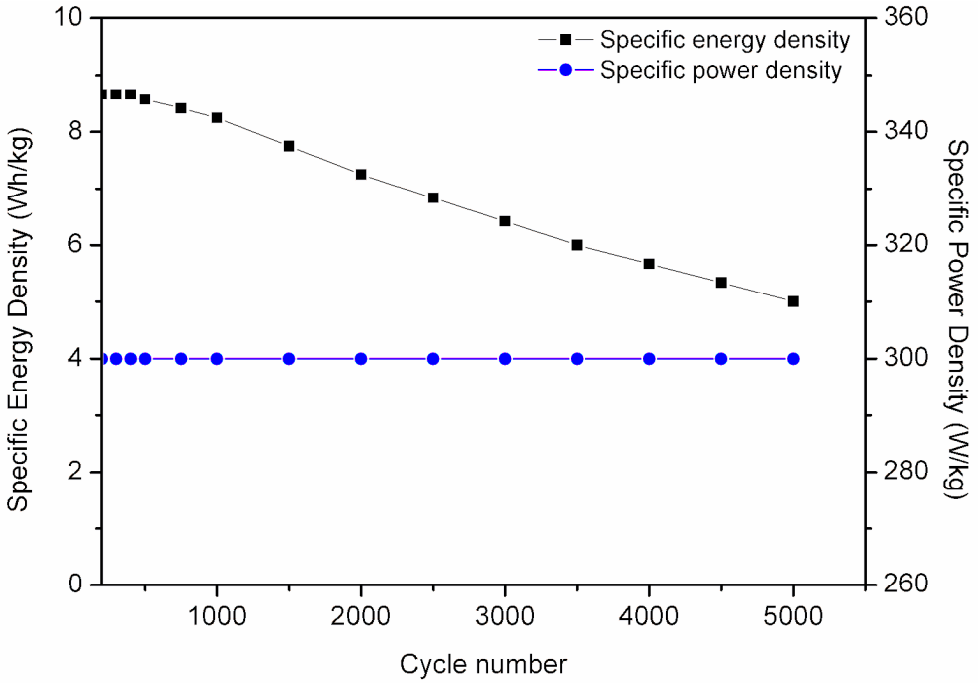

Figure 4.16. Specific energy density vs specific power density of supercapacitor cell with VA-CNT electrodes

Table 4.2. Specific energy density vs specific power density values before and after cycling test

Experiment	S.E.Density (Wh/kg)	S.P.Density (W/kg)
Before 5000 cycles	7,83	300
After 5000 cycles	5	300

5. Supercapacitor Cell Assembled With EN-CNT electrodes

5.1. Characterization of EN-CNT electrodes

5.1.1. Morphological Characterization of EN-CNT Electrodes

Morphological characterization of EN-CNT electrode is conducted with SEM and Figure 5.1 presents it. SEM image of EN-CNT film shows that there is a good adhesion between each tube so that there is no need any binder if CNTs are dispersed and dried well enough. SEM image also confirms that diffusion of the ions to the inside of the elecrolyte will be much harder in EN-CNT than VA-CNT one due to the destroyed ion path. Cross section image in Figure 5.2 shows that electrode consists of several layers. More SEM images can be seen in Appendix B.

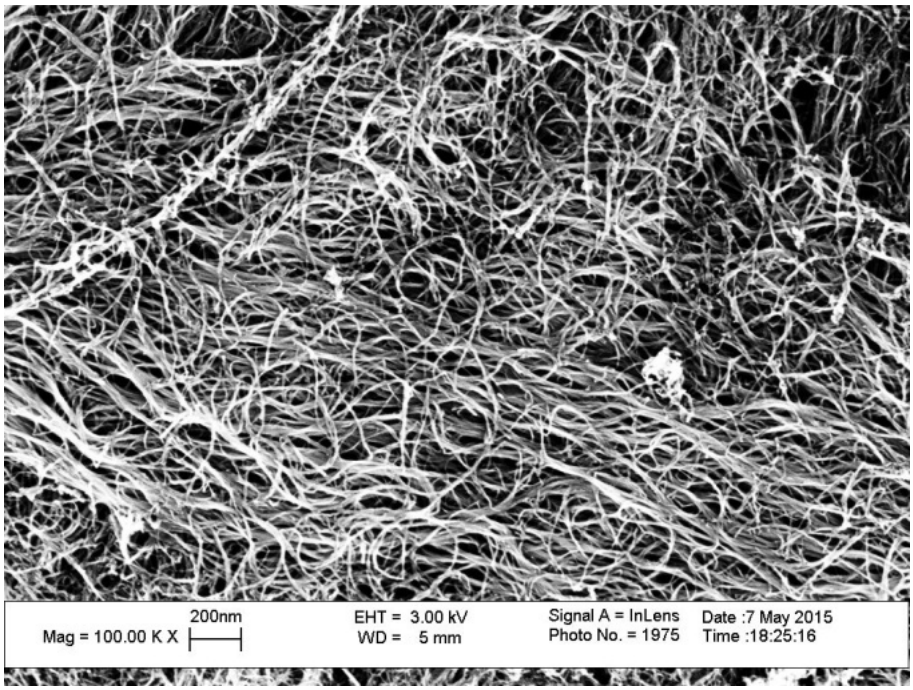

Figure 5.1. Scanning electron microscopy image of EN-CNT electrode

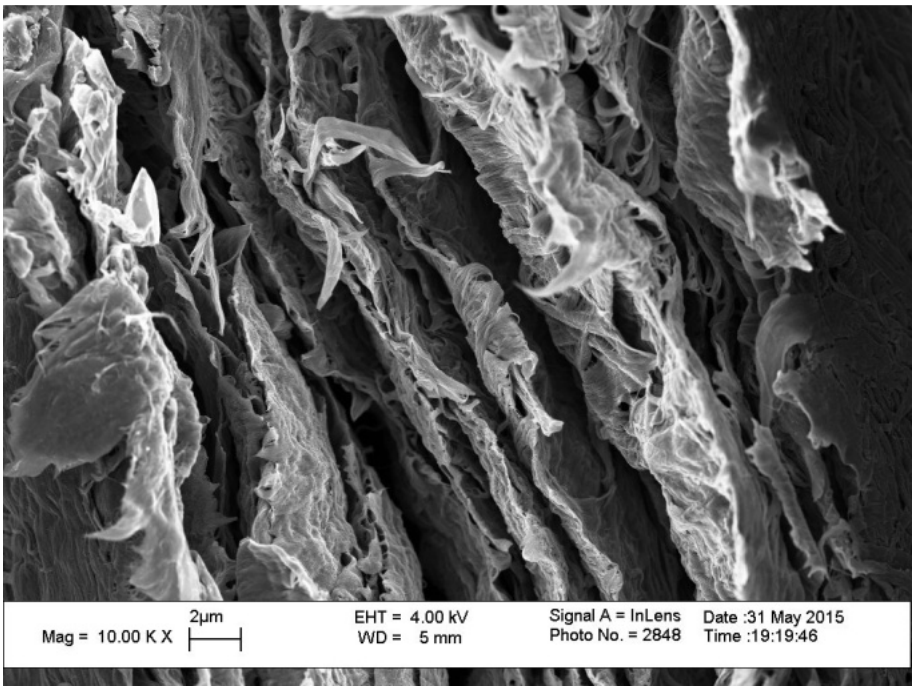

Figure 5.2. Scanning electron microscopy image of EN-CNT electrode from cross section

5.1.2. **Spectral Characterization of EN-CNT Electrodes**

Raman data (Figure 5.3) was also obtained for EN-CNT electrode. After ultrosonic dispersion of the aligned CNT, G/D ratio decreases slightly but this ratio is still acceptable.

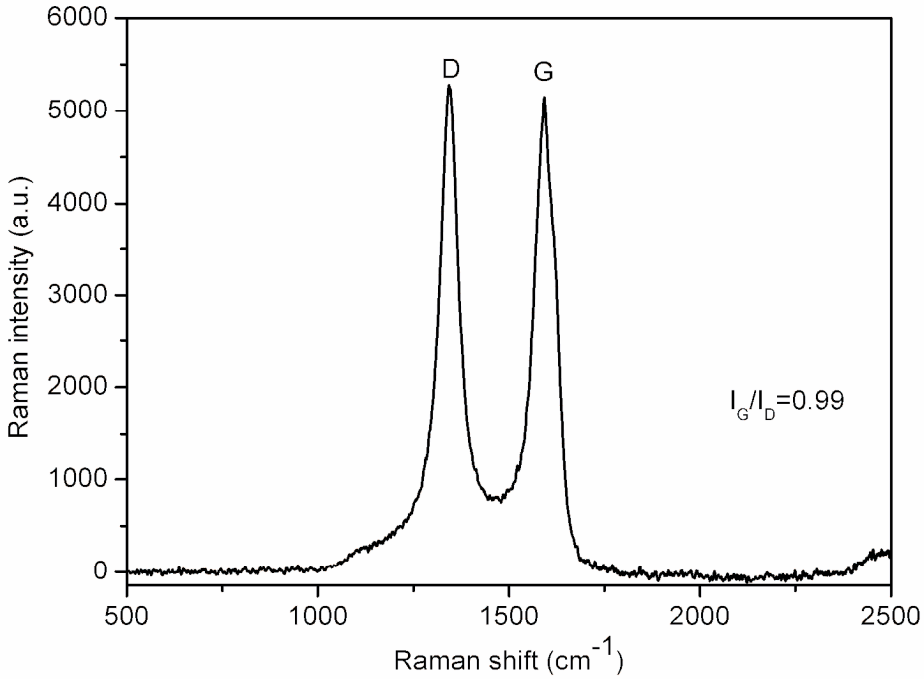

Figure 5.3. Raman spectra of EN-CNT electrode

5.1.3. **Thermal Characterizaiton of EN-CNT Electrodes**

TGA data (Figure 5.4) was also obtained for EN-CNT electrode. TGA data similar with VA-CNT one and proves that there is no trace of ethanol in electrode and purity is high.

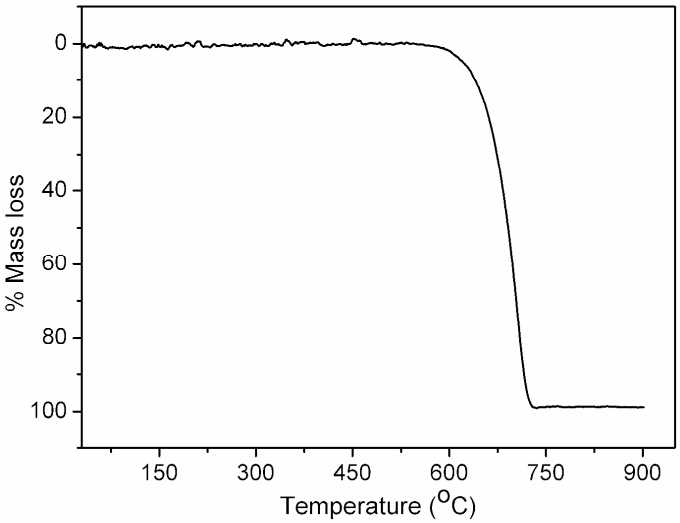

Figure 5.4. Thermo gravimetric analysis of EN-CNT electrode

5.2. Electrochemical Performance of Supercapacitor Cell with EN-CNT Electrodes

SC device assembled with EN-CNT electrodes were also electrochemically characterized in the same way with VA-CNT one. Figure 5.5 shows CV curves of SC, which weight 0.67mg in total, at different voltage scan rates with a range of 0V-1V in 1M H_2SO_4 electrolyte. As seen in the graph, CV curves show rectangular shape at slow scan rates however SC can not be able to give same respond so that rectangular shape in the curves is lost. Some works in literature also supports this result [95]. Also this was the reason not to repeat CV at high scan rates. We can conclude that SC with EN-CNT electrode is scan rate dependent. Also, the loss in rectangular shape with increasing scan rates is explained with two phenemones; one is that it can due to the electron transportation in the electrode materials and secon one is that ion absorption/desorption process at the interface of electrode/electrolyte can be limited [95].

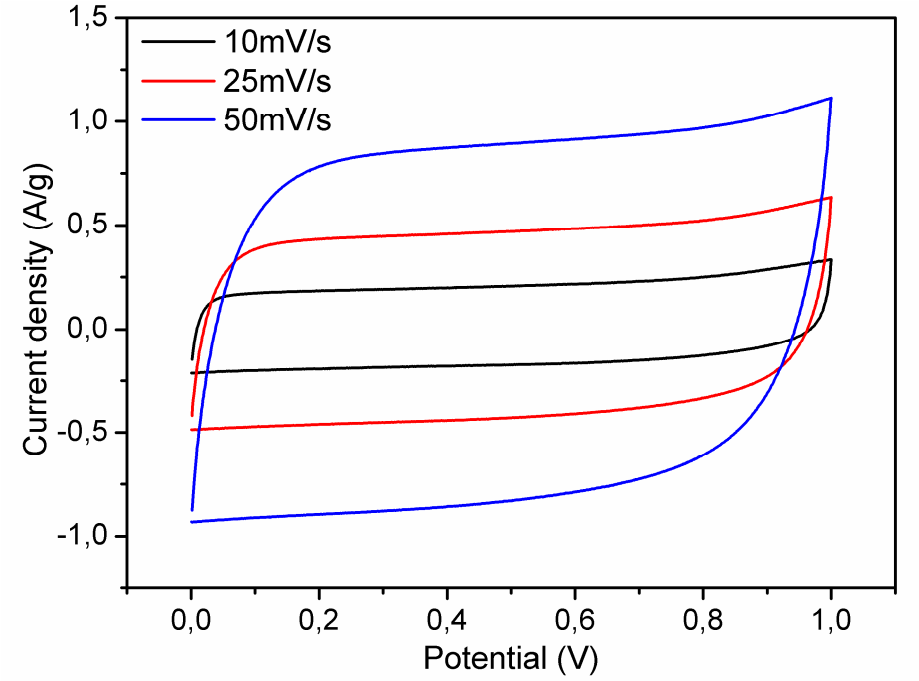

Figure 5.5. Cyclic voltammetry data of supercapacitor cell with EN-CNT electrodes at low scan rates

GCD testing presented in Figure 5.6 was also conducted at different current from 0V to 1V in 1M H_2SO_4 electrolyte. SC cell with EN-CNT electrodes from 0.1A/g to 0.5A/g showed also a typical ideal behavior analogous to VA-CNT one without any IR drop. Cycling stability was done upto 5000 cycles in 1M H_2SO_4 at 0.3A/g current density (Figure 5.7). EN-CNT electrode could not be tested for 1A/g because GCD behaviour of the electrode started to deviate ideality. Hence, It can be concluded that VA-CNT electrodes withstand to the higher current than EN-CNT one eventhough both have the same growth conditions. The specific capacitance of the SC cell calculated using Eqn. 2.2. which was around 40 F/g initially was decreased with increasing cycle number and at the end of the 5000 cycle it remained only 63% of its total specific capacitance. Specific energy and power densities of SC cell with EN-CNT electrodes calculated using Eqn. 2.3 and 2.4 were found 5.50 Wh/kg, 300 kW/kg respectively at 0.3A/g before the 5000 cycles. At the end of the 5000 cycles, specific energy density decreases to 3.42 Wh/kg and specific power density preserved the initial value. SC cell with VA-CNT electrodes had higher specific capacitance, specific power and energy density in contrast to EN-CNT electrodes.

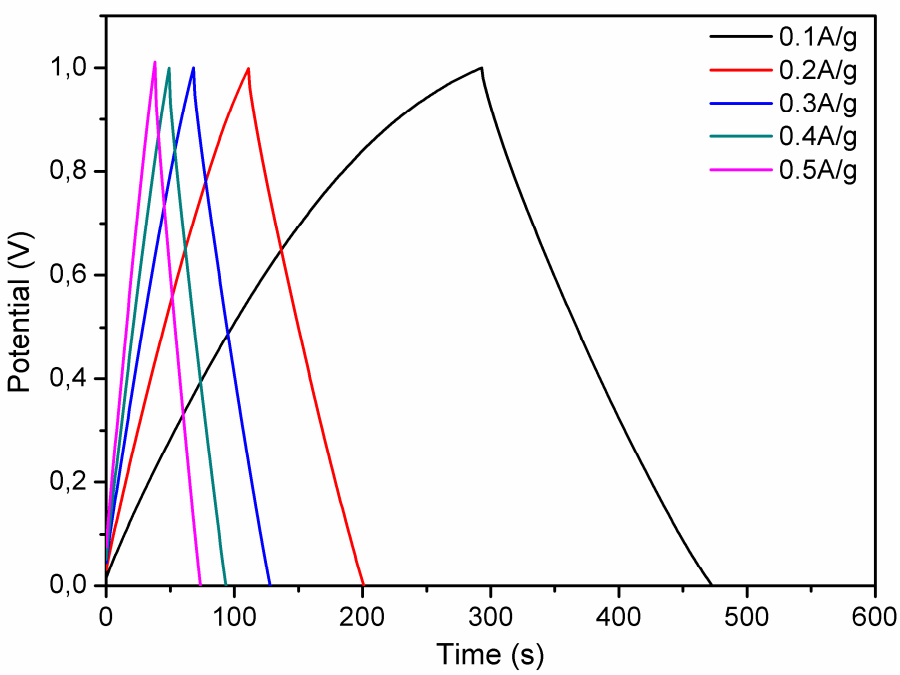

Figure 5.6. Galvanostatic charge/discharge data of supercapacitor cell with EN-CNT electrodes at different current densities

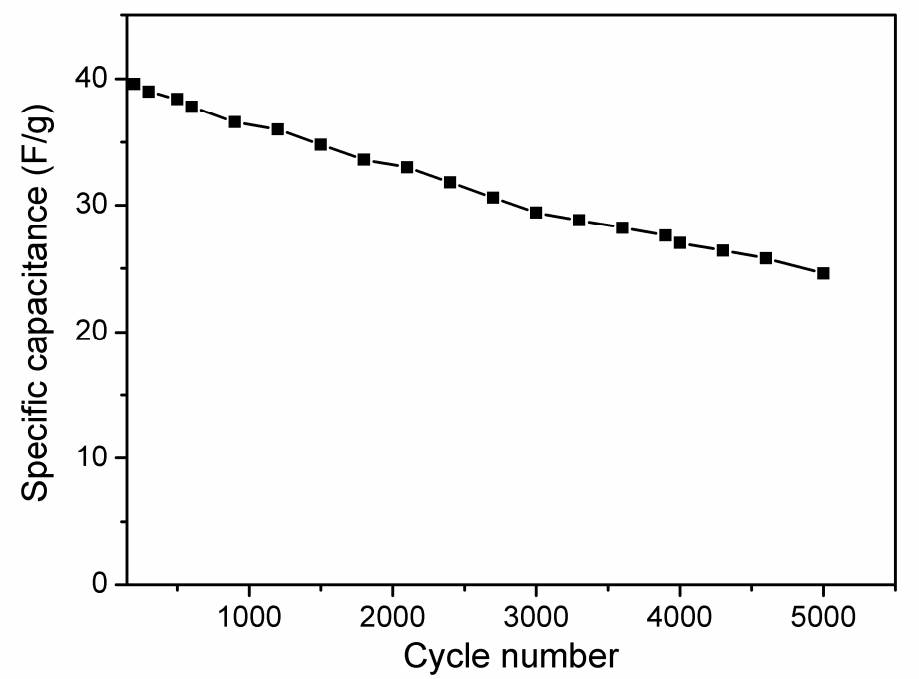

Figure 5.7. Cycling stability test for supercapacitor cell with EN-CNT electrodes

Both SC devices with VA-CNT and EN-CNT electrodes were unable to retain their capacitance retention after cycling tests in acidic aquaeous electrolyte, and subsequently raise the enquiry for this phenomenon. Some studies in literature has also similar result in

acidic electrolyte [96]. To analyze it further, the first attempt was to examine the digitial image of the EN-CNT electrodes before and after cycling test.

Two EN-CNT electrodes in the first row Figure 5.8 represents the electrodes before the electrochemical measurements, followed by the electrodes in second row in Figure 5.8 after testing verifies the change that has occured after 5000 cycles. It is apparent that the cycling test has affected negative electrode more than positive one. A physical shrinkage is evident in negative elecrode after 5000 cycles, whereas positive electrodes did not have any physical change. Carbon based materials can have functional groups such as –COOH, =CO, phenol, quinone and lactone groups depending on their preparation condition and precursors [97]. The reason behind this can be explanied in terms of insertion and deserption of the ions to the electrodes. In the SC cell, the positive electrode atracts the sulfat ions and the negative one atracts the hydrogen ions so that hydrogen ions age the negative electrode faster and a greater extent in contrary to the sulfat ions reaction to the positive electrode. The investigation of the structural change was carried out using Raman spectroscopy and Figure 5.9 presents the Raman data of electrodes before and after the cycling test. The positive electrode has almost the same G/D ratio with the fresh electrode after the cycling test, however negative electrode has totally different raman data. G/D ratio of the negative electrode is less than one after the cycling test which implies that surface defects such as vacancies, interstitials and adatoms has increased during cyling test for the negative electrode.

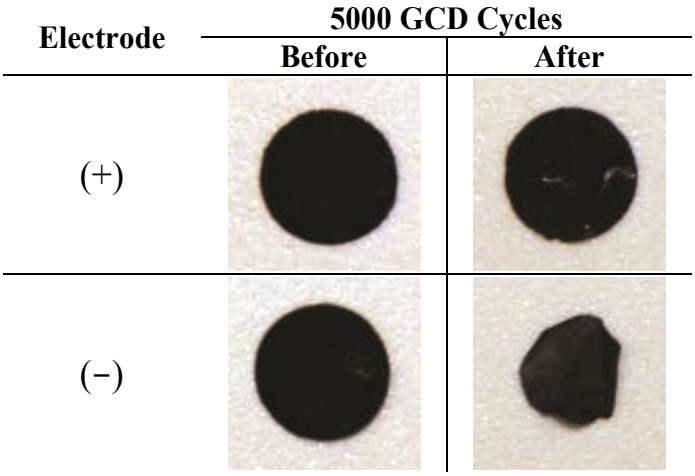

Figure 5.8. Digital image of electrodes before and after cycling test

This raman data is in close agreement with the literature [98]. Furthermore, 2D and G+D peaks have appeared for all electrodes, however intensity of G+D peak increased for

negative electrode after the cycling test. Also, this peak is also attributed to the defects [93]. This Raman data suggests the structural change in the negative electrode.

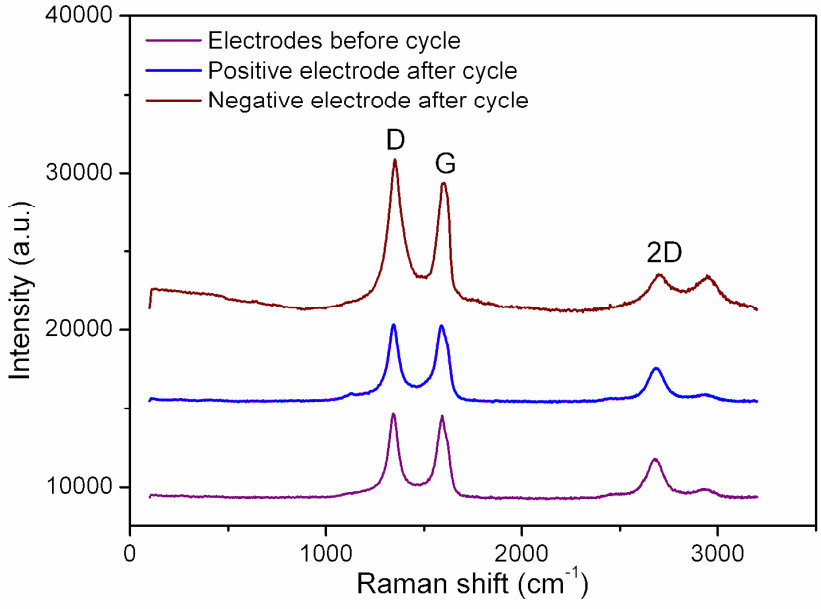

Figure 5.9. Raman spectra of supercapacitor cell before and after cycling test

Morphological characterization was conducted after cycling test and Figure 5.10 and Figure 5.11 presents the SEM results of positive and negative electrodes, respectively. There is not any clear morphological change in positive electrode when it is compared to the SEM image in Figure 5.1.

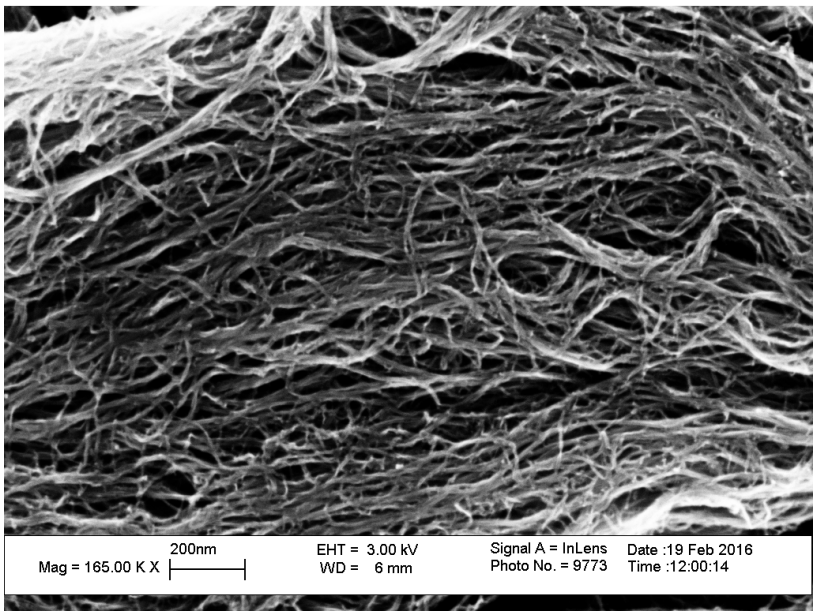

Figure 5.10. Scanning electron microscopy image of positive electrode after cycling test

However, negative electrode shows a big change in morphology as seen in SEM image. It seems that CNT electrode has agglemorated structure and it also explaines the shrinkage in electrode.

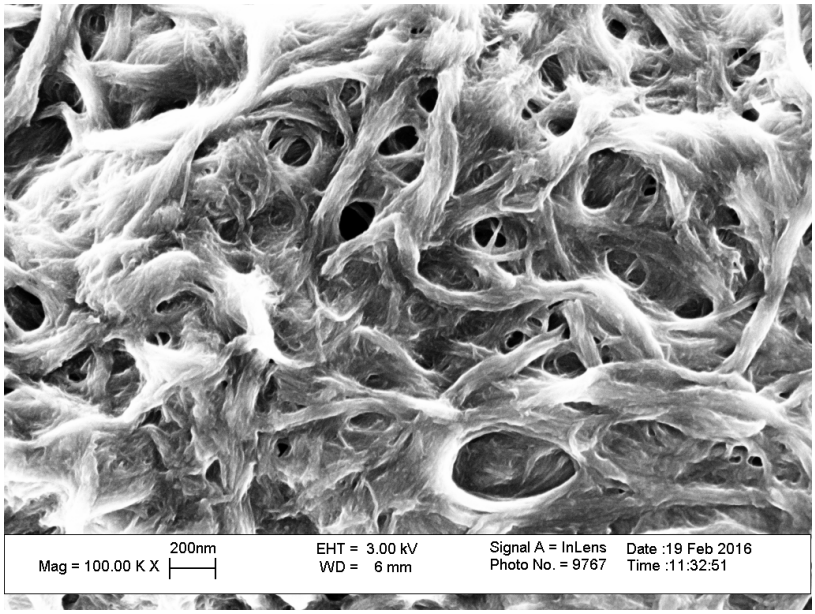

Figure 5.11. Scanning electron microscopy image of negative electrode after cycling test

EIS measurement was also conducted at the same experiment conductions with VA-CNT one before and after cycle test Figure 5.12. The radius of semicircle in high frequency region increased after cycling test and also had two different part as seen in the graph inset. EIS data also proves that one electrode behaves differently after cycling test. Bode phase graph in Figure 5.13 presents the phase angle degrees of the SC device before and after cycling test. Both degress are very close to 90 degree which ideal capacitior has this value. Additionally, in high frequency region, the effect of the electrodes is clearly seen after 5000 cycles.

To understand the effect of electrolyte for the electrode materials in detail, SC device was electrochemically analized in 1M $TBABF_4$/AN and compared with results in 1M H_2SO_4 electrolyte. Supercapacitor cell assembled with EN-CNT electrodes were tested in the same way which explained previous chapters. The advantage of the organic electrolytes is their wide voltage window so that CV measurements were conducted between 0-2 voltage range at different scan rates as shown in Figure 5.14.

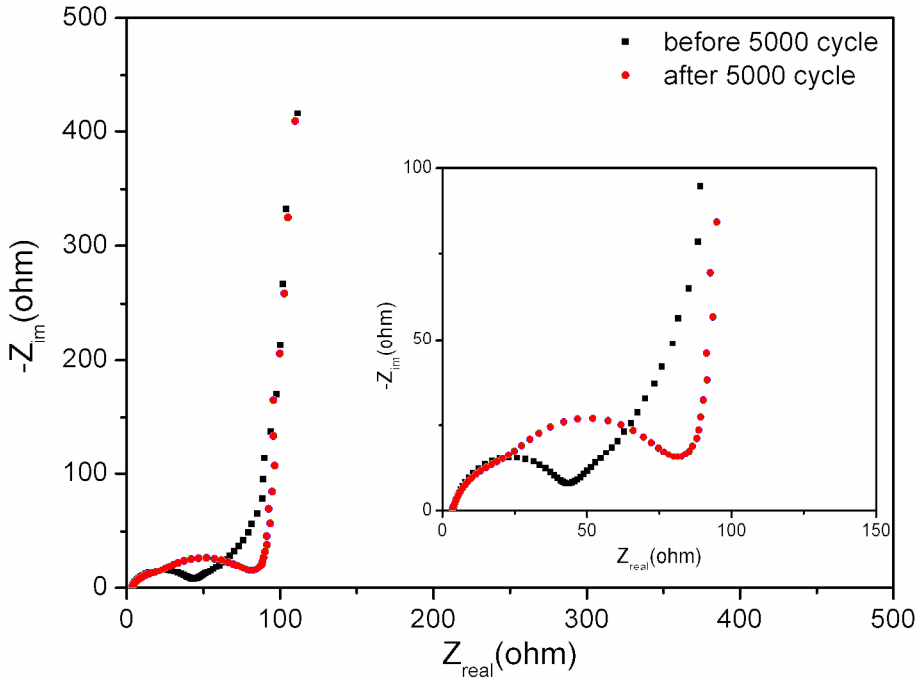

Figure 5.12. Electrochemical impedance spectra of supercapacitor cell with EN-CNT electrodes

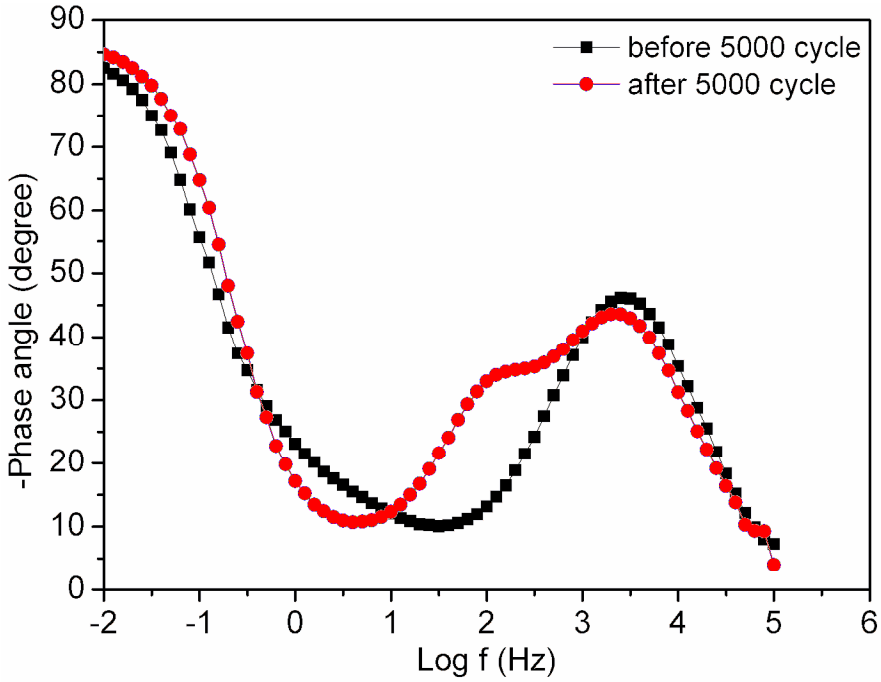

Figure 5.13. Bode phase data of supercapacitor cell with EN-CNT electrodes

Current slightly increases between 1.5V and 2V at slow scan rates so we can call the shape of the curves as quasi-rectangular and this type of CV curve is also common in organic electrolytes [99]. Figure 5.15 shows the CV data at high scan rates and still CV curves remain the shapes. Also SC in $TBABF_4$/AN electrolyte is scan rate independent.

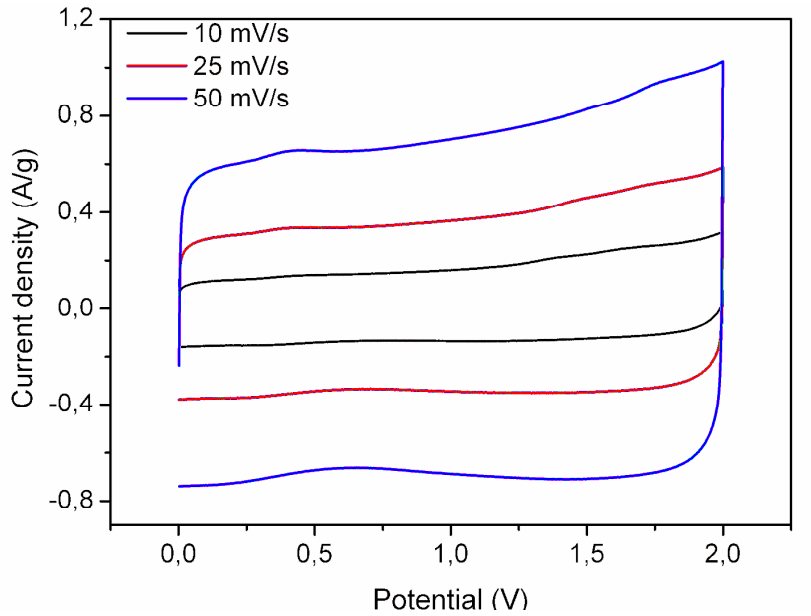

Figure 5.14. Cyclic voltammetry data of supercapacitor cell with EN-CNT electrodes in 1M $TBABF_4$/AN electrolyte at slow scan rates

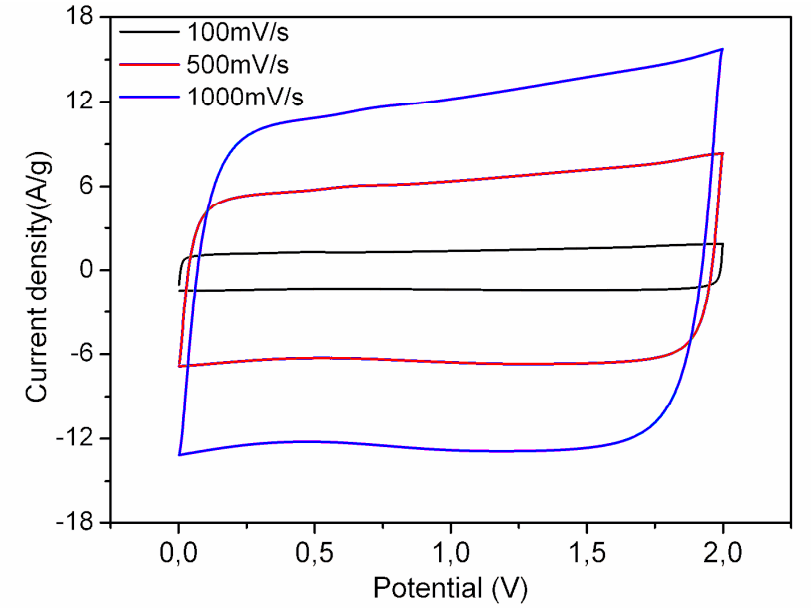

Figure 5.15. Cyclis voltammetry data of supercapacitor cell with EN-CNT electrodes in 1M TBABF4/AN electrolyte at slow scan rates

Figure 5.16 compares the CV curves of EN-CNT electrodes in 1M H_2SO_4 and 1M $TBABF_4$/AN at 10mV/s scan rate. Current is lower in organic electrolytes in the same voltage range because aquaous electrolytes is more conductive than organic one. Besides, SC device conduct the same current in organic electrolyte with the one in acidic aquaous

electrolyte at 1.5V-2.0V. So it means that TBA and BF_4 ions need that much potential to increase their mobility to compete with small ions.

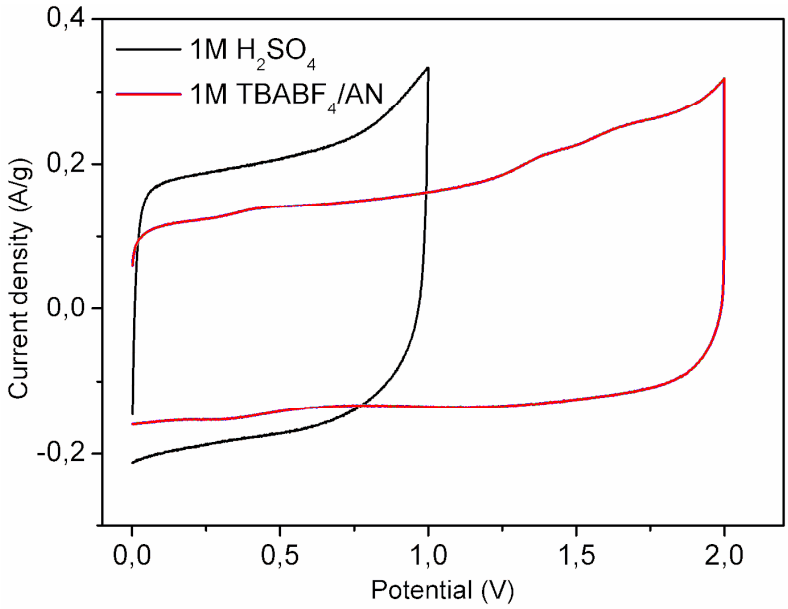

Figure 5.16. Cyclic voltammetry curves of SC cells with EN-CNT electrodes at 10mV/s in 1M H_2SO_4 and 1M $TBABF_4$/AN

GCD measurement was conducted from 0.2A/g to 2A/g between 0V to 2V in 1M $TBABF_4$/AN electrolyte. As seen in Figure 5.17, discharge stages of the SC show a linear line independently of current densities whereas charge stages of the SC show curvy character at low current densities but a linear line at high current densities. This behaviour is also common in organic electrolytes [95]. Cyclic stability of the SC device was also conducted in organic electrolyte. SC device in organic electrolyte shows better cyclic stability then other SC devices in acidic one. Even the digital image of the electrodes after cycling test does not show any change in the materials. Figure 5.19 presents the raman data of the electrodes before and after cycling test. There is a negligible change in the data but there is not any strong peak before 2D peak which was observed for the negative electrode in acidic aqueous electrolyte.

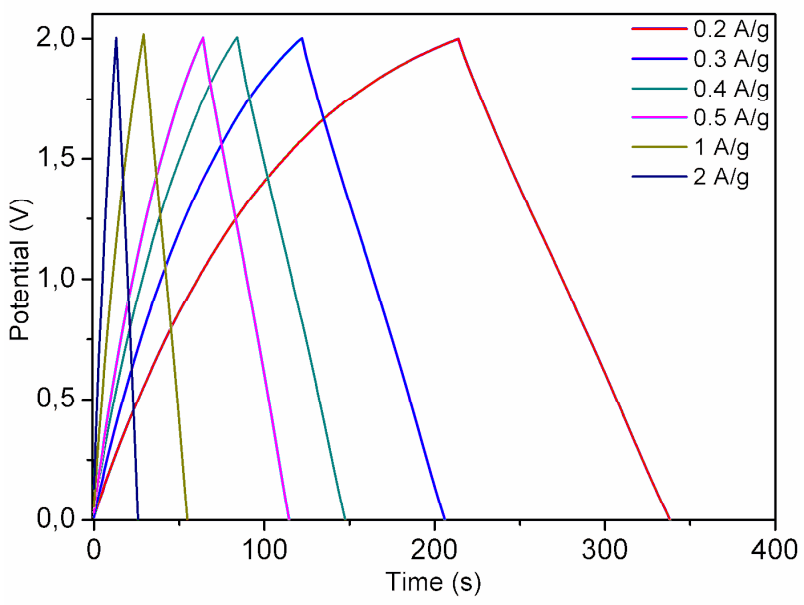

Figure 5.17. Galvanostatic charge/discharge data of supercapacitor cell with EN-CNT electrodes in 1M $TBABF_4$/AN

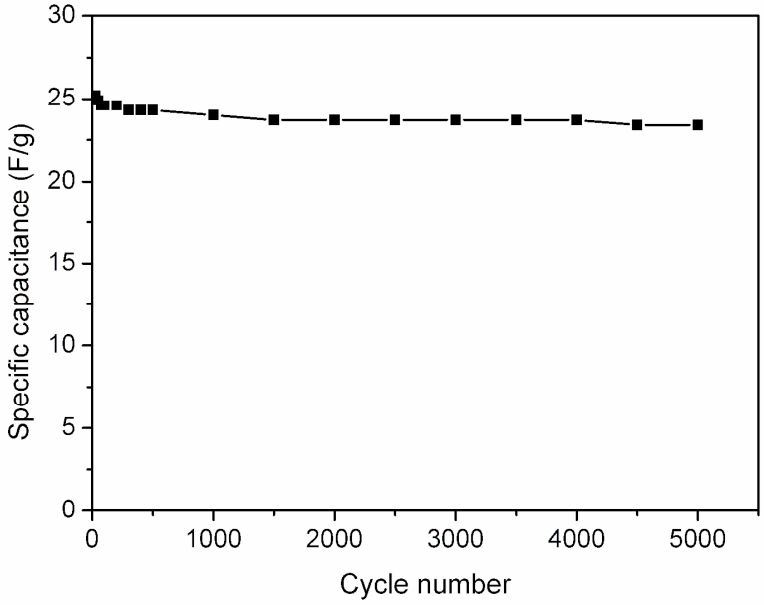

Figure 5.18. Cycling stability of supercapacitor cell with EN-CNT electrodes in 1M $TBABF_4$/AN

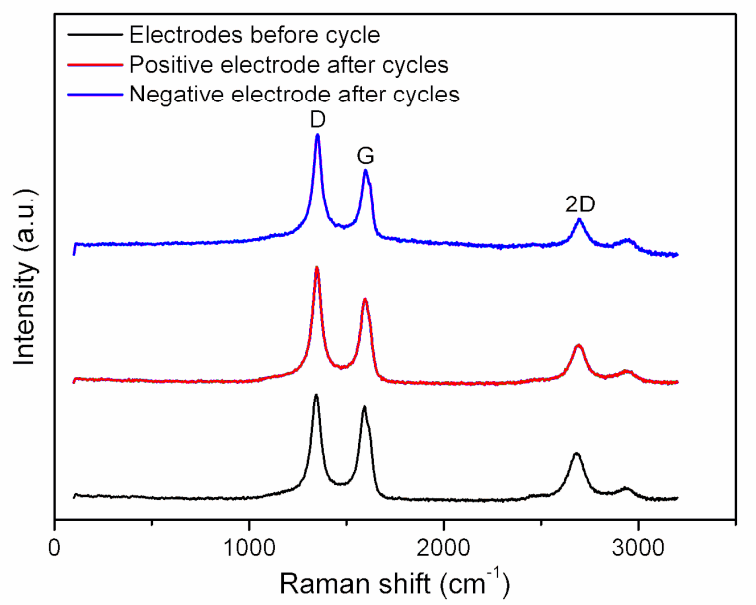

Figure 5.19. Raman spectra of SC cell with EN-CNT electrodes in 1M $TBABF_4$/AN before and after cycling test

EIS measurement was also conducted for SC in $TBABF_4$/AN electrolyte using the same experiment conditions. Figure 5.20 shows EIS data before and after 5000 cycle tests.

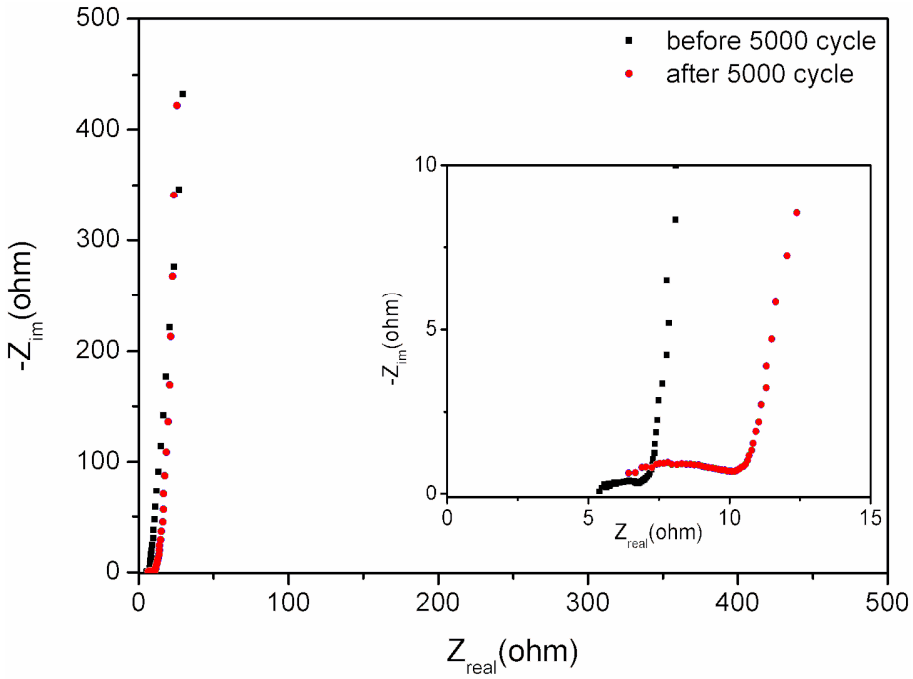

Figure 5.20. Electrochemical impedance data of supercapacitor cell with EN-CNT electrodes in 1M $TBABF_4$/AN before and after cycling test

Unlike from acidic aqueous electrolyte, SC device in organic one has only one semicircle after cycling test and radius of the semicircle is wider than the one at the begining as expected. Also, R_s value is higher in organic electrolytes (around 5 ohm) before and after cycling test when compared with acidic aquaous solution which R_s value is around 3 ohm. This is due to the poor ionic conductivity of the organic electrolytes and also the wettebality and compatibility between electrode and electrolyte [100]. Figure 5.21 shows the bode phase graph of SC device in 1M $TBABF_4$/AN electrolyte. Device has almost similar phase angle before and after cycling test and in high frequency region there is a slight difference. It can be concluded that SC device in 1M $TBABF_4$/AN electrolyte shows slightly more ideal behavior than one in 1M H_2SO_4 electrolyte when the phase angle degrees are compared. Depending on the what type of active material used, this conclusion could be in the opposite direction. For example, researchers in Korea concluded that porous silicon carbide electrode shows better result in aquaous electrolyte than organic one [100].

Complex capacitance analyses were done in both organic and acidic aquaous electrolytes before and after cycling test. Both specific capacitance values before and after cycling test at 1MHz are very close to the specific capacitance values calculated by GCD measurements. At the end of the 5000 cycle, specific capacitance value for the SC device in 1M H_2SO_4 decreases upto the value which SC device in 1M $TBABF_4$/AN has after 5000 cycle test. Time constants, specific energy densities and average power densities were calculated before and after cycling test and Table 5.1 presents them. Time constants for SC device assembled with EN-CNT electrodes in organic electrolyte is much more less than the one in acidic aquaous electrolyte However, SC device assembled with VA-CNT electrodes is the one which has the lowest time constant. For specific energy density values SC device in organic electrolyte has the highest value because of the wide voltage window and SC device with VA-CNT electrode in acidic aqueous is the second one. The same trend in average power density is in the same trend with specific energy density except the aqueous electrolyte results. Both device assembled with VA-CNT and EN-CNT electrodes have the same average power densities before and after cycling test. These results confirm that specific power density is independent from the form of CNT but dependent to the electrolyte. Also, energy density is directly related to the form of CNT and electrolyte. Figure 5.24 and Figure 5.25 show how specific energy and power density change with increasing cycle.

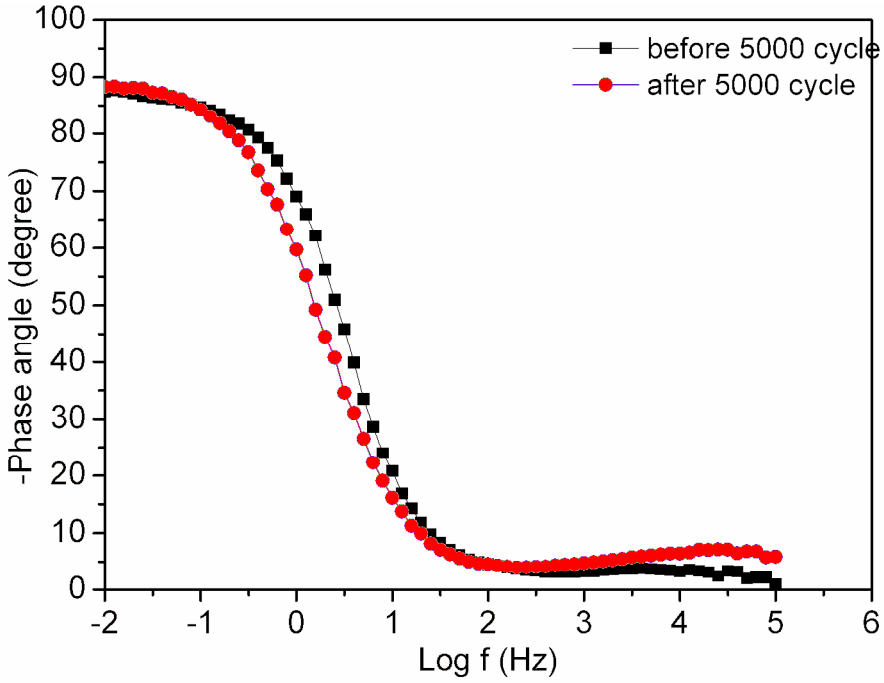

Figure 5.21. Bode phase curves of supercapacitor cell with EN-CNT electrodes in 1M $TBABF_4$/AN before and after cycling test

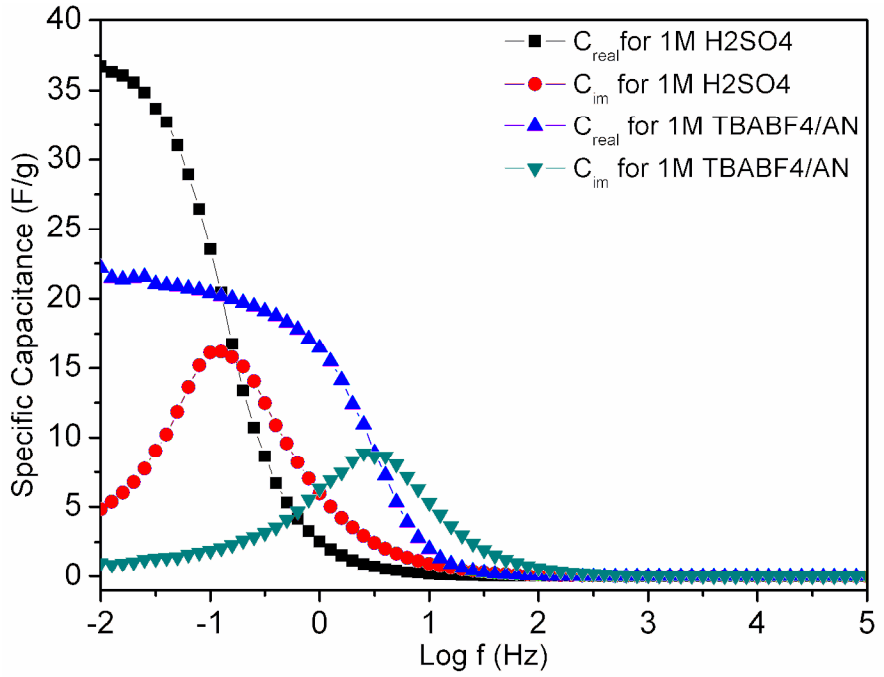

Figure 5.22. Complex capacitance analysis of supercapacitor cells with EN-CNT electrodes in 1M $TBABF_4$/AN and 1M H_2SO_4 before cycling test

As seen in the figures, SC device in both electrolytes have decreasing specific energy densities due to the decreasing specific capacitance. Besides, specific power densities remain stabile during the cycling tests.

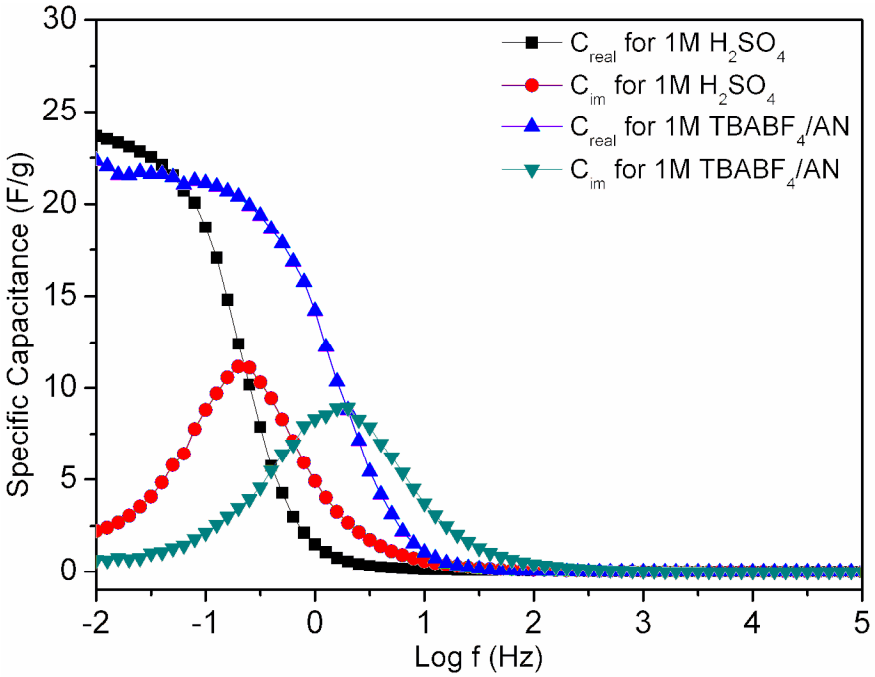

Figure 5.23. Complex capacitance analysis of supercapacitor cells with EN-CNT electrodes in 1M $TBABF_4$/AN and 1M H_2SO_4 after cycling test

Table 5.1. Specific energy and specific power densities of supercapacitor cells before and after cycling test in 1M H_2SO_4 and 1M $TBABF_4$/AN

Type of the measurements	1M H_2SO_4 before cycling test	1M H_2SO_4 after cycling test	1M $TBABF_4$/AN before cycling test	1M $TBABF_4$/AN after cycling test
S.E. Density (Wh/kg)	5,16	3,42	14	13,17
S. P. Density(W/kg)	300	300	600	600

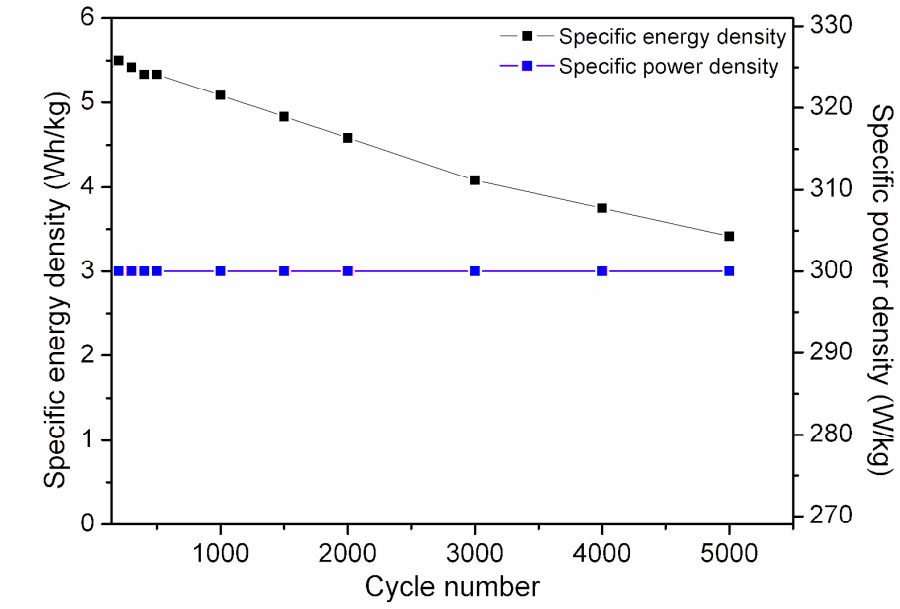

Figure 5.24. Change in specific energy density and power density of supercapacitor cell with EN-CNT electrodes in 1 M H_2SO_4 with cycling test

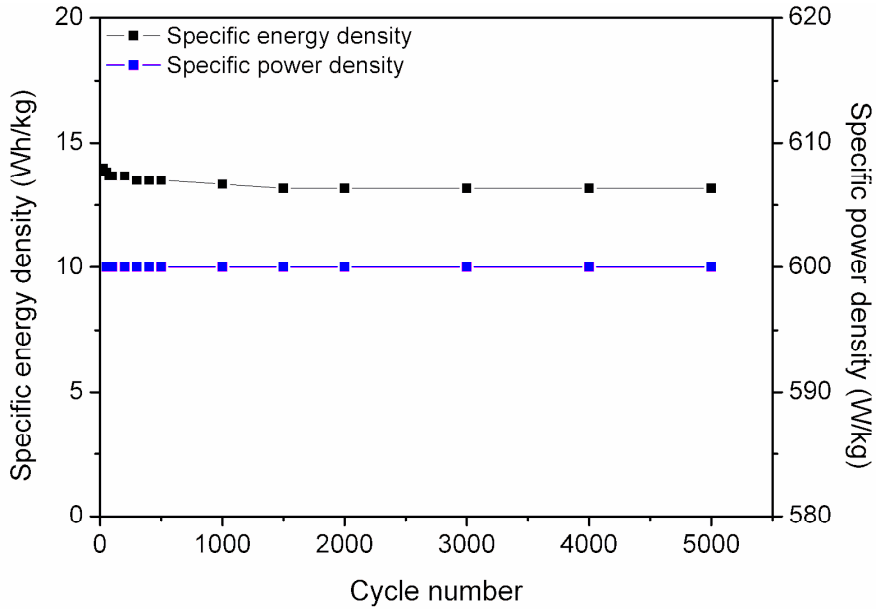

Figure 5.25. Change in specific energy density and power density of supercapacitor cell with EN-CNT electrodes in 1 M $TBABF_4$/AN with cycling test

6. Supercapacitor Cell Assembled With CNT/PANi Hybrid Electrode

6.1. Characterization of CNT/PANi Hybrid Electrodes

6.1.1. Morphological Characterization of CNT/PANi Hybrid Electrodes

SEM images of EN-CNT/PANi hybrid electrodes prepared with electrochemical method and chemical method were shown in Figure 6.1 and Figure 6.2 respectively. SEM image in Figure 6.3 belongs to the VA-CNT/PANi hybrid electrode. As seen in the images, the coating of PANi on VA-CNT is very homogene and still vertically aligned direction is retained. Both polymerization method worked well to prepare hybrid electrode structure however electrochemical method is more easier and user friendy than chemical method. Because there are less parameters to control the tickness of the polyaniline and requires short time. Thickness of the PANi is very important parameter because when the tickness of PANi increases, surface area of the as-prepared electrode will decrase so it will result in lower capacitance value.

Figure 6.4 shows the TEM image of PANi coated CNT. Unfortunatelly, image does not show any scale bar due to the software problem of the equipment so that we could not decide the tickness of PANi. However we can clearly say that PANi can be coated onto the CNT with these methods. More SEM and TEM images can be seen in Appendix C.

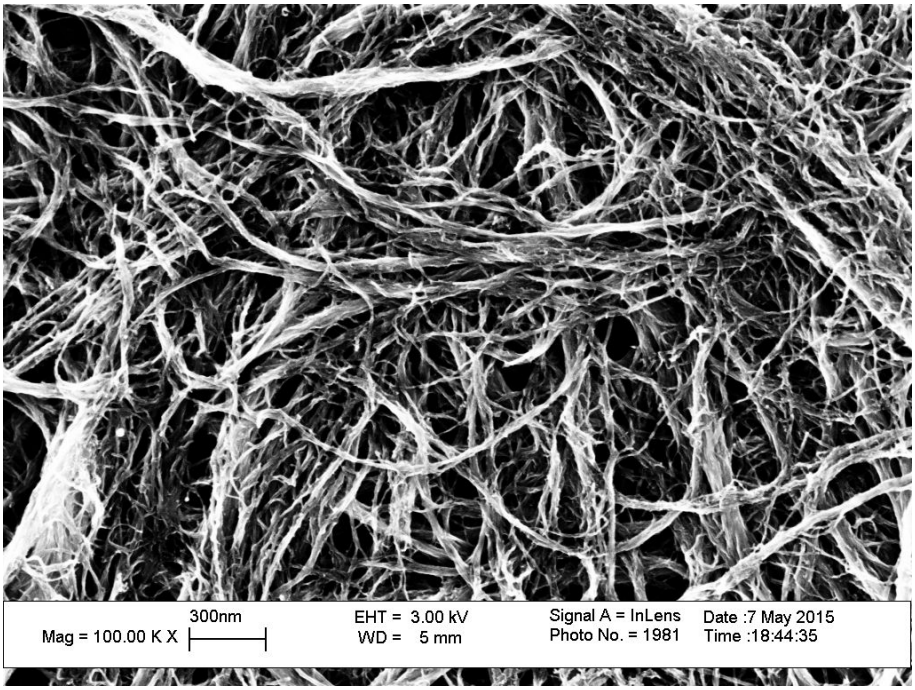

Figure 6.1. Scanning electron microscopy iamge of EN-CNT/PANi electrode prepared with electrochemical method

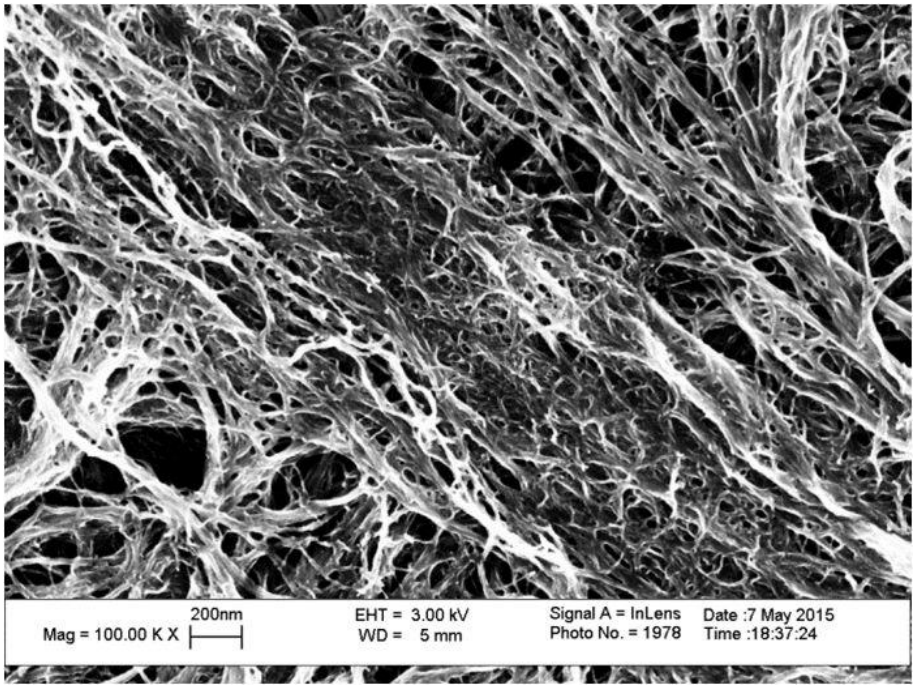

Figure 6.2. Scanning electron microscopy image of EN-CNT/PANi electrode prepared with composit method

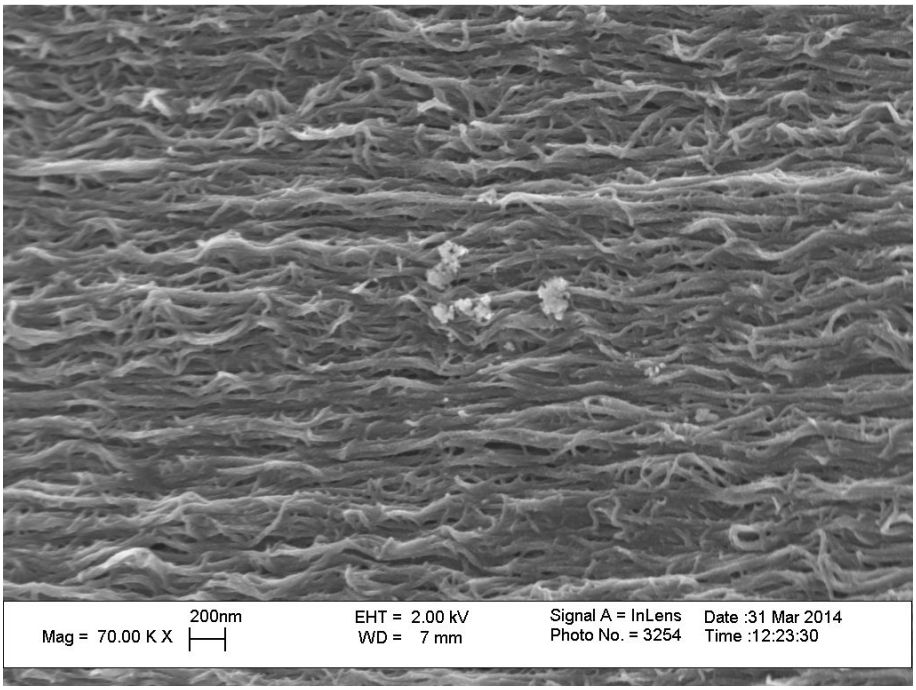

Figure 6.3. Scanning electron microscopy image of VA-CNT/PANi electrode prepared with electrochemical method

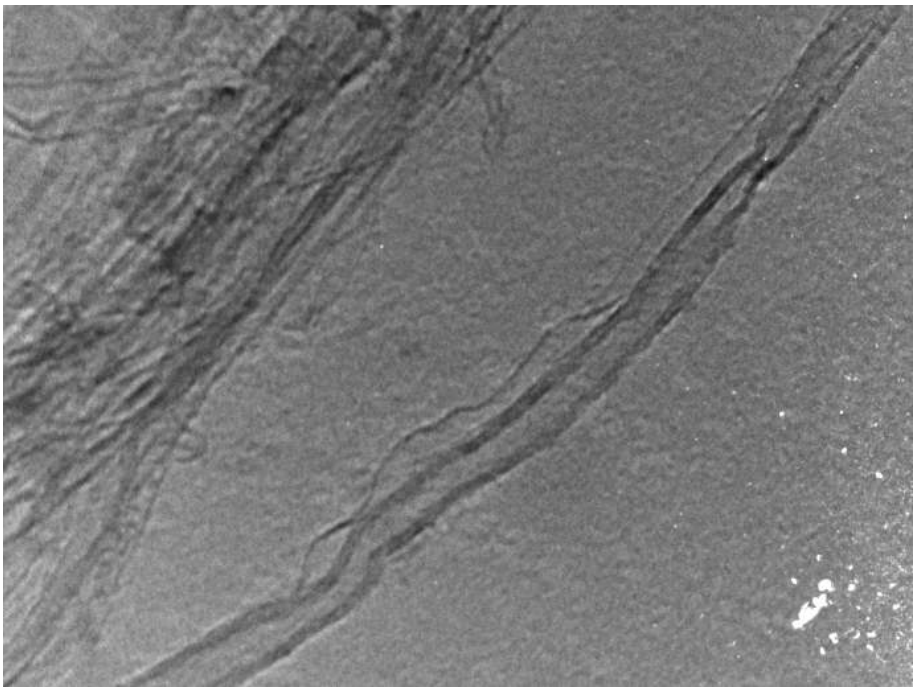

Figure 6.4. Transmission electron microscopy image of PANi coated CNT

6.1.2. **Spectral Characterization of CNT/PANi Hybrid Electrodes**

Raman scattering was used to observe the structural change and also to be sure about coating for aligned CNT/PANi composites. Figure 6.5 shows Raman spectra of CNT/PANi electrode. As seen in the data, the peaks for CNT are not obvious anymore besides PANi peaks appear. It also shows that CNT was covered well with PANi.

Three new peaks occured at around 1170 cm^{-1}, 1480 cm^{-1} and 1600 cm^{-1}. Those peaks are related to the C-H bending deformation in the quinoed-phenyl groups, C=N streching vibration of the quinoid units and C-C streching deformations in benzoid ring of PANi, respectively [94].

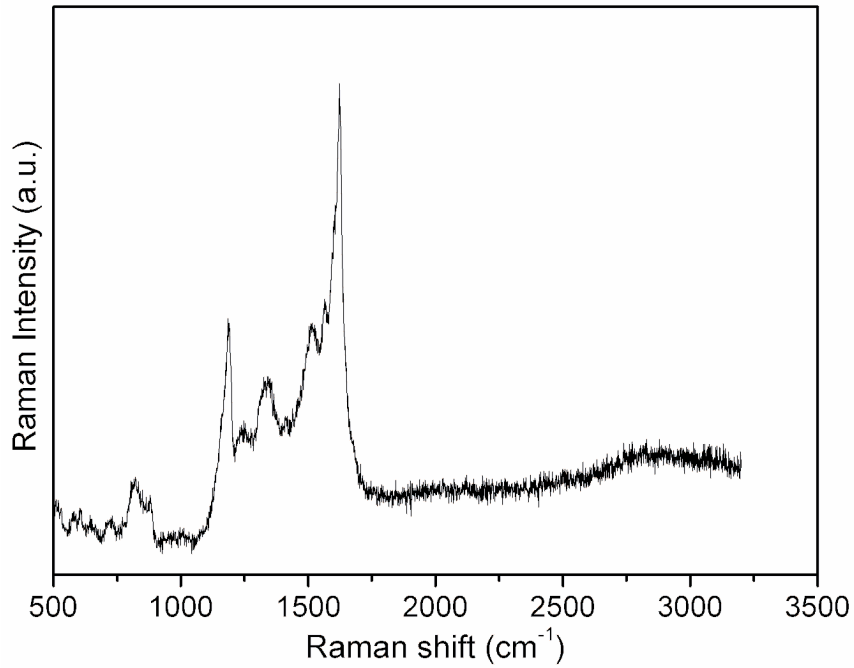

Figure 6.5. Raman spectra of CNT/PANi electrode

6.1.3. **Thermal Characterization of CNT/PANi Hybrid Electrodes**

Figure 6.6 shows the TGA graph of hybrid CNT/PANi electrode. TGA data was conducted at a heating rate of 10^{o}C under dry air atmposphere. There are three main losses in the graph; one is between 30^{o}C-100^{o}C, other one is between 150^{o}C-250^{o}C and the last one is between 500^{o}C-600^{o}C. The first loss is due to the water trace in the sample and the second one is associated with the monomer traces. Last one belongs to the polyaniline chain and the carbon nanotube. When the TGA of pure CNT and CNT/PANi electrode are compared, it is clearly said that hybrid electrode material decomposes at lower temperature than

virgin one and oxidation temperature shifts to the lower value. TGA indicates that hybrid electrode is also stable upto the high temperature.

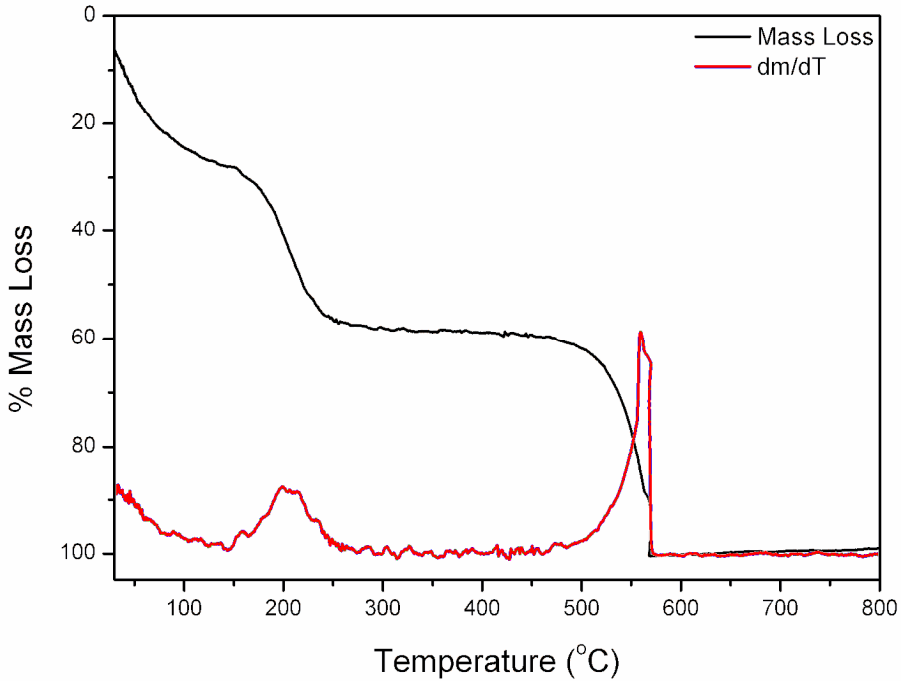

Figure 6.6. Thermo gravimetric analysis of CNT/PANi electrode

6.2. Electrochemical Performance of Supercapacitor with CNT/PANi Hybrid Electrodes

6.2.1. Electrochemical Performance of CNT/PANi Hybrid Electrodes

Hybrid electrodes were prepared as explained in chapter 3.3. Electrochemical measurements of prepared hybrid electrodes conducted using 3 electrode systems and then two electrode system was used to test the full SC assembled with asymmetic cell configuration, where bare CNT is negative electrode and hybrid CNT/PANi is positive electrode.

Firstly, hybrid electrodes prepared using electrochemical methods (called as e-CNT/PANi electrode) were tested using three electrode system. In three electrode system, e-CNT/PANi hybrid electrode was used as working electrode, Pt wire as counter electrode and Ag/AgCI saturated electrode as reference electrode. Figure 6.7 shows the CV curves of e-CNT/PANi electrode from -0.2V to 0.8V at different scan rates. Unlike double layer capacitors which covered in chapter 3, CV curves have peak around 0.4V which

corresponds to one of the PANi peaks. Also this peak indicates that there is a faradic process due to the electron transfer between electrode and electrolyte. Actually PANi has two peaks at slow scan rates like 5mV/s however this peak disappears with inscreasing scan rate as seen in Figure 6.8. These two peaks show two electrons transfer.

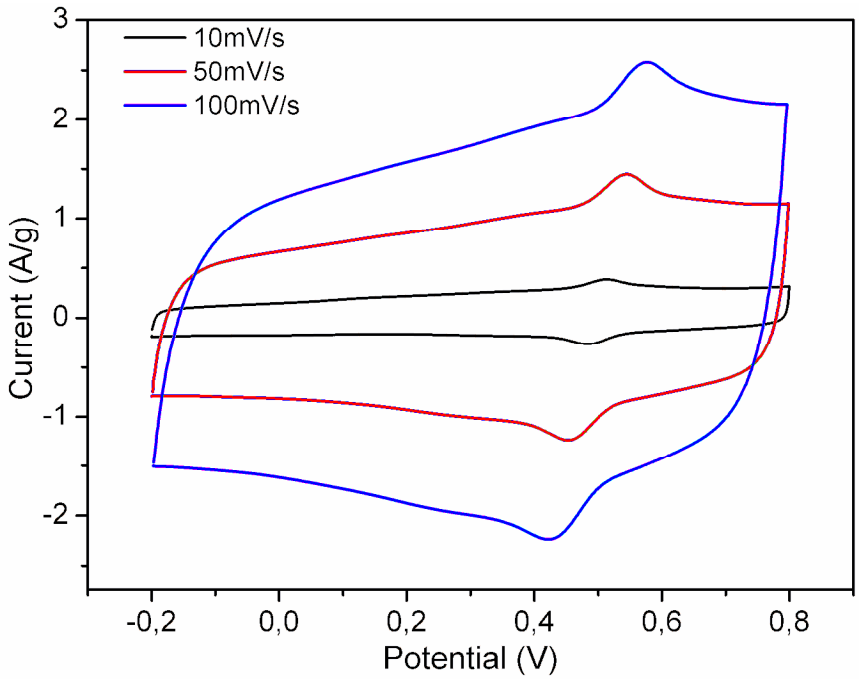

Figure 6.7. Cylic voltammetry curves of e-CNT/PANi electrode at different scan rates.

GCD measurements were conducted between 0V and 1V range and is presented in Figure 6.9. GCD curve of hybrid electrodes is different than bare electrode due to the faradic process. The effect of electron transfer is also seen in GCD curve easily. The linearity in discharge curves appears for a short time and then non-linearity appears. This non-linearity stems from the pseudocapacitive property of PANi chains.

Secondly, hybrid electrode was prepared using chemical methods and here called as c-CNT/PANi electrode. The same electrochemical tests were applied to this electrode using three electrode system. As seen in Figure 6.10, CV curves look similiar to Figure 6.7 expect that peaks are more clear even at high scan rates like 50 mV/s. Also, curve shapes change at 100 mV/s so we can conclude this behavior as scan rate dependent process of this electrode. To see the peaks clearly, CV curve at 10mV/s is presented indivually in Figure 6.11.

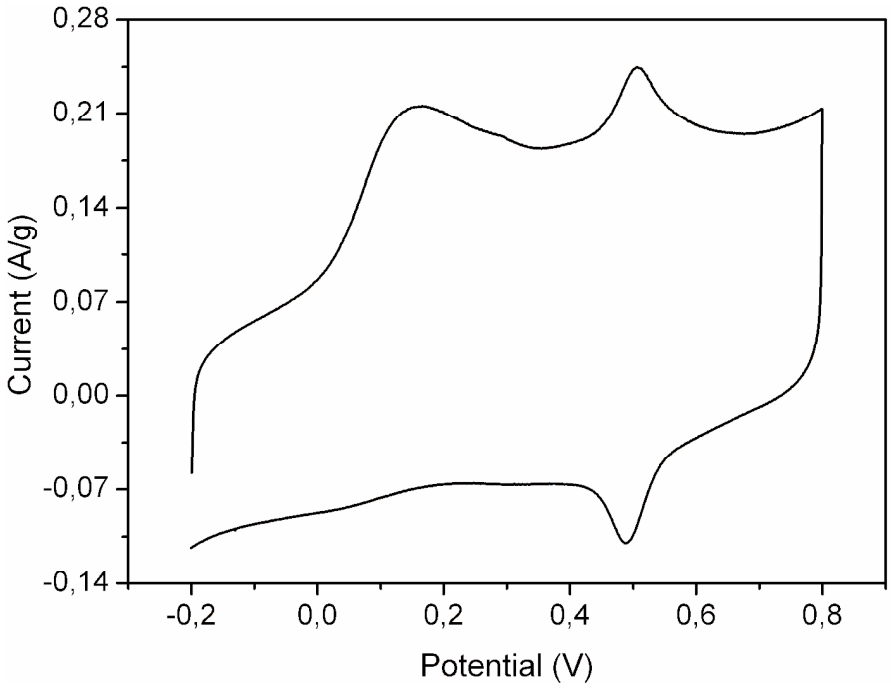

Figure 6.8. Cyclic voltammetry curves of e-CNT/PANi electrode at 5 mV/s scan rate.

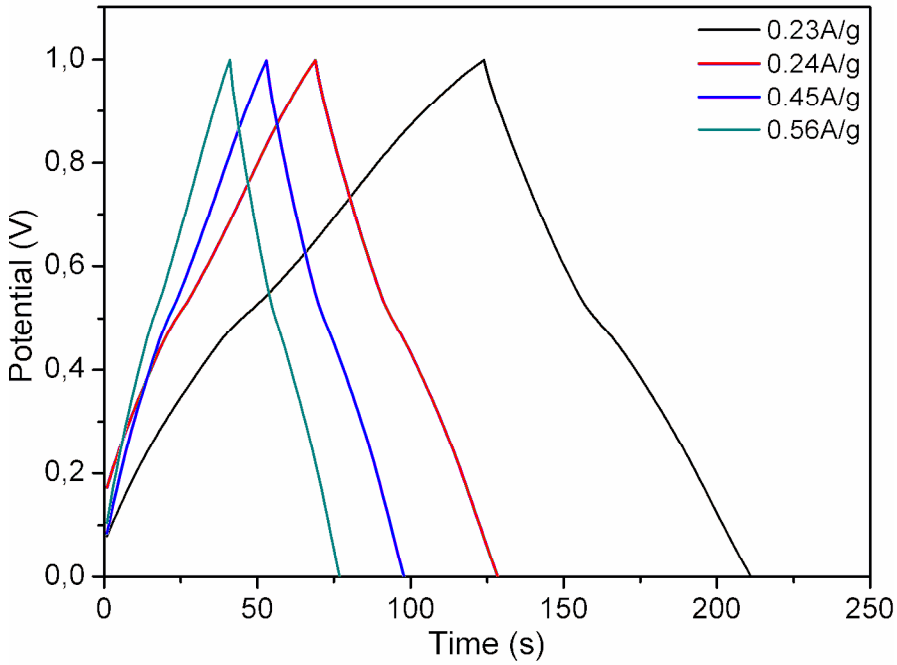

Figure 6.9. Galvanostatic charge/discharge curves of e-CNT/PANi electrodes at different current densities.

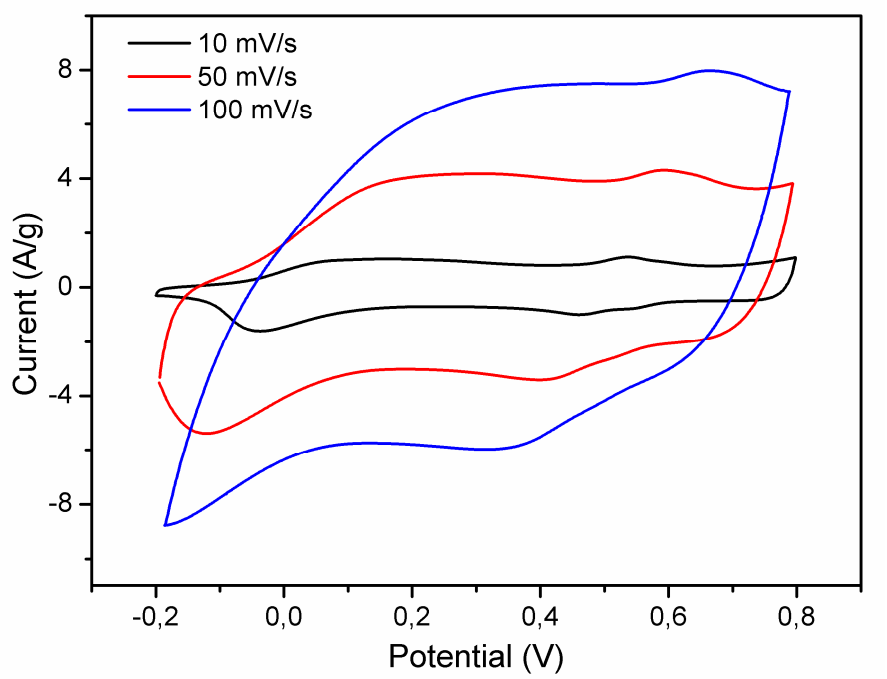

Figure 6.10. Cyclic voltammetry curves of c-CNT/PANi electrode at different scan rates

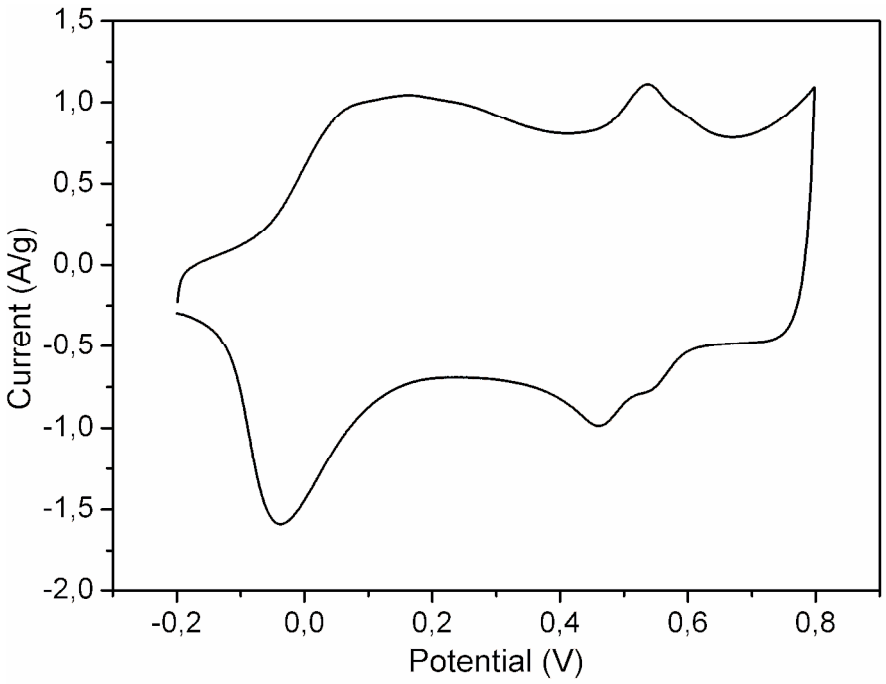

Figure 6.11. Cyclic voltammetry curve of c-CNT/PANi electrodes at 10mV/s scan rate.

To compare the effect of hybrid structure, CV data for these two hybrid CNT/PANi electrodes and bare CNT electrodes are compared as seen in Figure 6.12. Chemically prepared hybrid electrode at the same scan rate has hold more charge than electrochemically hybrid electrode and bare electrode. There also can be another approach

to explain this CV graphs; in electrochemical method, 1.5 minutes should not be enough for full PANi coating so that there is not clear difference between bare CNT electrode and e-CNT/PANi electrode. However, in chemically prepared one the effect of PANi for holding the charge is seen clearly. We can also conclude that in bare CNT electrode electrochemical double layer capacitor (EDLC) is dominant whereas in chemical one pseudocapacitance is more dominant.

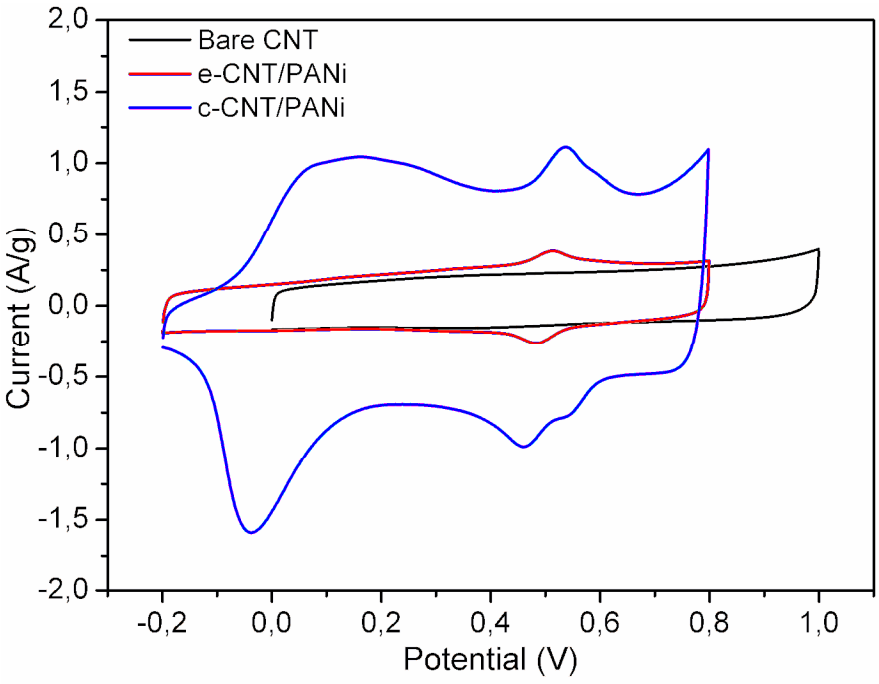

Figure 6.12. Cyclic voltammetry curves of CNT, e-CNT/PANi and c-CNT/PANi electrodes

GCD test results for c-CNT/PANi hybrid electrode is shown in Figure 6.13. GCD tests were done at higher current densities because e-CNT/PANi electrode has total 100s charge/discharge time at 0.45A/g whereas c-CNT/PANi electrode has total 120s at 1A/g. Also it shows that c-CNT/PANi hybrid electrode is more desirable electrode at high current applications when compared with e-CNT/PANi and bare CNT electrodes.

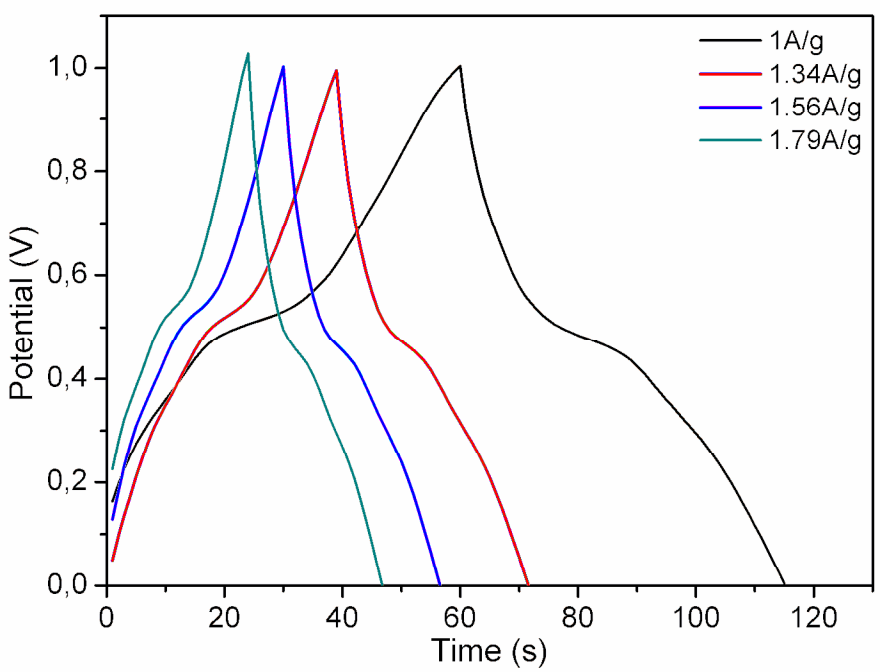

Figure 6.13. Galvanostatic charge/discharge curves of EN-CNT/PANi electrodes prepared with chemical method

GCD curves in Figure 6.13 are slightly different than in Figure 6.9. These curves are slightly similar to GCD test results in electrodes for battery applications. It means that ions are not absorbed or desorbed physically anymore but there is chemical reactions on the electrode surface as it happens in battery electrodes.

6.2.2. **Electrohemical Performance of Supercapacitor with Different Electrode Configuration**

Upto this chapter, SC cell was assembled with symmetric configuration which includes the same materials in both positive and negative electrode. In this part, asymmetric configuration will be investigated in detail using bare CNT electrode as a negative electrode and e-CNT/PANi as a positive electrode.

In a symmetric design, both sides have the same weight to compensate the charge equality between electrodes. In an asymmetric design, due to the different electrode structure which has different capacitance values, mass balance should be satisfied and Eqn. 6.1 is used for it; .

$$\frac{m_-}{m_+} = \frac{C_- \times U_-}{C_+ \times U_+} \qquad \text{(Eqn. 6.1)}$$

where, C_- and C_+ are the specific capacitance values of negative and positive electrodes, U is the voltage window and m is the mass of the electrodes [101]. For the fabrication of the asymetric SC device, the mass ratio of the positive (CNT/PANi) and negative electrode (CNT) was 2.56 according to the specific capacitance values of each electrode calculated using three electrode system in 1M H_2SO_4.

CNT/PANi electrode was prepared using electrochemical methods as it was explained in chapter 3. The coating time was 3 minutes with 5 seconds for polymerization step and 60 seconds for open circuit step. Figure 6.14 presents the TGA curves of CNT, PANi and CNT/PANi at a heating rate of 10^{o}C/min under nitrogen atmosphere. The weight percentage of PANi in hybrid electrode was determined as 40% using Eqn. 6.2 [102].

$$wt\% = \frac{\Delta w_1 - \Delta w_2}{\Delta w_3 - \Delta w_2} \qquad \text{(Eqn. 6.2)}$$

where, Δw_1, Δw_2 and Δw_3 refer to the weight loss of CNT/PANi, PANi and CNT from 100 to 700 ^{o}C, respectively.

Electrochemical characterization of the asymmetric SC device was conducted with CV, EIS and GCD tests. Figure 6.15 shows the CV curves of symmetric SC device assembled with CNT electrodes and asymetric device assembled with CNT and CNT/PANi electrodes at 10mV/s scan rate between 0V and 1V potential range. As seen in the figure, asymmetric SC device hold more charge than symmetric one due to the charge transfer mechanism.

EIS data in Figure 6.16 compares the frequency response of the both SC device under 10mV AC voltage from 100000 Hz to 0.01 Hz in 1M H_2SO_4. In high frequency region, asymmetric SC device has smaller semi-circle than symmetric one, which means that charge transfer resistance in asymmetric SC device is less than symmetric one. In the transition region from high to low frequency, Warburg impedance differs in each SC device. Asymmetric device has shorter Warburg impedance, which is interpreted as the transition from resistive behavior to capacitive behaviour, than symmetric one. Besides, Bode phase graph in Figure 6.17 presents the phase angle in low frequency region and asymmetric device has around 85^o whereas symmetric device has around 80^o, which is less than asymmetric one.

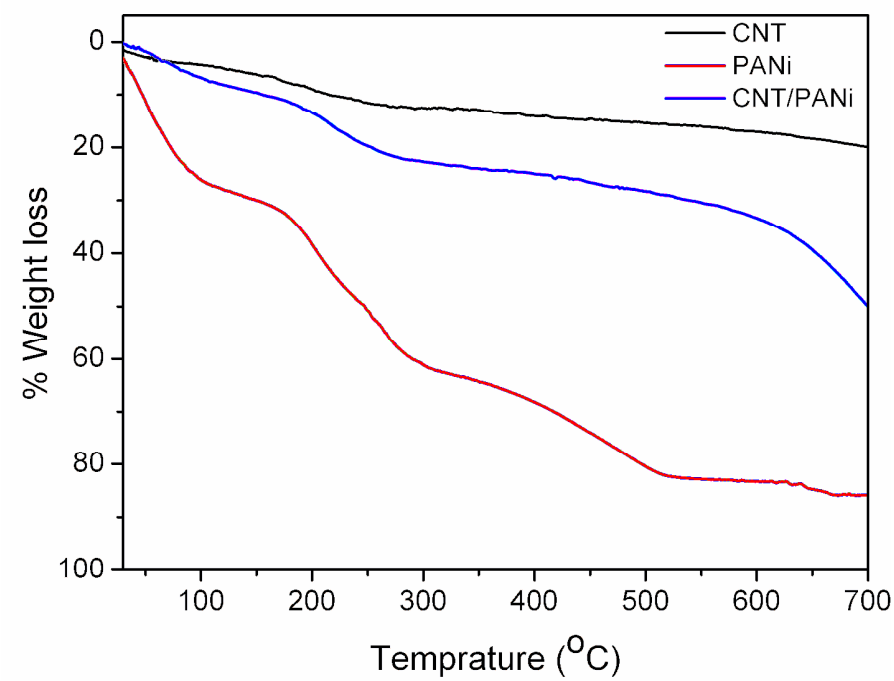

Figure 6.14. Thermo gravimetric analysis of CNT, PANi and CNT/PANi at nitrogen environment

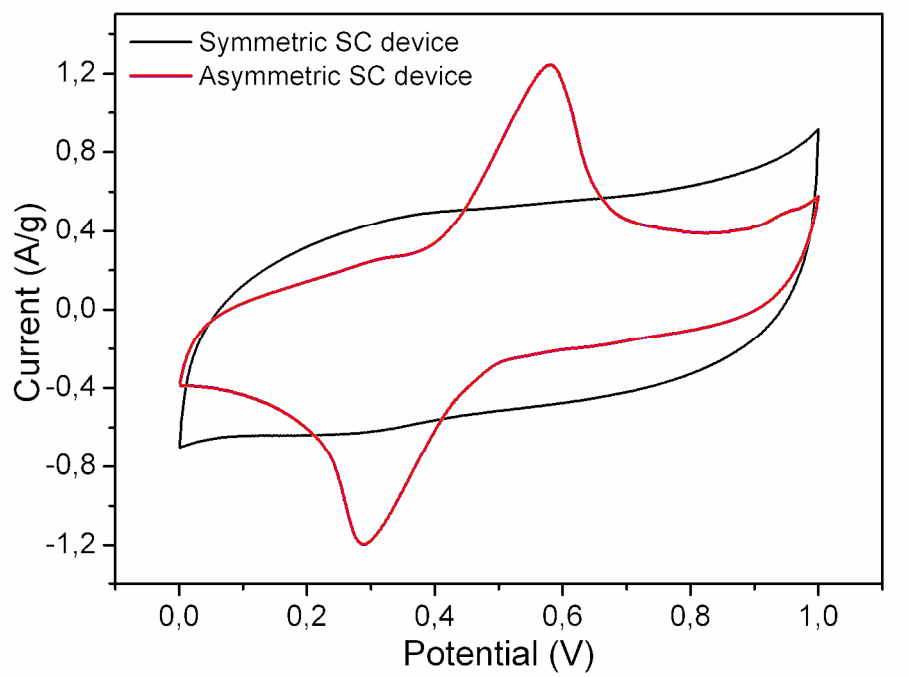

Figure 6.15. Cyclic voltammetry curves of supercapacitor cells with symmetric and asymmetric configuration

Complex impedance analysis was performed to investigate the time constant of both devices. Figure 6.18 presents the imaginary part of the specific capacitance versus frequency. Asymmetric device has smaller time constant, 3.99s, than symmetric one, 10s.

This results show that PANi fibers in hybrid electrode used in the asymmetric device design give faster respond to the current so that times constant is short.

The cycling stability of both SC device was investigated at 0.25A/g in 1M H_2SO_4 as seen in Figure 6.19. After 3500 charge/discharge cycles, the capacitance retention of symmetric and asymmetric SC devices are 60% and 80%, recpectivelly. It is noticeable that capacitance retention of the asymmetric device assembled with hybrid electrode over a long cycle is superior than symmetric one assembled with virgin CNT electrodes.

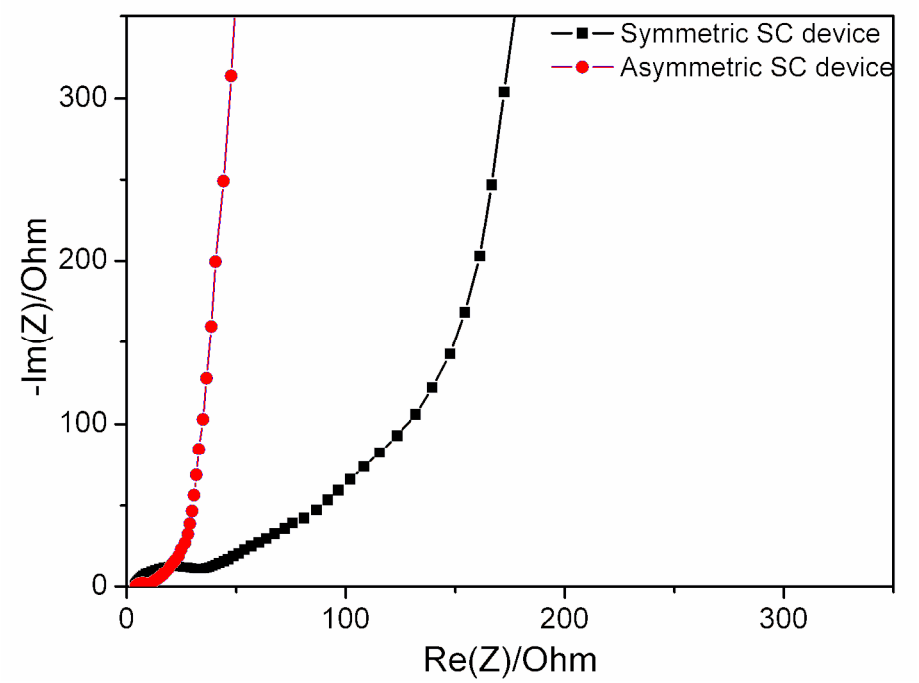

Figure 6.16. Complex impedance spectrum of supercapacitor cells with symmetric and asymmetric configuration

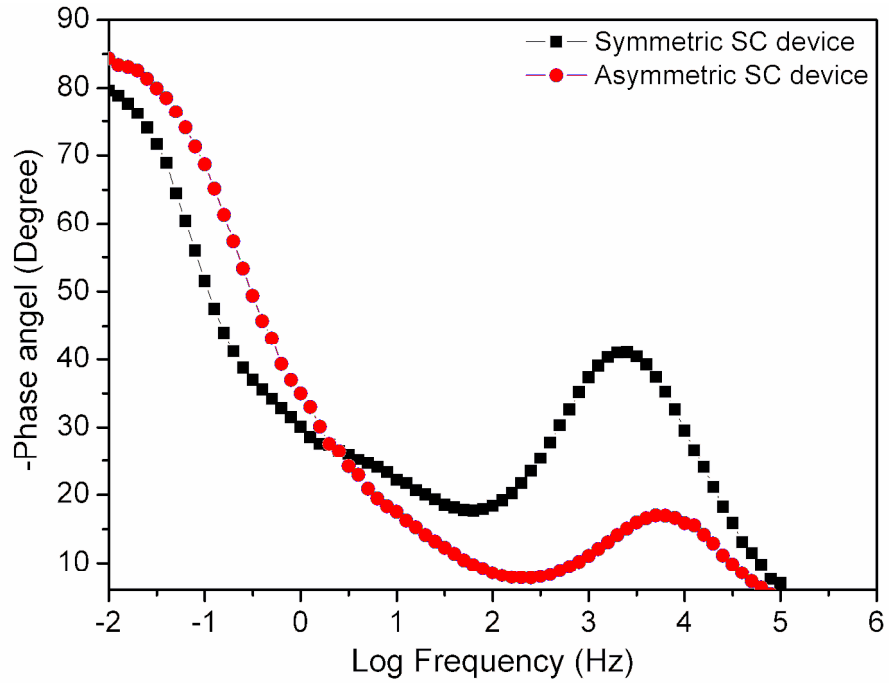

Figure 6.17. Dependence of phase change of supercapacitor cells with symmetric and asymmetric configuration

Furthermore, as mentioned in chapter 5, CNT electrodes in acidic aqueous electrolyte is affected by insertion of H^+ ion and capacitance retention decreases with increasing cycles. However, hybrid electrode shows better result in the same electrode so we can conclude that we can decrease the negative effect of H^+ ion using CNT/PANi electrode.

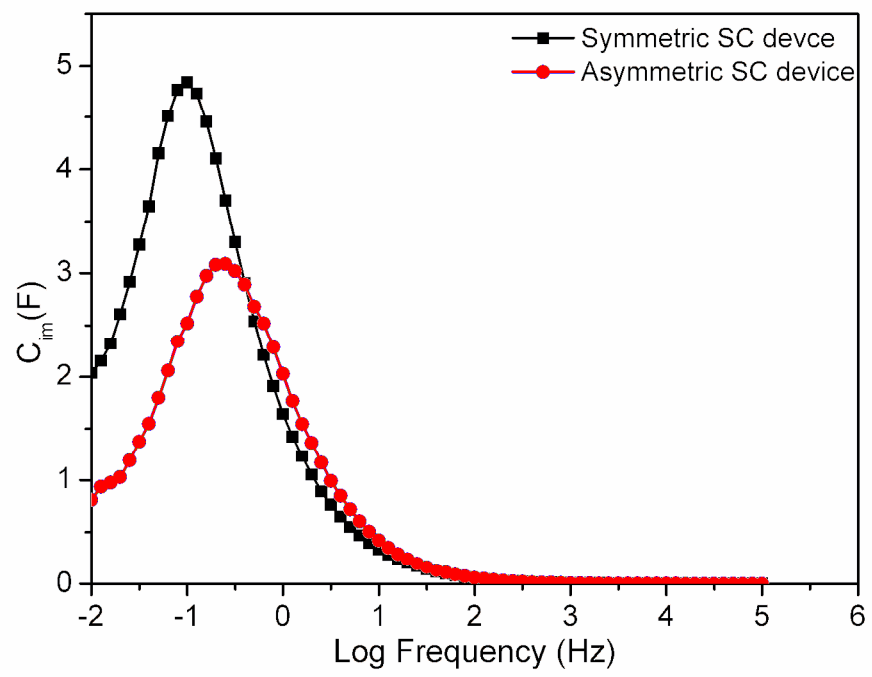

Figure 6.18. Imaginary part of complex capacitance of supercapacitor cells with symmetric and asymmetric configuration

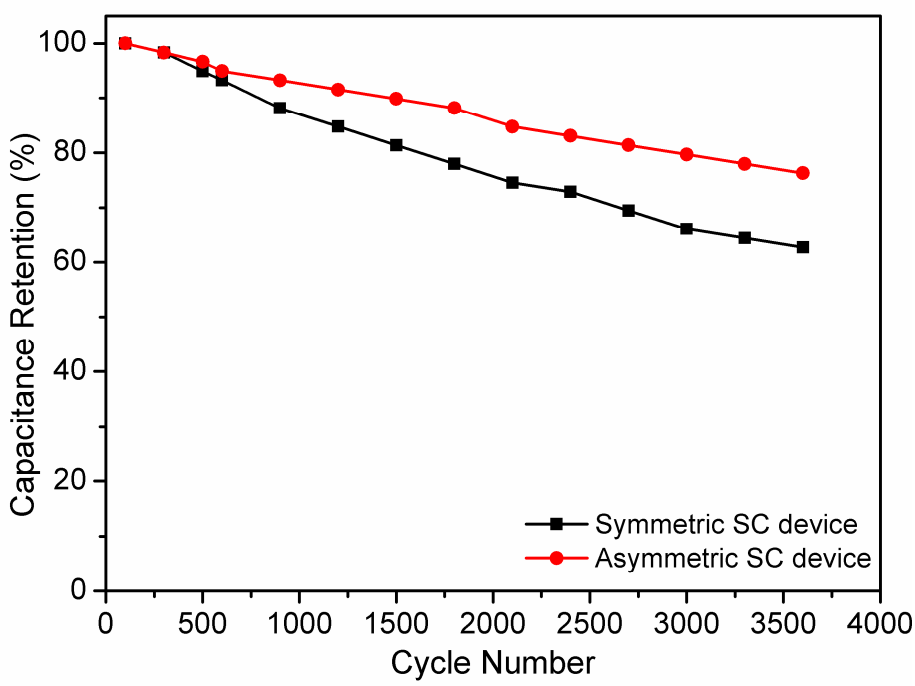

Figure 6.19. Capacitance retention of supercapacitor cells with symmetric and asymmetric configuration

7. Conclusion and Future Work

This study was attributed to the detailed investigation of the electrochemical performance of the supercapacitor cells fabricated with as grown VA-CNT electrodes, as prepared EN-CNT electrodes and hybrid CNT/PANi electrodes. VA-CNT growth was achieved on silicon substrate using thermal chemical vapor deposition method using ethylen as carbon source, helium and hydrogen as carrier gases. EN-CNT electrodes were prepared dispersing VA-CNT in ethanol and drying it oven for four hours. EN-CNT electrodes does not include any binder and filler. Hybrid CNT/PANi electrodes were prepared with using electrochemical and chemical methods. Before testing electrochemical performance of the electrodes, they were characterized with morphological, spectral and thermal characterization methods using SEM, TEM, Raman spectroscopy, and TGA, respectively.

Supercapacitor device was assembled with symmetric and asymmetric configuration. Symmetric device was assembled with VA-CNT and EN-CNT electrodes using 1M H_2SO_4 as electrolyte. According to the CV, EIS and GCD test results, device with VA-CNT electrodes show more promising electrochemical performance as compared to EN-CNT electrodes in terms of specific capacity, specific power and energy density. Furthermore each device was tested for cycling stability. At the begining of cycling test, SC device with VA-CNT electrodes had around 60F/g specific capacity, 7.83 Wh/kg specific energy density and 300 W/kg specific power density. Also SC device with EN-CNT electrodes had around 40F/g specific capacity, 5.16Wh/g specific energy density and 300 W/kg specific power density. Both SC device had unexpectedly low capacitance retention at the end of the 5000 cycles. Only 60% of the specific capacitance was retained by both device. In reality, EDLC should not have that much decline in specific capacitance. This decline in specific capacitance was explained underlying the fact of the structural change in negative electrode firstly examining the digital images and SEM images of both positive and negative electrodes. While there was not any morphological change in positive electrode before and after cycling test based on the digital and SEM images, negative electrode had very clear morphological change. According to SEM image, CNTs looked like

agglomerated. Also Raman data of both electrodes before and after cycling test showed different trend. In negative electrode, defect peak increased after 5000 cycles, whereas there is not any intensity change in defect for positive electrode. The functional groups on the electrode surface which comes from the growth condition in negative electrode and hydrogen ion insertion and desorption are the main reasons of this decline in capacity. Because hyrdrogen ion is absorbed and desorbed by the negative electrode during charging and discharging due to the electrostatşc forces so that hydrogen reacts with functional groups on the negative electrode surface. The same SC cell with EN-CNT electrode was tested in 1M TBABF4/AN electrolyte to ensure about the effect of acidic aquaeous electrolyte to the CNT based electrodes. Based on the cycling test result, SC cell in organic electrolyte preserved 97% of its capacitance value in 5000 charge/discharge cycles. However SC device in organic electrolyte showed smaller specific capacitance value because ions are bigger in organic electrolyte compared to the aqueous acidic one. Advantage of the organic electrolyte is its wide voltage window so that energy and power densities 2 times more compared to the acidic one, which is 14 Wh/kg and 600 W/kg, respectively. These results can be concluded that acidic aqueous electrolyte destroys the CNT based electrode structure and limits its usage for a long term, subsequently the life cycle of the SC device decreases. For a long term usage, organic electrolyte is more appropriate and promising choice for CNT based electrodes, nevertheless acidic aquaeous electrolyte satisfies high specific capacitance for short time usage.

Furthermore, hybrid electrode was prepared with PANi conducting polymer and CNT. Firstly electrodes were characterized with SEM, TEM, Raman and TGA to observe the morphological, spectral and thermal behaviour and also to be sure about the PANi coating on the CNT surface. SC device was assembled with asymmetric configuration using CNT as a negative electrode and hybrid PANi/CNT as a positive electrode. According to the test results in 1M H_2SO_4, asymmetric SC device showed better cycling stability than symmetric one. This results confirm that instead of using only PANi and CNT as electrode material, hybrid CNT/PANi electrode provides more promising results. Also asymmetric device configuration has lower time constant value than symmetric one.

The most important research area in supercapacitor field is to find appropriate electrode materials and to test them using different device configurations. So that the future research suggestions in the light of the outcomes of this thesis can be;

1. Due to the battery type property of the hybrid electrodes, capacitance calculations give error when the same capacitance equations are used. Also the calculated energy and power densities can not show the correct results because both values are directly related to the each other. So that a detail work including energy and power density calculations should be done for SC system with asymmetric electrode configurations.
2. Here, only hybrid electrode which sytnhesized electrochemical method was used in SC cell using two electrode configuration and as it explained maybe longer time should used for PANi polymerization on CNT and used as electrode in asymmetric SC cell. So that better capacitance performance can be obtained.
3. Another suggestion for hybrid electrode is to integrate PANi nanofibers into the CNT after functionalizing CNT using electrochemical activation method or any other method.
4. VA-CNT electrodes are very promising however it is very tough to handle this electrode when it is prepared with PANi. Because it does not stay aligned anymore after the coating with PANi. Solution based method is not a good way to prepara hybrid electrode with VA-CNT. So that oxidative chemical vapour deposition is a good method to prepare hybrid electrode.
5. Recently, preparation of ternary type hybrid electrodes and their usage in SC applications attract attention of reseachers. This electrode system provied higher capacitance, higher energy and power densities. As a next step, this electrode system should be prepared and used in SC cell system.

8. References

1. Winter, M. and R.J. Brodd, *What are batteries, fuel cells, and supercapacitors?* Chemical reviews, 2004. **104**(10): p. 4245-4270.

2. Pandolfo, G.A., Hollenkamp, F.A., *Carbon properties and their roles in supercapacitors.* Journal of Power Sources, 2006. **157**: p. 11-27.

3. Zhu, Y., et al., *Carbon-Based Supercapacitors Produced by Activation of Graphene.* Science, 2011. **332**(6037): p. 1537-1541.

4. Wang, G., L. Zhang, and J. Zhang, *A review of electrode materials for electrochemical supercapacitors.* Chemical Society Reviews, 2012. **41**(2): p. 797-828.

5. Simon, P., Gogotsi, Y., *Materials for electrochemical capacitors.* Nature Materials, 2008. **7**.

6. Zhang, L.L. and X. Zhao, *Carbon-based materials as supercapacitor electrodes.* Chemical Society Reviews, 2009. **38**(9): p. 2520-2531.

7. Yu, Z., et al., *Supercapacitor electrode materials: nanostructures from 0 to 3 dimensions.* Energy & Environmental Science, 2015. **8**(3): p. 702-730.

8. Dyatkin, B. and Y. Gogotsi, *Effects of structural disorder and surface chemistry on electric conductivity and capacitance of porous carbon electrodes.* Faraday Discussions, 2014.

9. Arie Borenstien, M.N., Sivan Okashy and Doron Aurbach, *Composite Carbon Nano-Tubes (CNT)/Activated Carbon Electrodes for Non-Aqueous Super Capacitors Using Organic Electrolyte Solutions.* Journal of The Electrochemical Society, 2013. **160**(8): p. A1282-A1285

10. Byungwoo Kim, H.C.a.K., *High-performance supercapacitors based on vertically aligned carbon nanotubes and nonaqueous electrolytes.* Nanotechnology, 2012. **23**.

11. Feng, H.P.J.L.Y.P., *Carbon Nanotubes for Supercapacitor.* Nanoscale Res Lett 2010. **2010**(5): p. 654-668.

12. Basirico, L. and G. Lanzara, *Moving towards high-power, high-frequency and low-resistance CNT supercapacitors by tuning the CNT length, axial deformation and contact resistance.* Nanotechnology, 2012. **23**(30): p. 305401.

13. Zhou, Y., et al., *High volumetric electrochemical performance of ultra-high density aligned carbon nanotube supercapacitors with controlled nanomorphology.* Electrochimica Acta, 2013. **111**(0): p. 608-613.

14. Iijima, S., *Helical microtubules of graphitic carbon.* nature, 1991. **354**(6348): p. 56-58.

15. Terrones, M. and N. Grobert, *Controlled production of aligned-nanotube bundles.* Nature, 1997. **388**(6637): p. 52.

16. Ren, Z.F., et al., *Synthesis of Large Arrays of Well-Aligned Carbon Nanotubes on Glass.* Science, 1998. **282**(5391): p. 1105-1107.

17. Hao Zhang, G.C., Yusheng Yang, Zhennan Gu *Comparison Between Electrochemical Properties of Aligned Carbon Nanotube Array and Entangled Carbon Nanotube Electrodes.* J. Electrochemical Society, 2008. **155**(2): p. K19-K22.

18. Lagoutte, S., et al., *Poly(3-methylthiophene)/Vertically Aligned Multi-walled Carbon Nanotubes: Electrochemical Synthesis, Characterizations and Electrochemical Storage Properties in Ionic Liquids.* Electrochimica Acta, 2014. **130**(0): p. 754-765.

19. Liu, C.-C., et al., *Electrochemical micro-capacitors of patterned electrodes loaded with manganese oxide and carbon nanotubes.* Journal of Power Sources, 2011. **196**(13): p. 5761-5768.

20. Dörfler, S., et al., *High power supercap electrodes based on vertical aligned carbon nanotubes on aluminum.* Journal of Power Sources, 2013. **227**(0): p. 218-228.

21. Honda, Y., et al., *Vertically aligned double-walled carbon nanotube electrode prepared by transfer methodology for electric double layer capacitor.* Journal of Power Sources, 2008. **185**(2): p. 1580-1584.

22. Lachman, N., et al., *Tailoring Thickness of Conformal Conducting Polymer Decorated Aligned Carbon Nanotube Electrodes for Energy Storage.* Advanced Materials Interfaces, 2014: p. n/a-n/a.

23. Ghaffari, M., et al., *Hybrid supercapacitor materials from poly(3,4-ethylenedioxythiophene) conformally coated aligned carbon nanotubes.* Electrochimica Acta, 2013. **112**: p. 522-528.

24. Saghafi, M., et al., *Preparation of vertically aligned carbon nanotubes and their electrochemical performance in supercapacitors.* Synthetic Metals, 2014. **195**(0): p. 252-259.

25. Abbas, Q., et al., *Effect of binder on the performance of carbon/carbon symmetric capacitors in salt aqueous electrolyte.* Electrochimica Acta, 2014. **140**(0): p. 132-138.

26. Kang, J., et al., *Development of an equivalent circuit model for electrochemical double layer capacitors (EDLCs) with distinct electrolytes.* Electrochimica Acta, 2014. **115**: p. 587-598.

27. Dubal, D.P., et al., *Hybrid energy storage: the merging of battery and supercapacitor chemistries.* Chemical Society Reviews, 2015. **44**(7): p. 1777-1790.

28. Jiang, X., et al., *Polyaniline/graphene/carbon fiber ternary composites as supercapacitor electrodes*. Materials Letters, 2015. **140**(0): p. 43-47.

29. Han, G., et al., *Sandwich-structured MnO2/polypyrrole/reduced graphene oxide hybrid composites for high-performance supercapacitors*. RSC Advances, 2014. **4**(20): p. 9898-9904.

30. Achilleos, D.S. and T.A. Hatton, *Surface design and engineering of hierarchical hybrid nanostructures for asymmetric supercapacitors with improved electrochemical performance.* Journal of Colloid and Interface Science, 2015. **447**(0): p. 282-301.

31. González, A., et al., *Review on supercapacitors: Technologies and materials.* Renewable and Sustainable Energy Reviews, 2016. **58**: p. 1189-1206.

32. Béguin, F., et al., *Supercapacitors: Carbons and Electrolytes for Advanced Supercapacitors (Adv. Mater. 14/2014).* Advanced Materials, 2014. **26**(14): p. 2283-2283.

33. Miller, J.R., *Market and Applications of Electrochemical Capacitors*, in *Supercapacitors*. 2013, Wiley-VCH Verlag GmbH & Co. KGaA. p. 509-526.

34. Chen, T. and L. Dai, *Carbon nanomaterials for high-performance supercapacitors.* Materials Today, 2013. **16**(7–8): p. 272-280.

35. Nor Syafira Abdul Manaf, M.S.A.B., Mohd Asyadi azam, *Development of High Performance Electrochemical Capacitor: A Systematic Review of Electrode Fabrication Technique Based on Different Carbon Materials.* ECS Journal of Solid State Science and Technology, 2013. **2**(10): p. M3101-M3119.

36. Borenstien, A., et al., *Composite Carbon Nano-Tubes (CNT)/Activated Carbon Electrodes for Non-Aqueous Super Capacitors Using Organic Electrolyte Solutions.* Journal of The Electrochemical Society, 2013. **160**(8): p. A1282-A1285.

37. Taberna, P.L., P. Simon, and J.F. Fauvarque *Electrochemical Characteristics and Impedance Spectroscopy Studies of Carbon-Carbon Supercapacitors.* Journal of The Electrochemical Society, 2003. **150**(3): p. A292-A300.

38. Jung, H.Y., et al., *Transparent, flexible supercapacitors from nano-engineered carbon films.* Sci. Rep., 2012. **2**.

39. Hu, S., R. Rajamani, and X. Yu, *Flexible solid-state paper based carbon nanotube supercapacitor.* Applied Physics Letters, 2012. **100**(10): p. 104103.

40. Quintero, R., et al., *Important factors for effective use of carbon nanotube matrices in electrochemical capacitor hybrid electrodes without binding additives.* RSC Advances, 2015. **5**(21): p. 16101-16111.

41. Ameen, S., et al., *Metal Oxide Nanomaterials, Conducting Polymers and Their Nanocomposites for Solar Energy.* 2013.

42. Liu, M., et al., *Hierarchical composites of polyaniline-graphene nanoribbons-carbon nanotubes as electrode materials in all-solid-state supercapacitors.* Nanoscale, 2013. **5**(16): p. 7312-7320.

43. Hu, H., et al., *Three-dimensional cross-linked carbon network wrapped with ordered polyaniline nanowires for high-performance pseudo-supercapacitors.* Journal of Power Sources, 2014. **268**(0): p. 451-458.

44. Song, E. and J.-W. Choi, *Conducting Polyaniline Nanowire and Its Applications in Chemiresistive Sensing.* Nanomaterials, 2013. **3**(3): p. 498.

45. Potphode, D.D., et al., *Polyaniline/partially exfoliated multi-walled carbon nanotubes based nanocomposites for supercapacitors.* Electrochimica Acta, 2015. **155**(0): p. 402-410.

46. Yu, D., et al., *Emergence of fiber supercapacitors.* Chemical Society Reviews, 2015. **44**(3): p. 647-662.

47. Francois Béguin, E.F., *Supercapacitors: Materials, Systems, and Applications*. 2013: Wiley-VCH Verlag GmbH & Co. KGaA.

48. R. Kotz, M.C., *Principles and applications of electrochemical capacitors.* Electrochimica Acta, 2000. **45**: p. 2483-2498.

49. Frackowiak, E., Q. Abbas, and F. Béguin, *Carbon/carbon supercapacitors.* Journal of Energy Chemistry, 2013. **22**(2): p. 226-240.

50. Frackowiak, E., *Carbon materials for supercapacitor application.* Phys Chem Chem Phys, 2007. **9**(15): p. 1774-85.

51. Noofeli, A., P.J. Hall, and A.J.R. Rennie, *Ionic liquid based EDLCs: influence of carbon porosity on electrochemical performance.* Faraday Discussions, 2014.

52. Sharma, P. and T.S. Bhatti, *A review on electrochemical double-layer capacitors.* Energy Conversion and Management, 2010. **51**(12): p. 2901-2912.

53. Ghosh, A. and Y.H. Lee, *Carbon-Based Electrochemical Capacitors.* ChemSusChem, 2012. **5**(3): p. 480-499.

54. Liu, S., S. Sun, and X.-Z. You, *Inorganic nanostructured materials for high performance electrochemical supercapacitors.* Nanoscale, 2014. **6**(4): p. 2037-2045.

55. Dirican, M., M. Yanilmaz, and X. Zhang, *Free-standing polyaniline-porous carbon nanofiber electrodes for symmetric and asymmetric supercapacitors.* RSC Advances, 2014. **4**(103): p. 59427-59435.

56. Zhu, H., S. Peng, and W. Jiang, *Electrochemical properties of PANI as single electrode of electrochemical capacitors in acid electrolytes.* ScientificWorldJournal, 2013. **2013**: p. 940153.

57. Zhou, Y., et al., *Advanced asymmetric supercapacitor based on conducting polymer and aligned carbon nanotubes with controlled nanomorphology.* Nano Energy, 2014. **9**: p. 176-185.

58. Meng, C., C. Liu, and S. Fan, *Flexible carbon nanotube/polyaniline paper-like films and their enhanced electrochemical properties.* Electrochemistry Communications, 2009. **11**(1): p. 186-189.

59. Yingqi Jiang, † Pengbo Wang,†,‡ Xining Zang,† Yang Yang,†,§ Alina Kozinda,† and Liwei Lin†, *Uniformly Embedded Metal Oxide Nanoparticles in Vertically Aligned Carbon Nanotube Forests as Pseudocapacitor Electrodes for Enhanced Energy Storage.* Nano Letters, 2013(13).

60. Yang, C., et al., *Freestanding and flexible graphene wrapped MnO2/MoO3 nanoparticle based asymmetric supercapacitors for high energy density and output voltage.* RSC Advances, 2015. **5**(56): p. 45129-45135.

61. Ramya, R., R. Sivasubramanian, and M.V. Sangaranarayanan, *Conducting polymers-based electrochemical supercapacitors—Progress and prospects.* Electrochimica Acta, 2013. **101**(0): p. 109-129.

62. Conway, B.E., *Transition from 'supercapacitor' to 'battery' behavior in electrochemical energy storage.* Journal of the Electrochemical Society, 1991. **138**(6): p. 1539-1548.

63. Zhao, Y., et al., *Vapor deposition polymerization of aniline on 3D hierarchical porous carbon with enhanced cycling stability as supercapacitor electrode.* Journal of Power Sources, 2015. **286**(0): p. 1-9.

64. Yu, G., et al., *Hybrid nanostructured materials for high-performance electrochemical capacitors.* Nano Energy, 2013. **2**(2): p. 213-234.

65. El-Kady, M.F., et al., *Engineering three-dimensional hybrid supercapacitors and microsupercapacitors for high-performance integrated energy storage.* Proceedings of the National Academy of Sciences, 2015. **112**(14): p. 4233-4238.

66. Shown, I., et al., *Conducting polymer-based flexible supercapacitor.* Energy Science & Engineering, 2015. **3**(1): p. 2-26.

67. S. Zhang, N.P., *Supercapacitors Performance Evaluation.* Advanced Energy Materials, 2014.

68. Hsia, B., et al., *Highly flexible, all solid-state micro-supercapacitors from vertically aligned carbon nanotubes.* Nanotechnology, 2014. **25**(5): p. 055401.

69. Frackowiak, E., et al., *Supercapacitors based on conducting polymers/nanotubes composites.* Journal of Power Sources, 2006. **153**(2): p. 413-418.

70. Khomenko, V., E. Frackowiak, and F. Béguin, *Determination of the specific capacitance of conducting polymer/nanotubes composite electrodes using different cell configurations.* Electrochimica Acta, 2005. **50**(12): p. 2499-2506.

71. Jinzhang Liu, F.M., Marco Notarianni, Matto Pasquali, Nunzio Motta, *High Performance All-Carbon Thin Film Supercapacitors.* Journal of Power Sources, 2015. **274**: p. 823-830.

72. Du, C. and N. Pan, *Supercapacitors using carbon nanotubes films by electrophoretic deposition.* Journal of Power Sources, 2006. **160**(2): p. 1487-1494.

73. Taberna, P.-L. and P. Simon, *Electrochemical Techniques*, in *Supercapacitors*. 2013, Wiley-VCH Verlag GmbH & Co. KGaA. p. 111-130.

74. Li, Z.-Y., M.S. Akhtar, and O.B. Yang, *Supercapacitors with ultrahigh energy density based on mesoporous carbon nanofibers: Enhanced double-layer electrochemical properties.* Journal of Alloys and Compounds, 2015. **653**: p. 212-218.

75. Biswal, M., et al., *From dead leaves to high energy density supercapacitors.* Energy & Environmental Science, 2013. **6**(4): p. 1249-1259.

76. Zhang, D., et al., *Enhanced capacitance and rate capability of graphene/polypyrrole composite as electrode material for supercapacitors.* Journal of Power Sources, 2011. **196**(14): p. 5990-5996.

77. Niu, Z., et al., *A "skeleton/skin" strategy for preparing ultrathin free-standing single-walled carbon nanotube/polyaniline films for high performance supercapacitor electrodes.* Energy & Environmental Science, 2012. **5**(9): p. 8726.

78. Nègre, L., et al., *Solvent-Free Electrolytes for Electrical Double Layer Capacitors.* Journal of The Electrochemical Society, 2015. **162**(5): p. A5037-A5040.

79. Majid Beidaghi, Z.W., Lin Gu, Chunlei Wang, *Electrostatic spray deposition of graphene nanoplatelets for high-power thin-film supercapacitor electrodes.* J. Solid State Electrochem., 2012. **16**: p. 3341-3348.

80. Portet, C., G. Yushin, and Y. Gogotsi, *Electrochemical performance of carbon onions, nanodiamonds, carbon black and multiwalled nanotubes in electrical double layer capacitors.* Carbon, 2007. **45**(13): p. 2511-2518.

81. Jang, Y., et al., *Activated carbon nanocomposite electrodes for high performance supercapacitors.* Electrochimica Acta, 2013. **102**(0): p. 240-245.

82. Nordheim, K.E., *Growth and Properties of Carbon Nanotubes.* 2013.

83. Mohd Asyadi Azam, N.S.A.M., Elyas Talib, Mohd Shahril Amin Bistamam, *Aligned carbon nanotube from catalytic chemical vapor deposition technique for energy storage device: a review.* Ionics, 2013. **19**(11): p. 1455-1476.

84. Polsen, E.S., *ROBUST SYNTHESIS AND CONTINUOUS MANUFACTURING OF CARBON NANOTUBE FORESTS AND GRAPHENE FILMS.* 2013.

85. Mohamed Shuaib Mohamed Saheed, N.M.M., and Zainal Arif Burhanudin, *Effect of Different Catalyst Deposition Technique on Aligned Multiwalled Carbon Nanotubes Grown by Thermal Chemical Vapor Deposition.* Journal of Nanomaterials, 2014. **2014**.

86. Seah, C.-M., S.-P. Chai, and A.R. Mohamed, *Synthesis of aligned carbon nanotubes.* Carbon, 2011. **49**(14): p. 4613-4635.

87. Choi, B.H., et al., *Effects of Al buffer layer on growth of highly vertically aligned carbon nanotube forests for in situ yarning.* Microelectron. Eng., 2010. **87**(5-8): p. 1500-1505.

88. Liu, H., et al., *Aligned multi-walled carbon nanotubes on different substrates by floating catalyst chemical vapor deposition: Critical effects of buffer layer.* Surface and Coatings Technology, 2008. **202**(17): p. 4114-4120.

89. Gilbert D. Nessim, A.J.H., Jin S. Kim, Donatello Acquaviva, Jihun Oh,Caitlin D. Morgan, Matteo Seita, Jeffrey S. Leib, and Carl V. Thompson, *Tuning of Vertically-Aligned Carbon Nanotube Diameter and Areal Density through Catalyst Pre-Treatment.* Nano Letters, 2008. **8**.

90. Oliver, C.R., et al., *Statistical Analysis of Variation in Laboratory Growth of Carbon Nanotube Forests and Recommendations for Improved Consistency.* ACS Nano, 2013. **7**(4): p. 3565-3580.

91. Fang, Y., et al., *Self-supported supercapacitor membranes: Polypyrrole-coated carbon nanotube networks enabled by pulsed electrodeposition.* Journal of Power Sources, 2010. **195**(2): p. 674-679.

92. Song, E. and J.-W. Choi, *Conducting Polyaniline Nanowire and Its Applications in Chemiresistive Sensing.* Nanomaterials, 2013. **3**(3): p. 498-523.

93. Lehman, J.H., et al., *Evaluating the characteristics of multiwall carbon nanotubes.* Carbon, 2011. **49**(8): p. 2581-2602.

94. Tong, Z., et al., *Layered polyaniline/graphene film from sandwich-structured polyaniline/graphene/polyaniline nanosheets for high-performance pseudosupercapacitors.* Journal of Materials Chemistry A, 2014. **2**(13): p. 4642.

95. Chen, W., R.B. Rakhi, and H.N. Alshareef, *High energy density supercapacitors using macroporous kitchen sponges.* Journal of Materials Chemistry, 2012. **22**(29): p. 14394-14402.

96. Zhang, X., et al., *Effect of aqueous electrolytes on the electrochemical behaviors of supercapacitors based on hierarchically porous carbons.* Journal of Power Sources, 2012. **216**(0): p. 290-296.

97. Dennis Antiohos, M.R., Jun Chen and Joselito M. Razal *Carbon Nanotubes for Energy Applications*, in *Syntheses and Applications of Carbon Nanotubes and Their Composite*. 2013.

98. Kim, N.H., T. Kuila, and J.H. Lee, *Enhanced mechanical properties of a multiwall carbon nanotube attached pre-stitched graphene oxide filled linear low density polyethylene composite.* Journal of Materials Chemistry A, 2014. **2**(8): p. 2681-2689.

99. Yang, X., et al., *High voltage supercapacitors using hydrated graphene film in a neutral aqueous electrolyte.* Electrochemistry Communications, 2011. **13**(11): p. 1166-1169.

100. Kim, M., I. Oh, and J. Kim, *Effects of different electrolytes on the electrochemical and dynamic behavior of electric double layer capacitors based on a porous silicon carbide electrode.* Physical Chemistry Chemical Physics, 2015. **17**(25): p. 16367-16374.

101. Bello, A., et al., *Asymmetric supercapacitor based on nanostructured graphene foam/polyvinyl alcohol/formaldehyde and activated carbon electrodes.* Journal of Power Sources, 2015. **273**(0): p. 305-311.

102. Li, M., et al., *Fabrication of two-dimensional hybrid sheets by decorating insulating PANI on reduced graphene oxide for polymer nanocomposites with low dielectric loss and high dielectric constant.* Journal of Materials Chemistry, 2012. **22**(44): p. 23477-23484.

9. Appendix

9.1. Appendix A

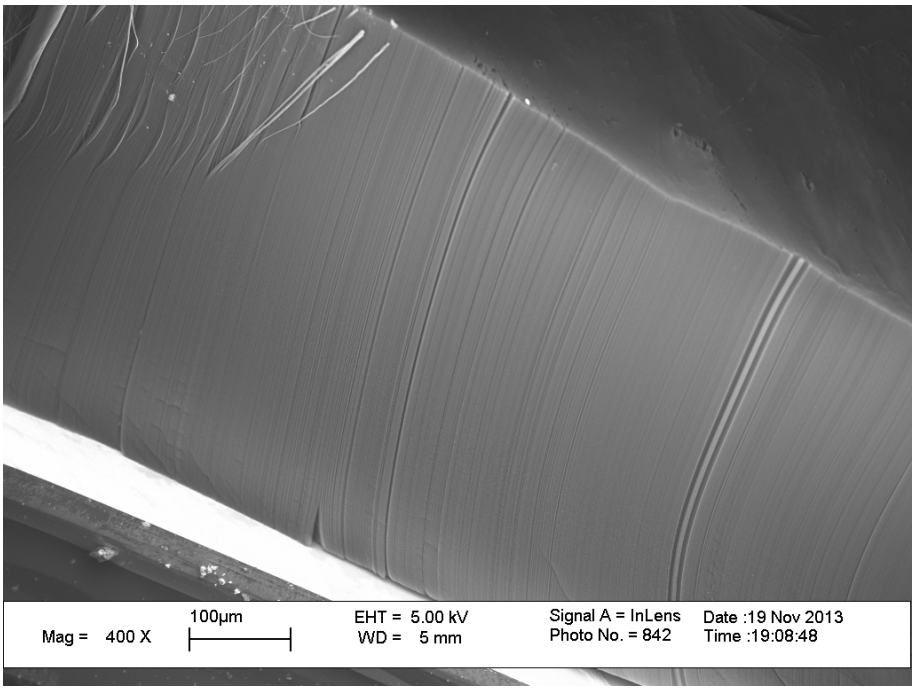

Figure 9.1. SEM image of VA-CNT

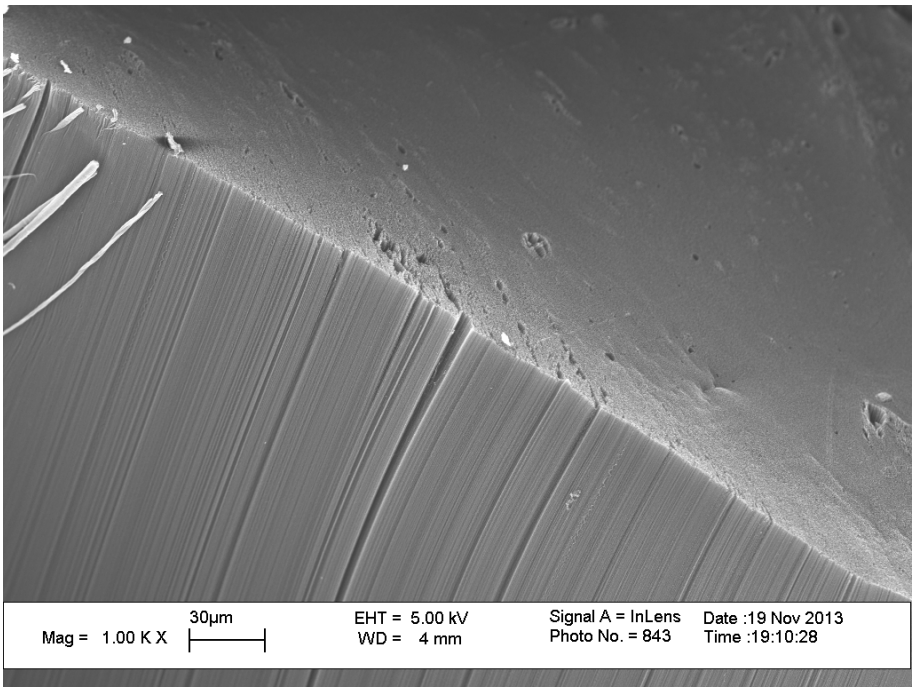

Figure 9.2. SEM image of VA-CNT

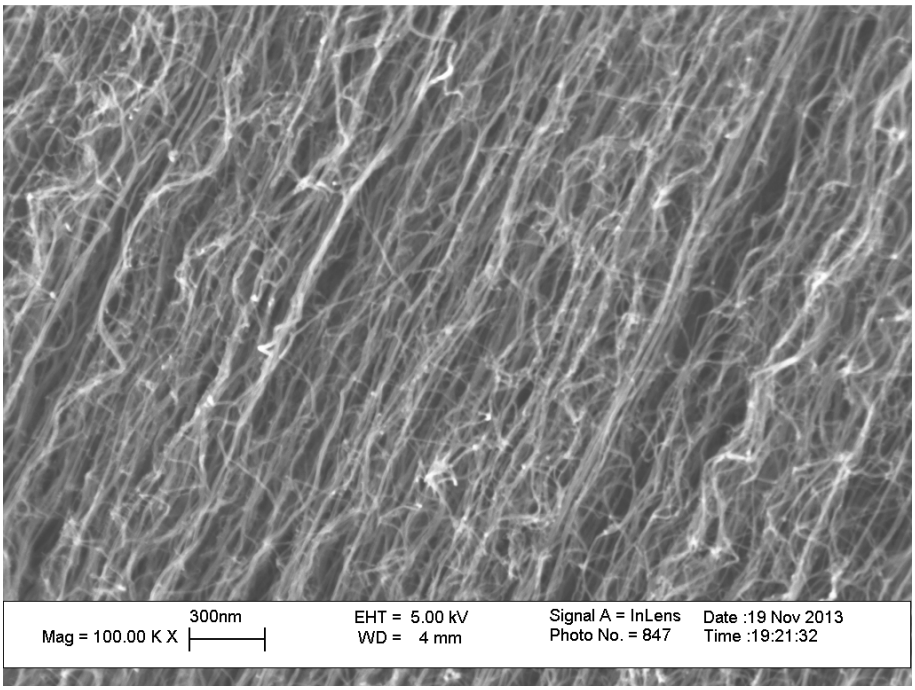

Figure 9.3 SEM image of VA-CNT

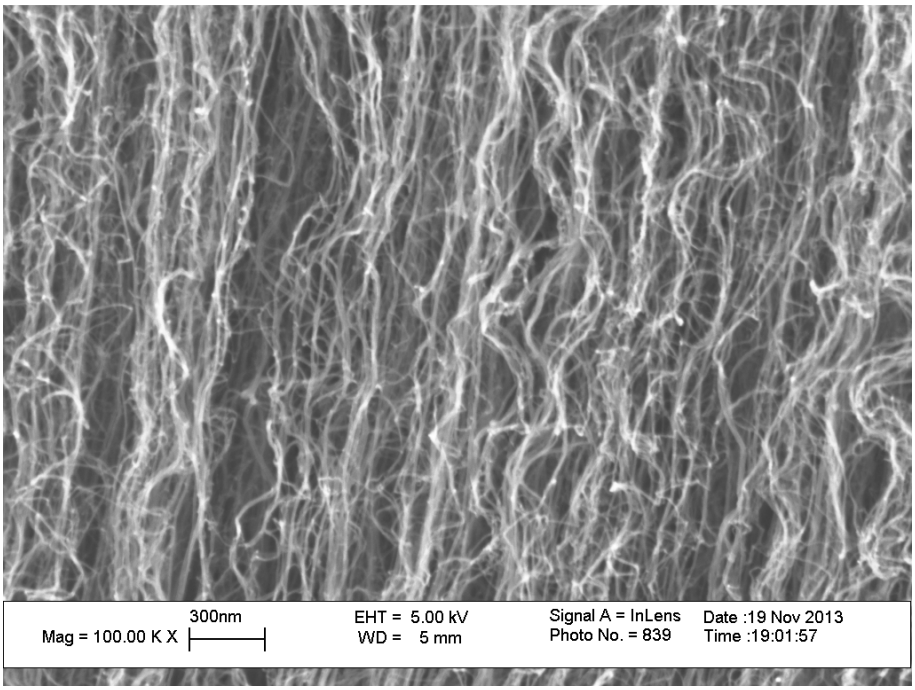

Figure 9.4. SEM image of VA-CNT

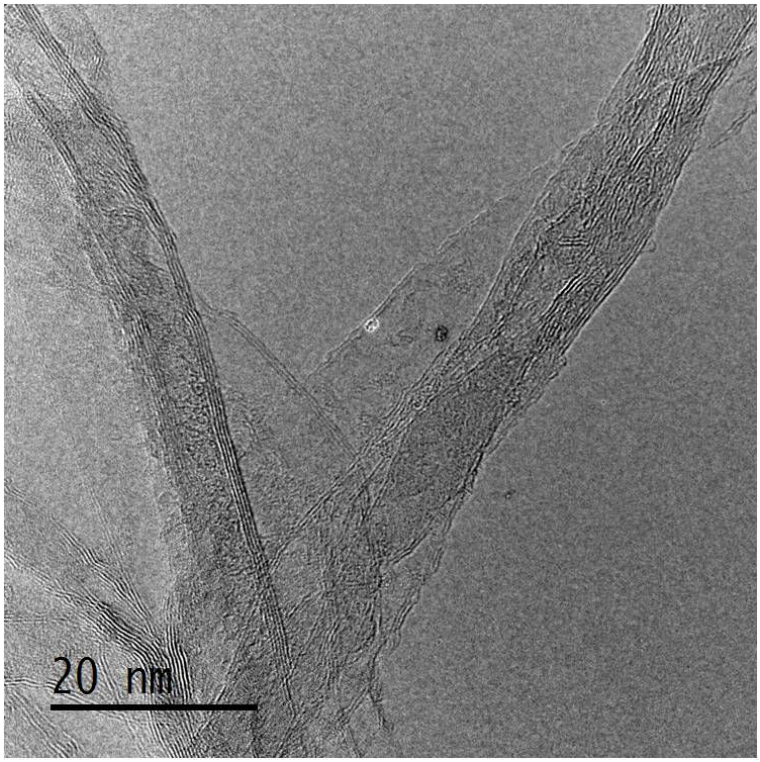

Figure 9.5. TEM image of CNT

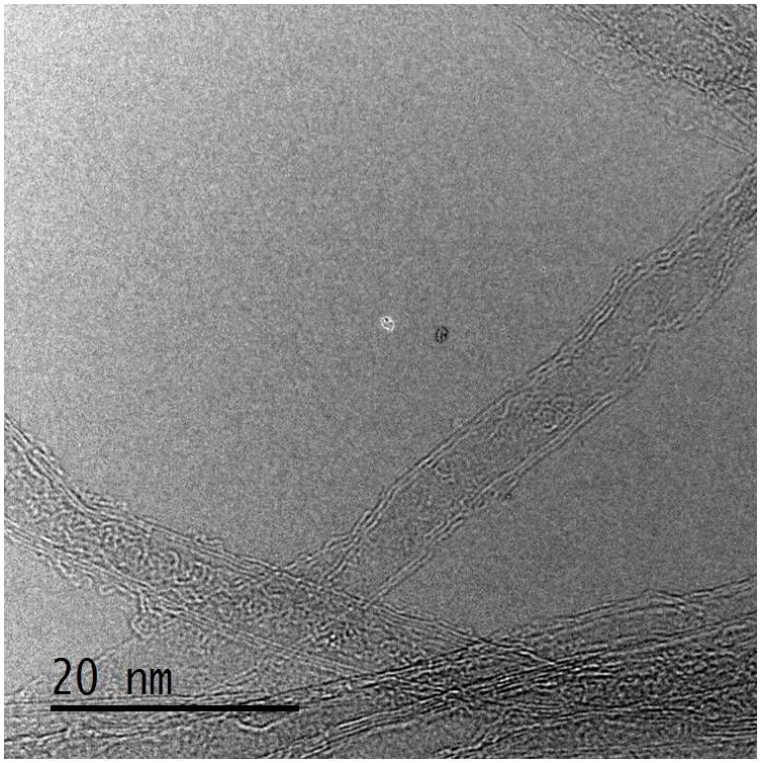

Figure 9.6. TEM image of CNT

9.2. Appendix B

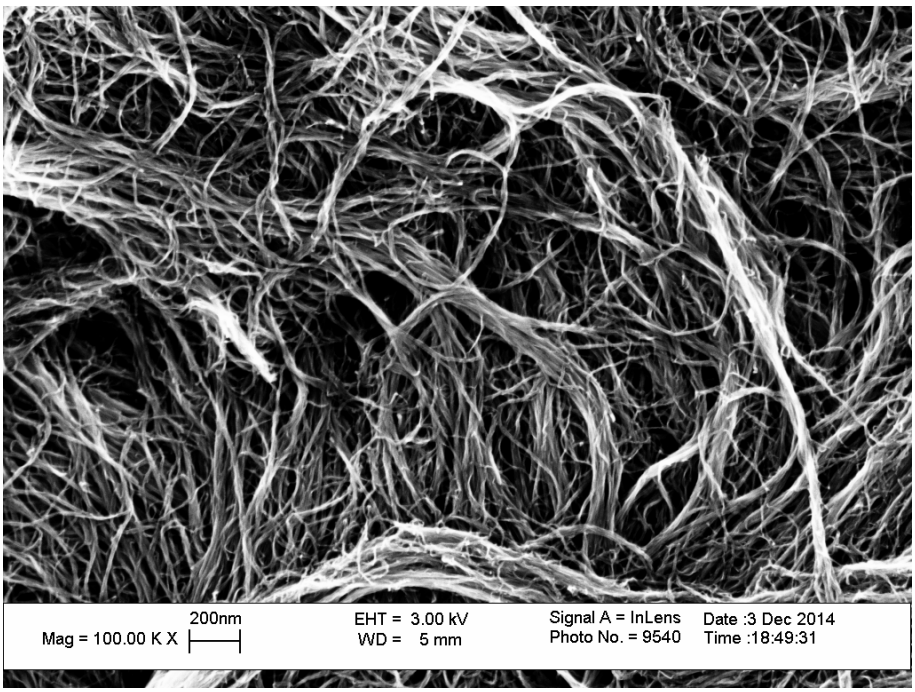

Figure 9.7. SEM image of EN-CNT

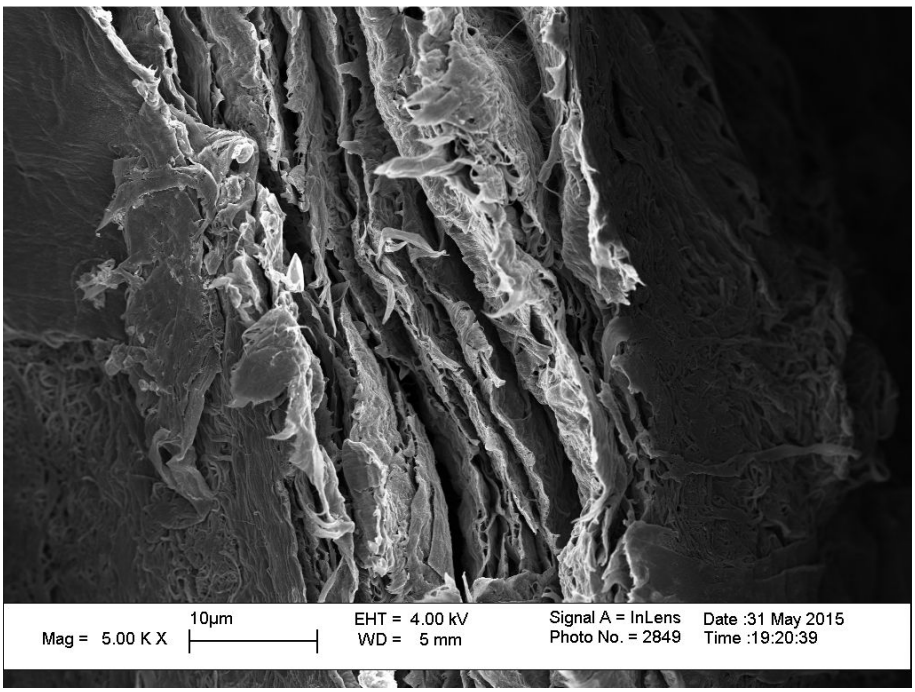

Figure 9.8. SEM image of EN-CNT from cross section

9.3. Appendix C

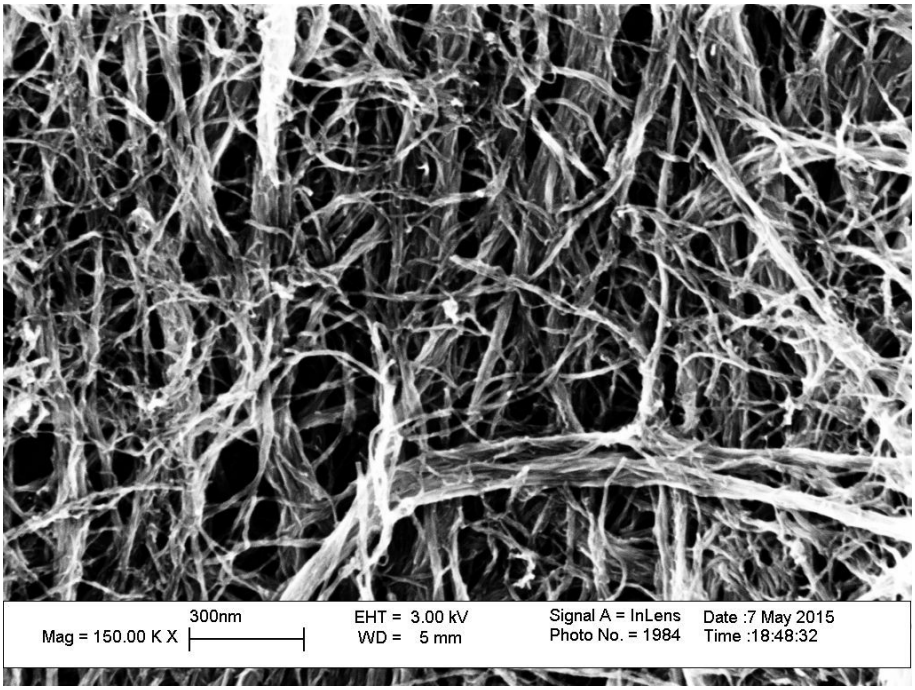

Figure 9.9. SEM image of electrochemically prepared EN-CNT/PANi

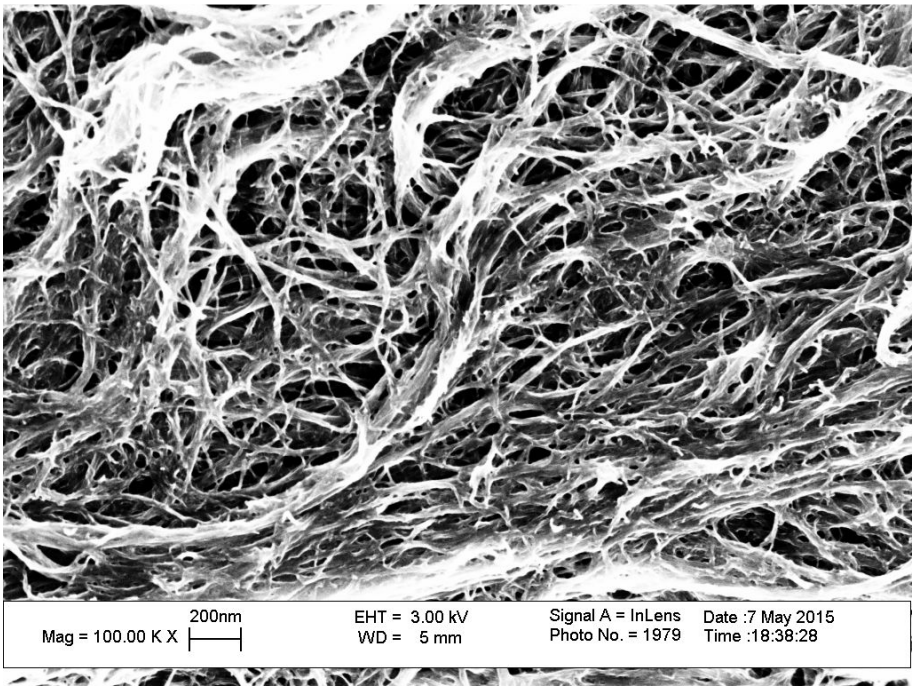

Figure 9.10. SEM image of chemically prepared EN-CNT/PANi

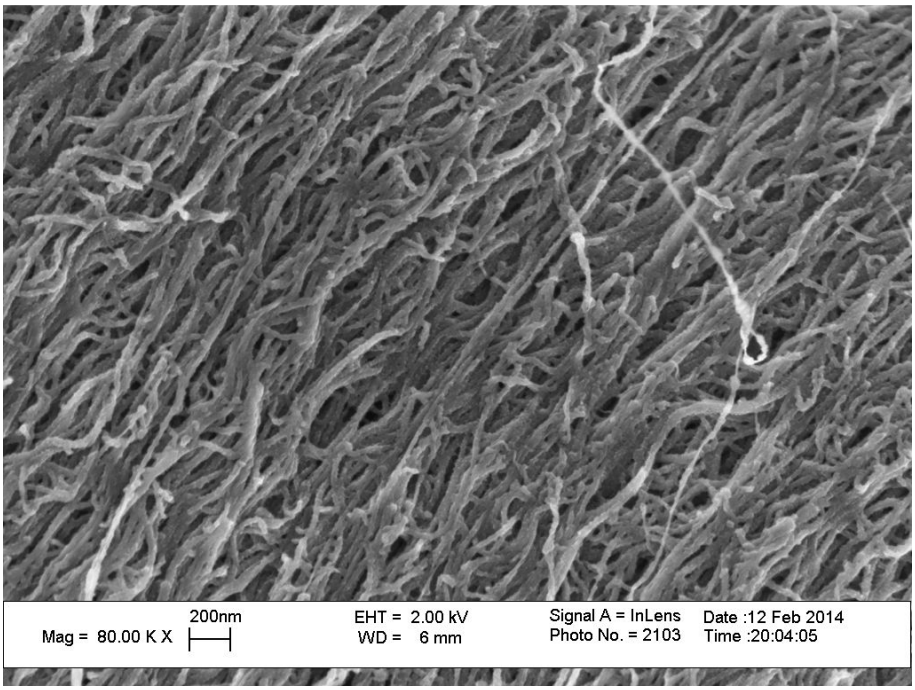

Figure 9.11. SEM image of VA-CNT/PANi

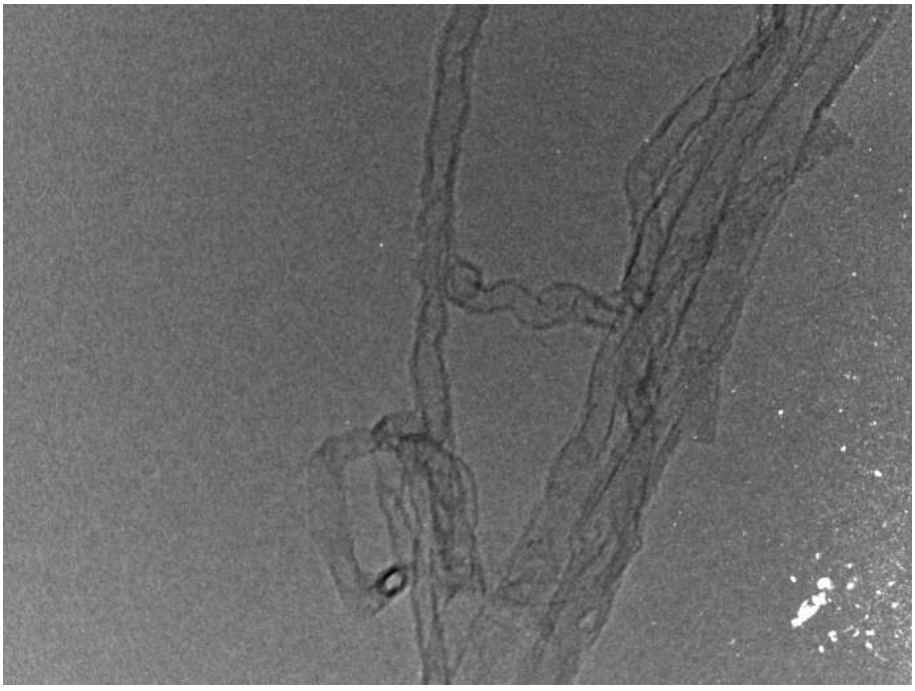

Figure 9.12. TEM image of CNT/PANi